4D-Earth
Planetary Mapping

Shannon Entropy as a Space Exploration Tool Using Hyperspectral Data On Mars

Raynouval Arief Amir
Student No. S2268914
raynouvalariefamir@student.utwente.nl

Supervisors:
Frank van Ruitenbeek (Department of Earth Systems Analysis)
Wim Harry Bakker (Department of Earth Systems Analysis)

UNIVERSITY OF TWENTE. | ITC

Table of Contents

List of Figures

List of Tables

1. Introduction

1.1. Background

Planetary mapping, or planetary cartography, is the mapping of objects other than the Earth. The development of planetary exploration is important in advancing the human understanding of the universe. The advancement of space exploration has developed greatly since Neil Armstrong has set foot on the moon in 1969 alongside others undergoing the lunar mission by the National Aeronautics and Space Administration (NASA). The challenges towards that advancement have been considerable due to the limitations of space exploration, such as the surface conditions, harsh environments, and the variety of planetary bodies. Now, by using satellites and hyperspectral images, researchers are able to identify and interpret surface lithologies of planets and chemical composition of atmospheres of other objects in the Universe. Planetary mapping has been continually developing, that researchers without any background in planetary mapping along with sufficient dataset can produce planetary maps (Naß et al., 2017).

Mars is one of the planets in our solar system that is relatively the most researched planetary body after Earth, due to the calmer environment than the other planetary bodies and a relatively close distance from Earth. Although Venus is closer to Earth, unlike Mars, Venus has a more harsh environment with a surface temperature of about 425°C (Singh, 2019) while Mars only goes up to 30°C (NASA, 2019b). Being the fourth planet in the Solar System, Mars is approximately 57 million kilometres from Earth at its nearest point (NASA, 2018), with the average distance from the Sun around 228 million kilometres (NASA, 2019b). Mars has a diameter of around 6,791 kilometres making it the second-smallest planet in volume on the Solar System after Mercury (NASA, 2019b). The atmosphere of Mars differs from that of Earth, consisting of mostly carbon dioxide with an average volume ratio of 94.9%, alongside trace elements such as Nitrogen (2.6%), Argon (1.9%), and Oxygen (0.174%) with trace gasses of acetylene, carbon monoxide, krypton, methane, neon, nitrogen oxide, ozone, water vapour, and xenon (ESA, 2018) (Franz et al., 2017). The atmosphere of Mars is only 1% in atmospheric density than that of Earth (ESA, 2018).

Different from Earth, Mars has epochs based on the crater density scale (Carr & Head, 2010), while the timescale on Earth is based on the study of relationships of rock layers, and also biostratigraphy. The epochs on Mars are Noachian, Hesperian, and Amazonian. The division of the epoch is based on the logic that older surfaces would have more craters than the younger ones. The 3 epochs are also named after the places on Mars belonging to the epochs. The Noachian epoch is the oldest ranging between 3.8 to 3.5 billion years ago. During the Noachian epoch, significant quantities of phyllosilicates is suspected to have formed, such as smectites. During the Noachian epoch, it has been proposed that Mars has an abundance of surface water (Carr, 1987), based on the geomorphology of the surface of Mars. The Hesperian epoch ranges from 3.5 to 1.8 billion years ago, during which the creation of lava plains occurs. The Amazonian epoch ranges from 1.8 billion years ago to the present day. During this time, only few meteorites has impacted Mars. The Olympus Mons formed during the Amazonian epoch.

A more recent timeline was proposed based on the mineralogical and geology of Mars that includes also 3 epochs; Phyllocian, Theiikian, and Siderikan (Bibring et al., 2006). The Phyllocian is the epoch starting from the planet creation to 4 billion years ago. The name Phyllocian is given due to the phyllosilicate minerals abundant during this time period (Bibring et al., 2006). The Theiikian is the time period ranging from 4 billion years ago to 3.5 billion years ago where there was the occurrence of volcanic activity and acidic aqueous alteration traced by sulfates (Bibring et al., 2006). Lastly, the Siderikan ranges from 3.5 billion years ago until the present, marked by the inactivity of volcanoes and

absence of water and aqueous-free alteration traced by ferric oxides (Bibring et al., 2006). During the Siderikan time period, oxidation of iron-rich rocks causes the planet to have a reddish colour as it is now. Based on the geological history of Mars, it is likely that the hydrothermal activity on Mars is magmatic-driven and impact-generated, assumed from the many occurrence of volcanic, impact, and water-related features that are often associated with each other (El Maarry, 2011). Figure 1 shows the geological time scale of both crater density scale and mineralogical scale.

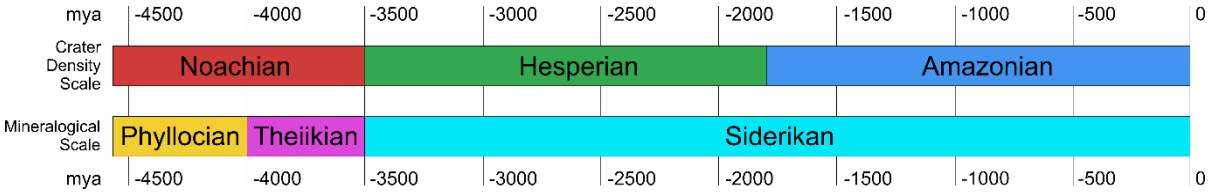

Figure 1. Geological time scales of Mars

The composition of Mars has been studied using remote sensing and spectral data to create geological maps of Mars. The USGS has created a geological map of Mars that has a record of geological units based on data acquired by orbiters since the Viking Orbiters (K. L. Tanaka et al., 2014).

One of the problems with remote sensing applications of Mars is that noise of the data causes difficulty in interpreting the spectral data when proceeding with the multispectral analysis. Another problem is the absence of surface validation measured on the ground. Ground samples from the Mars Rover may exist but their availability is dependent on the research area. In planetary images, noises are often specific to the planetary bodies, caused by the atmospheric effects, alongside the sensor itself which can also cause systematic noise (Gilmore et al., 2011). Other noise sources may also occur such as low light conditions, radiation spikes and dropouts, and transmission errors. Reddish sand and dust cover a high percentage of the surface of Mars, causing low reflectance in the multispectral analysis of the surface of Mars (Gilmore et al., 2011). This research aims to create a new exploratory tool to identify the existence of hydrothermal alteration by using Shannon entropy and the spectral data of Mars, while also considering the effects of noise and limitations, such as low reflectance, of planetary mapping.

Shannon entropy is the calculation that evaluates the amount of difference from the average number (Shannon, 1948). Combined with a hyperspectral dataset, Shannon entropy can be used as an indication process of hydrothermally altered rocks. Places with a low entropy will show more distinct absorption features due to the differences in absorption values and can be used to identify pixels containing hydrothermal alteration minerals (Ruitenbeek, Goseling, Bakker, & Hein, 2020). Hydrothermally altered rocks generally have minerals with a more distinct absorption feature, for instance at 2.2μm due to the vibration of the Al-OH (Podwysocki, Segal, & Jones, 1983) of the clay minerals.

1.2. Research Objectives and Research Questions

This research aims to use Shannon entropy to indicate hydrothermal alteration based on the surface spectral absorption values of minerals on Mars as a new exploratory tool. For this objective, areas of interest will be chosen based on previous research that show places with signs of hydrothermally altered rocks and unaltered rocks, to be used as a comparison for Shannon entropy calculations. Hyperspectral images from the CRISM or OMEGA satellite will be used in the research because of the higher number of spectral bands than multi-spectral images.

To achieve this objective, various sub-objectives are defined to help in the workflow and understanding of the research. The objectives are as follows:

Sub Objectives:

1. **Selecting areas on Mars that have been thoroughly researched for hydrothermally alterations as the research area to be used for comparison**
    - What requirements are used to select the area of interest which would be used as a comparison for the end result of this research?
2. **Reproducing mineralogical map of the research area based on past researches.**
    - Which minerals are needed to be mapped in the mineralogical map to be used for the comparison step?
3. **Calculation of Shannon entropy using spectral data of the research area**
    - Which comparison method and criteria can be used to conclude that Shannon Entropy is a viable exploratory tool?
    - How to interpret entropy values retrieved from the satellite data to identify low entropy anomaly on Mars?
4. **Interpreting the variation of entropy values calculated from absorption value on Mars to identify Hydrothermal Alterations**
    - Does the interpreted entropy value represent hydrothermal alterations or other phenomenon occurring on Mars?
    - How to differentiate low entropy values that may be caused by hydrothermal alteration or another occurring phenomenon?
5. **Using the Shannon entropy exploratory tool to analyse alternative areas for further comparison of the new exploratory tool**
    - Does the new exploratory tool work on a different research area to detect hydrothermal alterations?

1.3. Research Area

The research will use 4 research areas, which is comprised of 2 research areas using 2 different sensors. The data used in this research can be retrieved from the data repositories of OMEGA and CRISM instrument as they have recorded hyperspectral data of Mars. Other spectrometers orbiting Mars, such as the IRS, IRTM, ISM, TES, and THEMIS, all have either only multispectral data, or a very low spatial and spectral resolution (Brown & Storrie-Lombardi, 2014). For this research, hyperspectral data will be more useful than multispectral data due to the higher number of wavelength bands, which would make the research more accurate.

1.4. Dataset

The CRISM (The Compact Reconnaissance Imaging Spectrometer for Mars) sensor provides data with spatial resolution of 18.4 meter per pixel (at 300km altitude) and a spectral resolution ranging from 362nm to 3.92µm with 6.55nm per channel (NASA, 2019a). This means the CRISM satellite will provide a hyperspectral data cube with 544 bands. CRISM moves in an elliptical orbit and has a swath width of 11.1km at 300km altitude. If CRISM data is used, then the CRISM analysis tool (CAT) created by NASA will be used as a plugin for ENVI. The CAT is used in opening the CRISM data and applying standard corrections to the CRISM data. The OMEGA (Observatoire pour la Minéralogie, l'Eau, les Glaces et l'Activité) has a spectral range from 0.38µm to 5.1µm and a spatial resolution of < 350m when observed from an altitude of less than 300km (Bibring et al., 2004). CRISM and OMEGA data can be obtained online, on the Mars Orbital Data Explorer website (PDS Geosciences Node, 2017) which contains both the satellite data for OMEGA and CRISM. The original OMEGA data can be found in the OMEGA FTP directory managed by the PSA (Planetary Science Archive) (PSA, 2017).

2. Methodology

2.1. CRISM Processing methods

The typical processing work flow when working with CRISM data starts with conversion from PDS (Planetary Data System) to CAT (CRISM Analysis Toolkit) format, geometric correction, continued with photometric correction, atmospheric correction, despike & destripe, and lastly spectral subsetting to limit the wavelength to bands that shows absorption features for hydrothermal alteration. The workflow for the processing of the CRISM data can be seen in Figure 2. PDS file format is the standard format created by the planetary division of NASA (National Aeronautics and Space Administration) (Data Design Working Group, 2020). The CAT format is a format to be used with the CRISM analysis toolkit (Morgan, Seelos, & Murchie, 2017) that sorts the wavelength band from short-to-long. The data used is the TRDR (Targeted Reduced Data Record) downloaded from the Planetary Data System (PDS). TRDR data is CRISM data that has been radiometrically calibrated, which is calibration to convert digital number into reflectance, and is resampled in the spectral and spatial direction. TRDR data stores the wavelength bands in a descending order, from long to short. By converting the data from the original PDS format into the CAT format, the wavelength bands are sorted from the shortest wavelength band to the longest wavelength band. TRDR data is not yet geometrically projected and has to be reprojected into the correct projection system, which is the Mars 2000 spatial reference.

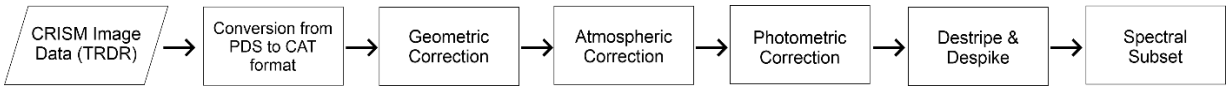

Figure 2. Processing method of a CRISM data includes conversion from PDS to CAT format, geometric correction, atmospheric correction, photometric correction, destripe & despike, and spectral subsetting.

- PDS to CAT
  Converts the PDS file into a CAT file with an ENVI header. The conversion causes the PDS file that has wavelength bands sorted from long-to-short into short-to-long. The process is done to ease the use of the CRISM data to be used with the CAT software.

- Atmospheric Correction
  Atmospheric correction is done to correct for the effects of the atmosphere on the data. Carbon dioxide is the main component of the Mars atmosphere. The chemical compound causes a triple deep absorption feature centered in the 2.0 µm, as shown in Figure 3a. Carbon dioxide also shows visible absorption features in the 1.4 and 1.6 µm as well (M. Tanaka & Yamanouchi, 1977). 1.4µm absorption feature may also be an indication of water or OH. The atmospheric correction uses the division by scaled volcano scan, which uses the division by a scaled atmospheric transmission method generated from the Martian surface, where the high and low altitude spectra are derived from the base and summit of the Olympus Mons volcano (Wiseman et al., 2016), hence the name. The result of the atmospheric correction can be seen in Figure 3b, where the triple absorption feature caused by carbon dioxide of the atmosphere is reduced. The carbon dioxide absorption features in 1.4 and 1.6µm bands have also been reduced by the atmospheric correction. If a correction is done to the extent of full removal of the CO2 absorption, it may cause the removal of other features, because the volcano scan method employs a division of the atmospheric transmission. The level of atmospheric correction is empirically optimized for the research area by the CAT software.

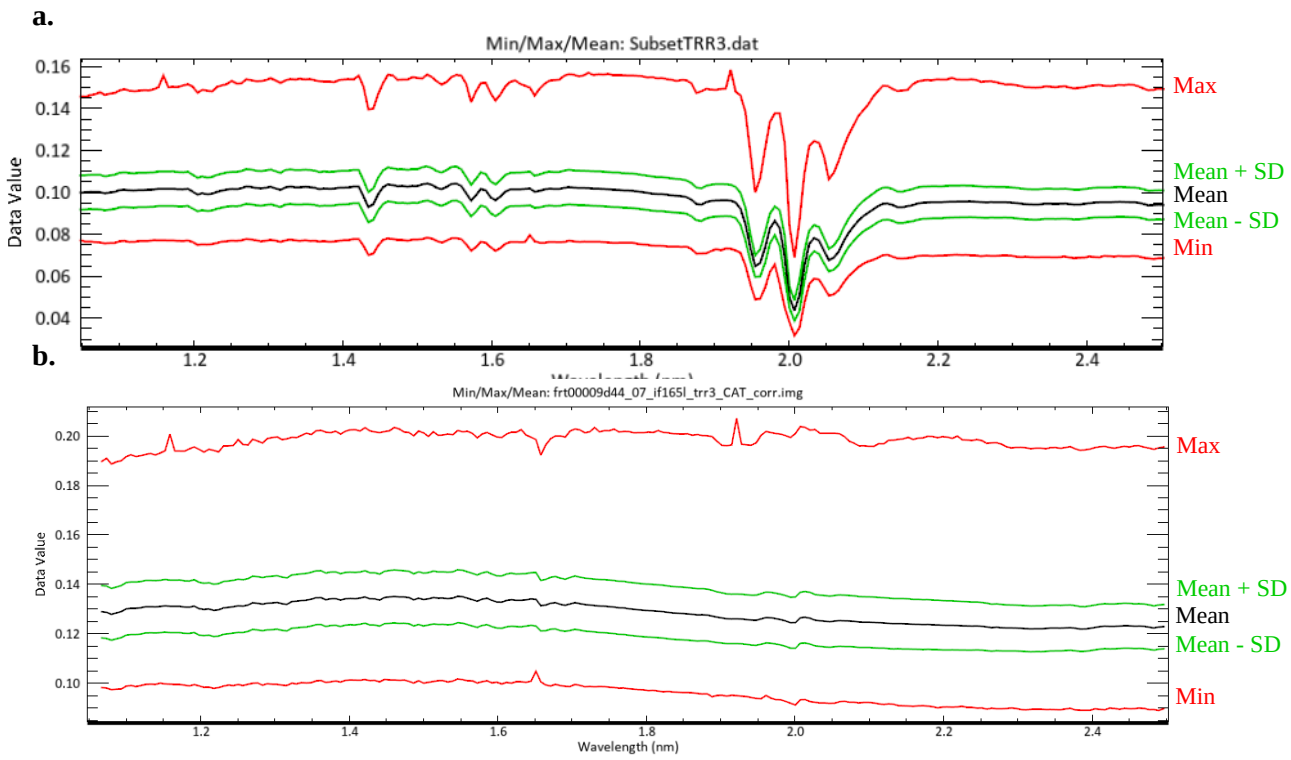

Figure 3. Mean, maximum, minimum, and mean +/- standard deviation spectral value of the research area in Nili Fossae before (Figure 3a) and after (Figure 3b) atmospheric correction is applied. A triple absorption feature caused by carbon dioxide can be seen centered in 2.0 µm, where it is then removed using atmospheric correction.

- Photometric Correction
  Photometric correction is the division by cosine of the incidence angle, which empirically corrects the surface to a common viewing condition, it is also called the cosine correction. Cosine correction is the correction of reflectance measurements that is affected by the incidence angle to create the Lambertian Reflectance, where the reflectance value is the same when viewed from different angles (Koppal, 2014).

- Despike & Destripe
  Despiking is done to remove noise spikes that may occur in the spectra of the research. The destripe process is done to remove scan line striping in the image data that may cause a misread of the spectral data. Striping is caused by systematic error of the instrument.

- Geometric Correction
  Geometric correction is the process of transforming the image data into its observed size and shape based on the projection system of the area, done by projecting a single data cube. Figure 4 shows the result before and after geometric correction of the CRISM Nili Fossae research area. Before geometric correction, the TRDR data was not projected. After applying a geometric correction by using the CAT software to project a single cube data, the TRDR data was projected into the Mars 2000 geographic coordinate system, the general coordinate system of Mars, which uses degrees. The coordinates are then displayed as degrees, minutes, and seconds.

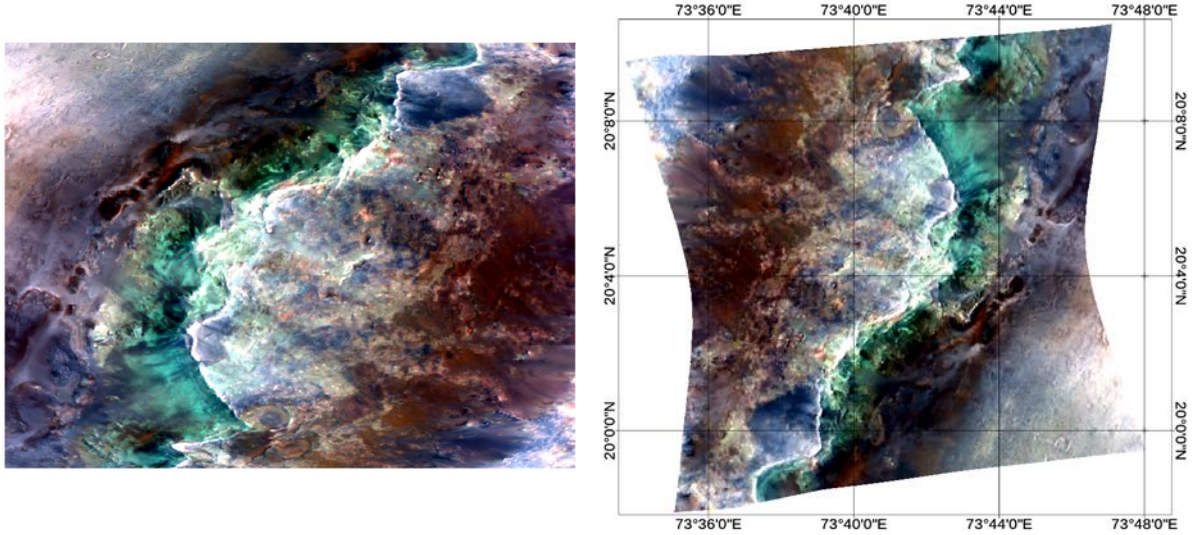

Figure 4. The result of geometric correction which changes the TRDR raw image data (left) into the correct projection (right) with the Mars 2000 IAU2000:49900 projection system shown in degrees, minutes, and seconds.

- Spectral Subset

The spectral subsetting procedure of the image depends on the intended use of the data by the user. This research uses the near-infrared to short-wavelength infrared range wavelength to determine the entropy value of each pixel. The SWIR range is used to the absorption features present that may be indicative of hydrothermal alteration. The TRDR data retrieved from the CRISM archive before it has been processed has 438 bands that range from 1.0014 µm to 4.0 µm after the conversion into CAT format from PDS format. This research uses the spectral subset of 1.0472µm to 2.5031µm, which includes the absorption features needed to identify hydrothermal alterations. In total, the subset image has 222 bands.

2.2. OMEGA Processing method

The OMEGA processing method, similar to the CRISM processing method, involves the calibration of the raw-data cube, removal of bad bands, geometric correction, solar correction, transmittance model, and lastly atmospheric correction (Bakker et al., 2014). The OMEGA data used in this research has already been processed following these steps and would not need anymore processing.

2.3. Entropy Map

Entropy maps are created using spectral math available in the HypPy software. The software applies the formula (Shannon, 1948) (Cover & Thomas, 2005):

$$Hspec\ (P) = -\sum_{1=1}^{m} p_i \cdot log_2\, p_i$$

The formula is used calculate the entropy value of each pixel spectrum on a pixel-by-pixel basis, creating an entropy map in the absorption spectra, which is the subtraction of 1 with the reflectance spectra. The calculation uses Shannon entropy as Hspec, probability distribution as P, m as the number of possible outcomes, and pi as the probability of outcome i (Ruitenbeek et al., 2020).

2.4. Entropy Map Comparison

To see the effects of processing that includes geometric correction, atmospheric correction, photometric correction, despike & destripe, and spectral subsetting on the calculated entropy, three entropy maps are created for comparison. The data used are 1) the TRDR data that has only undergone geometric correction conducted by me, 2) TRDR data that has been processed by me for geometric correction, atmospheric correction, photometric correction, and destripe & despiking, and 3) MTRDR (Map-projected Targeted Reduced Data Record) data which is CRISM data that has been processed by the CRISM team. The result should show the differences between the data that are caused by differences in the processing of the data. Following the visual comparison, a regression statistic alongside a regression model is done to quantify the similarities or differences between the entropy maps, by analyzing the coefficient of determination and the standard error.

R squared is the coefficient of determination, which shows how many points is located on the regression line. It shows the percentage where the differences in the first variable can be explained by the difference in a second variable, which means the higher the coefficient of determination, the better the model fits the data. Standard Error of the regression is the measure of the distance of data points that does not fall in the regression line.

2.5. Geological Structure

Analyzing the geological structure is crucial in understanding the mineralogy of the research area. The creation of the geological structure uses digital elevation model (DEM) to understand the topography of the research area and the geological process that may have caused said topography. The DEM data is taken from the instrument Mars Orbiter Laser Altimeter (MOLA), an instrument on the Mars Global Surveyor (MGS) spacecraft that was launched in November 7, 1996. A greyscale map using MOLA elevation data can be seen in Figure 5.

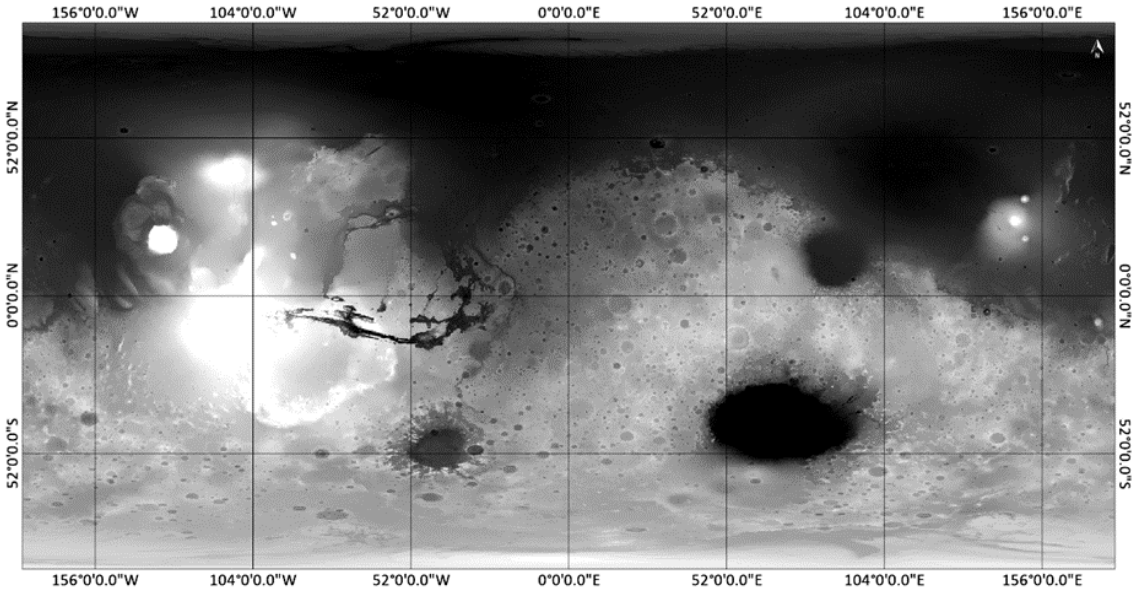

Figure 5. Mars Orbiter Laser Altimeter (MOLA) data showing the elevation of Mars in Mars 2000 Coordinate system.

2.6. Wavelength Map

Wavelength maps are maps that indicates the deepest absorption features, where the location and depth of the deepest absorption feature is represented by colour (Van Ruitenbeek et al., 2014). The wavelength map is used to create the mineral maps in this research. Mineral maps are used in this research as a

comparison with the entropy maps as a mean of validation of the Shannon entropy method. The mineral map is created using the wavelength mapper, where the deepest absorption feature of the area is represented by a colour based on its wavelength. Figure 6 shows the result of the creation of the wavelength map with the legend that shows the wavelength representation in colour. The wavelength map is used as the base for the creation of a mineral map. The wavelength map is digitized by using a region of interest tool, creating a polygon of the region of interest, according to the groups of color that may be representative of a certain mineral based on its absorption feature. The resulting region of interest (ROI) is then calculated for its mean spectra, to be interpreted for which mineral it may represent. The mean spectrum is compared with the spectrum of a potential mineral from the CRISM spectra library and identified based on the absorption features of the mean spectrum of the ROI.

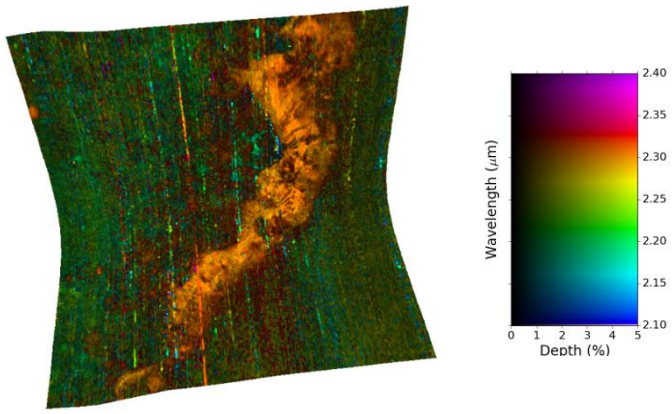

Figure 6. The result of wavelength mapping. The map shows deepest absorption features of a pixel represented by color as shown in the legend.

2.7. Summary Product Maps

Alongside the wavelength maps, the summary product maps which are indexes that highlights locations of geological features are also created for further analysis and creation of mineral maps. Summary product maps are created using band calculations to indicate the locations of geological features such as carbonates, phyllosilicates, pyroxene, and olivine among others. The summary product calculations in this research uses formulas proposed by Pelkey et al., 2007 which includes all the summary products needed for this research, and uses the full spectra of the CRISM and OMEGA images. The tables for the summary product calculations (Pelkey et al., 2007) can be seen in Table 1.

Table 1. Summary product formulas used in the research.

Name	Parameter	Formula	Rationale
Surface Parameters			
OLINDEX	Olivine index	(R1695/(0.1*R1050 + 0.1*R1210 + 0.4*R1330 + 0.4*R1470)) − 1	Olivine will be strongly positive; based on fayalite
LCPINDEX	pyroxene index	((R1330-R1050)/(R1330 + R1050)) * ((R1330-R1815)/(R1330 + R1815)	Pyroxene will be strongly positive; favors LCP
HCPXINDEX	pyroxene index	((R1470-R1050)/(R1470 + R1050)) * ((R1470-R2067)/(R1470 + R2067)	Pyroxene will be strongly positive; favors HCP
BD2290	2.29 μm band depth	1 − (R2290/(a*R2250 + b*R2350))	Mg,Fe-OH minerals (@ 2.3); ALSO CO_2 ice (@ 2.292)
BDCARB	2.33 & 2.53 μm band depth	1 − (sqrt [(R2330/(a*R2230 + b*R2390)) *(R2530/(c*R2390 +	Carbonate overtones

2.8. Mineral Maps

The mineral map of the research area is created by digitizing the areas that shows diagnostic absorption features of certain minerals. The diagnostic features can be seen in the wavelength maps with further validation using the summary product indexes.

2.9. Entropy Map Validation

The purpose of the research area is to analyze whether or not the entropy method works in finding interesting phenomenon of a research area. The minerals mapped using the wavelength and summary products map are overlain in the entropy map as an ROI. The overlain entropy map is then analyzed as to whether or not the low entropy values identify the minerals that has a deeper absorption feature in the research area. If the entropy method works, the low entropy areas should match with the ROI of the mapped minerals. The different entropy areas are also created an ROI representative to be analyzed further on how the different entropy values represent a spectrum. The entropy ROI will be used to calculate the mean spectra of the ROI.

2.10. Log-residuals

The satellite imagery of Mars contains systematic noise, in particular the CRISM images shows noisy spectra in the first zone of the spectra, ranging from 1.0μm to 1.8μm. Log residuals are applied to create ratioed space which is a pseudo-reflectance spectrum. It is a 2-step normalization method where the pixel spectra are normalized and divided using the mean spectra of the image, creating a pseudo-reflectance. These pseudo-reflectance spectra are used to identify diagnostic absorption features that may occur in the noisy bands. The comparison between reflectance and pseudo-reflectance can be seen in Figure 7. The log residuals method also provides the Robust Least Upper Bound (RLUB) spectra, which contains the reflectance of the least upper bound of the image. The RLUB can be seen in Appendix 1. If there is a spectral feature that is present in the whole image, then that feature will be taken as atmospheric effects and will not be present in the resulting pseudo-reflectance, which is why the use of log-residuals must be used with caution.

a. **b.**

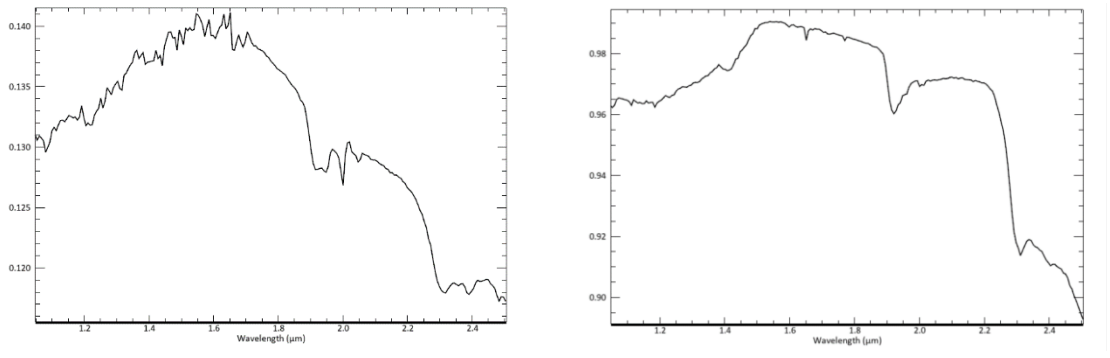

Figure 7. Comparison between the spectra with reflectance (a.) and spectra with pseudo-reflectance (b.) of the same area.

3. Results

3.1. Processing

The processing including geometric correction, atmospheric correction, photometric correction, despike & destripe, and spectral subsetting was applied to the TRDR CRISM data, which was radiometrically calibrated into reflectance. The processing is conducted on the CRISM data instead of the OMEGA data because of the availability of the processed and raw CRISM data, while the OMEGA data acquired for this research has already been processed and will be used for the exploratory phase.

Atmospheric correction of the data removes any absorption features that may have been caused by the atmospheric transmission. The data is also processed for noises such as random noises, and systematic errors such as striping. The result of the processing of the TRDR data and MTRDR data can be seen in Figure 8. Figure 8a shows the result of the TRDR data that is conducted by me, while Figure 8b shows the processing result of the MTRDR data that has been conducted by the CRISM team.

a.

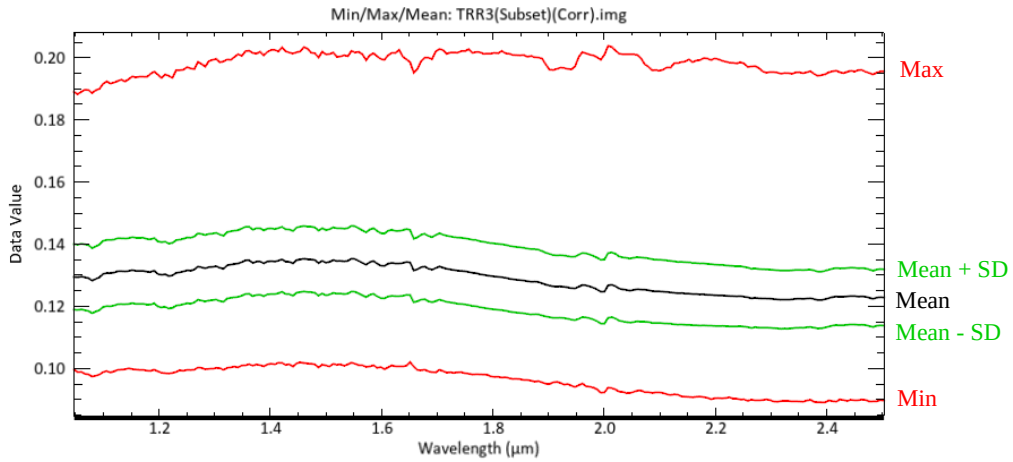

b.

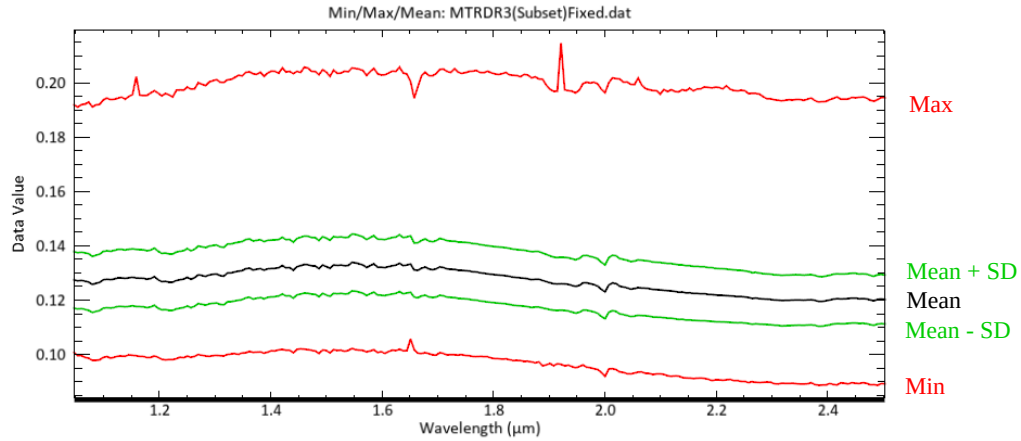

Figure 8. Result of the processed CRISM Nili Fossae image TRDR data (a) and the processed CRISM Nili Fossae image MTRDR data (b) that shows the maximum, minimum, mean, mean + standard deviation, mean – standard deviation of the spectra. The spectral variance of the processed TRDR data and MTRDR data shows visual similarities. Both showing the remains of the carbon dioxide absorption feature at 2.0 µm.

3.2. Entropy Map Comparison

The entropy maps are created using the corrected MTRDR data, the TRDR data, and the raw TRDR data are shown in Figure 9. Figure 9 shows the maximum, minimum, mean, and standard deviation of the MTRDR entropy map, the TRDR corrected entropy map, and the TRDR raw entropy map. Visually, the patterns of the 3 entropy maps are similar, only the contrast differs.

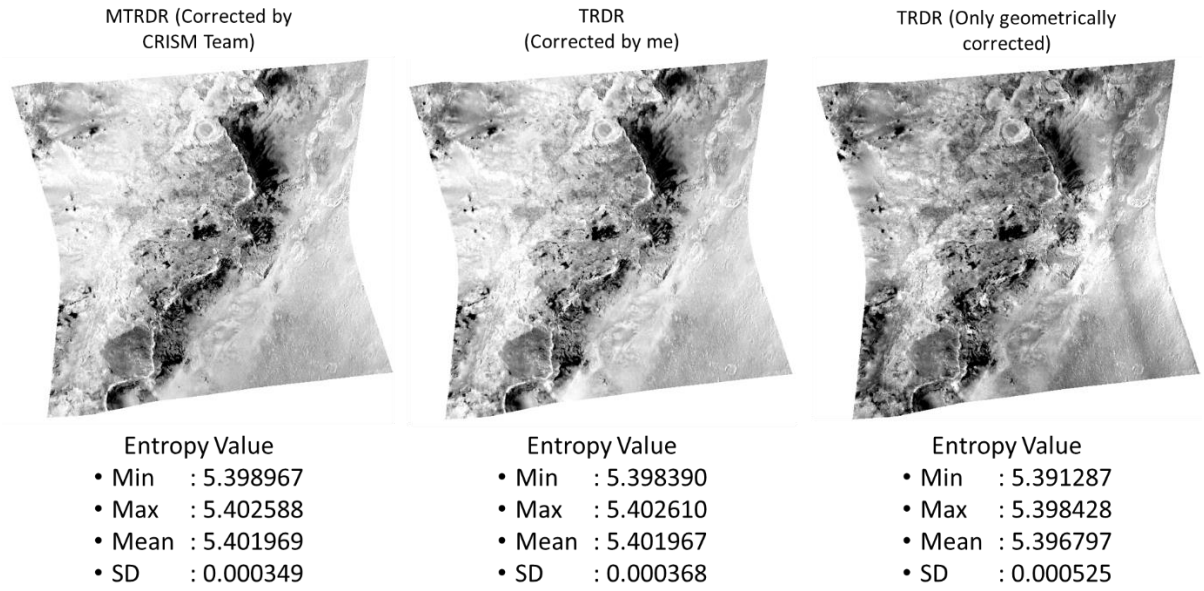

Figure 9. Comparison between the corrected MTRDR data, TRDR data, and raw TRDR data. The MTRDR and the corrected TRDR data has similar entropy values (minimum, maximum, mean, and standard deviation), while the TRDR data that has not been corrected shows a higher standard deviation and lower entropy values.

To analyse further the differences and similarities between the 3 entropy maps, a scatterplot is used using the entropy values of the entropy maps as the x and y axis. Scatterplot is used to plot the entropy values to analyse the relationship between 2 entropy maps. Regression statistics is then conducted to quantify the similarities and differences between the entropy maps alongside the creation of a regression line in the scatter plot. Figure 10 shows the scatter plots between the entropy maps and the regression statistics. Regression statistics in Figure 10 shows the value for R-squared, or the coefficient of determination. The coefficient of determination is the coefficient to determine the strength of the relationship between the 2 variables. The closer the value is to 1, the stronger the relationship between the 2 variables. Standard Error of the regression statistics in Figure 10 measures the distance of the variable values from the regression line. The smaller the number the less spread the values are.

a.

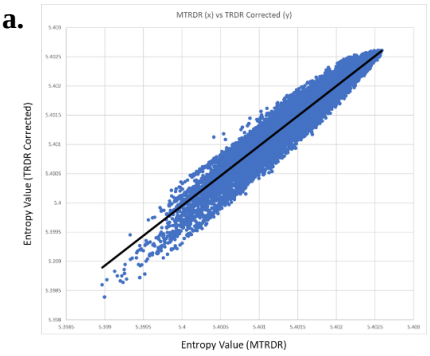

MTRDR vs TRDR Corrected

REGRESSION STATISTICS	
R Squared	0.94249439
Standard Error	8.36188E-05
Observations	382055

b.

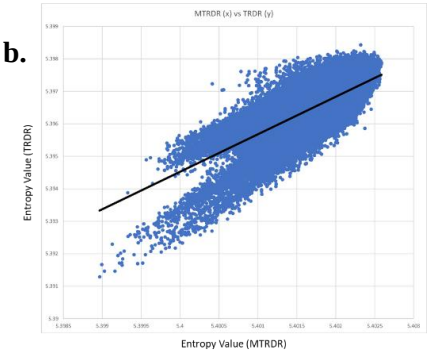

MTRDR vs TRDR (Raw)

REGRESSION STATISTICS	
R Squared	0.587808105
Standard Error	0.000337238
Observations	382055

c.

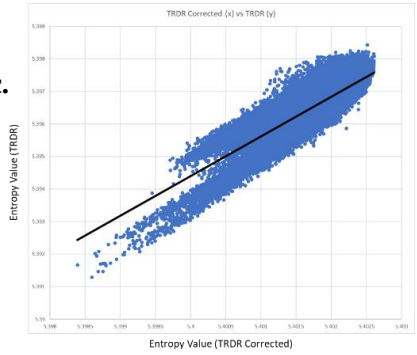

TRDR Corrected vs TRDR (Raw)

REGRESSION STATISTICS	
R Square	0.729838161
Standard Error	0.000273023
Observations	382055

Figure 10. Regression model with R-square, standard error, and number of observations between; a) MTRDR entropy map and TRDR corrected entropy map, b) MTRDR entropy map and TRDR raw entropy map, c) TRDR corrected entropy map and TRDR raw entropy map.

3.3. CRISM Images

3.3.1. Nili Fossae Research Area

The Nili fossae research area is labeled as FRT00009D44, located on the graben walls of the trough in Nili Fossae region. Nili Fossae itself is located in the Syrtis Major quadrangle. This location has been selected because of the high number of studies that have been conducted in the area, which is needed for the validation of the entropy method as an exploration tool. From past studies, there has been reported phyllosilicates and low calcium pyroxene present in the area (Mustard et al., 2009), which is why Nili Fossae is an optimal candidate for this research. The location of the Nili Fossae research area can be seen in Figure *11*.

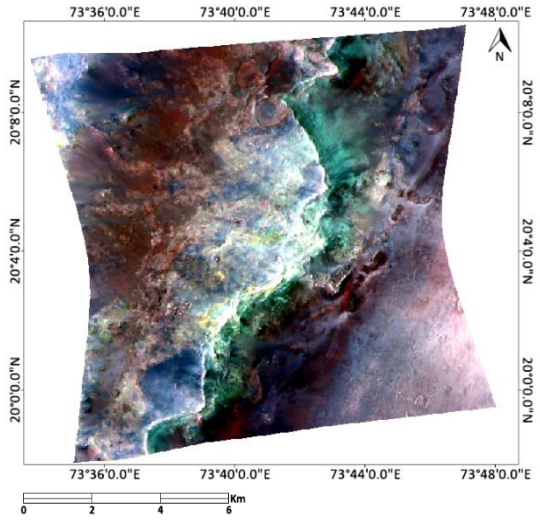

R: 2.5295µm
G: 1.3292µm
B: 0.7684µm

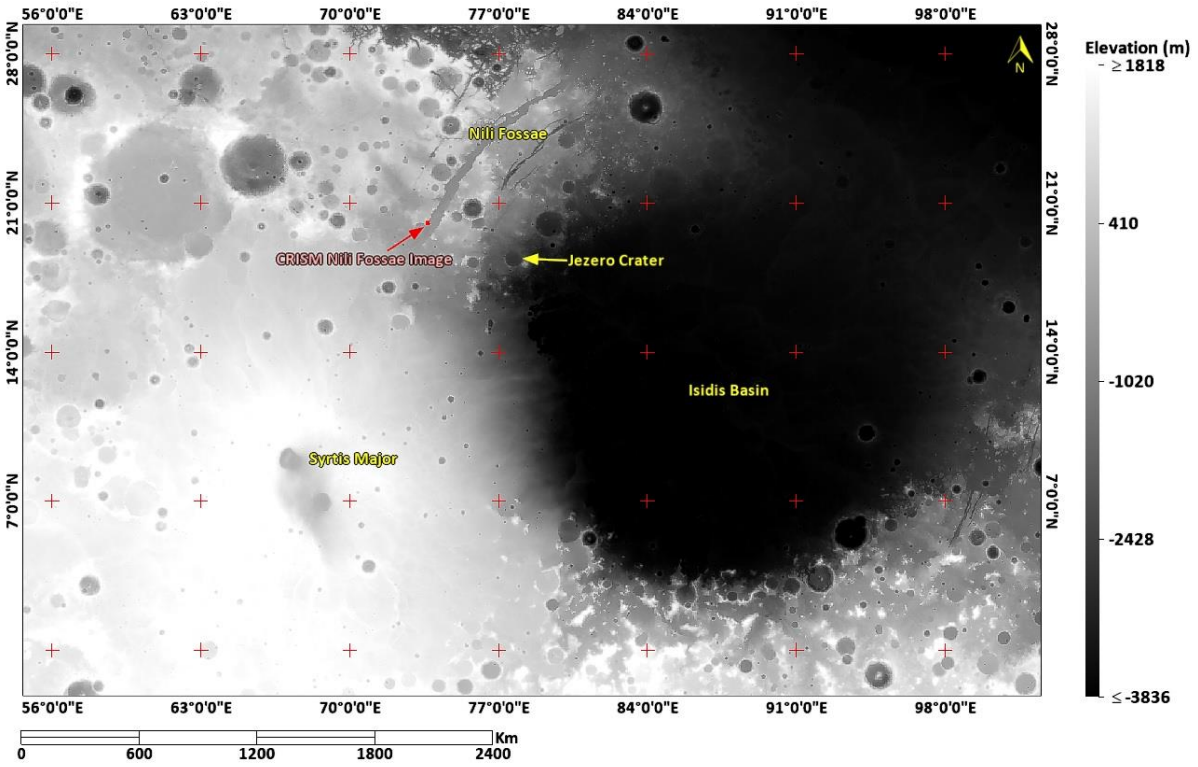

Figure 11. Location of the Nili Fossae research area (FRT00009D44) shown on a greyscale map of the MOLA elevation data.

3.3.1.1. Geological Structure

The CRISM Nili Fossae image is located in the walls of the graben in the Nili Fossae region. The graben of the Nili Fossae region was caused by tectonic activity (Ritzer & Hauck, 2009). The research area shows ridges along the graben wall, formed by faulting, indicated by the yellow color in Figure 12.. The graben wall is a slope that has a difference of ±500m between the ridges and the graben floor. Craters caused by impacts have been seen in the research area, these are the most recent geological structures visible of the research area. The outline of the graben wall, impact craters, graben floor, and ridges present in the CRISM Nili Fossae research area can be seen in Figure 12.

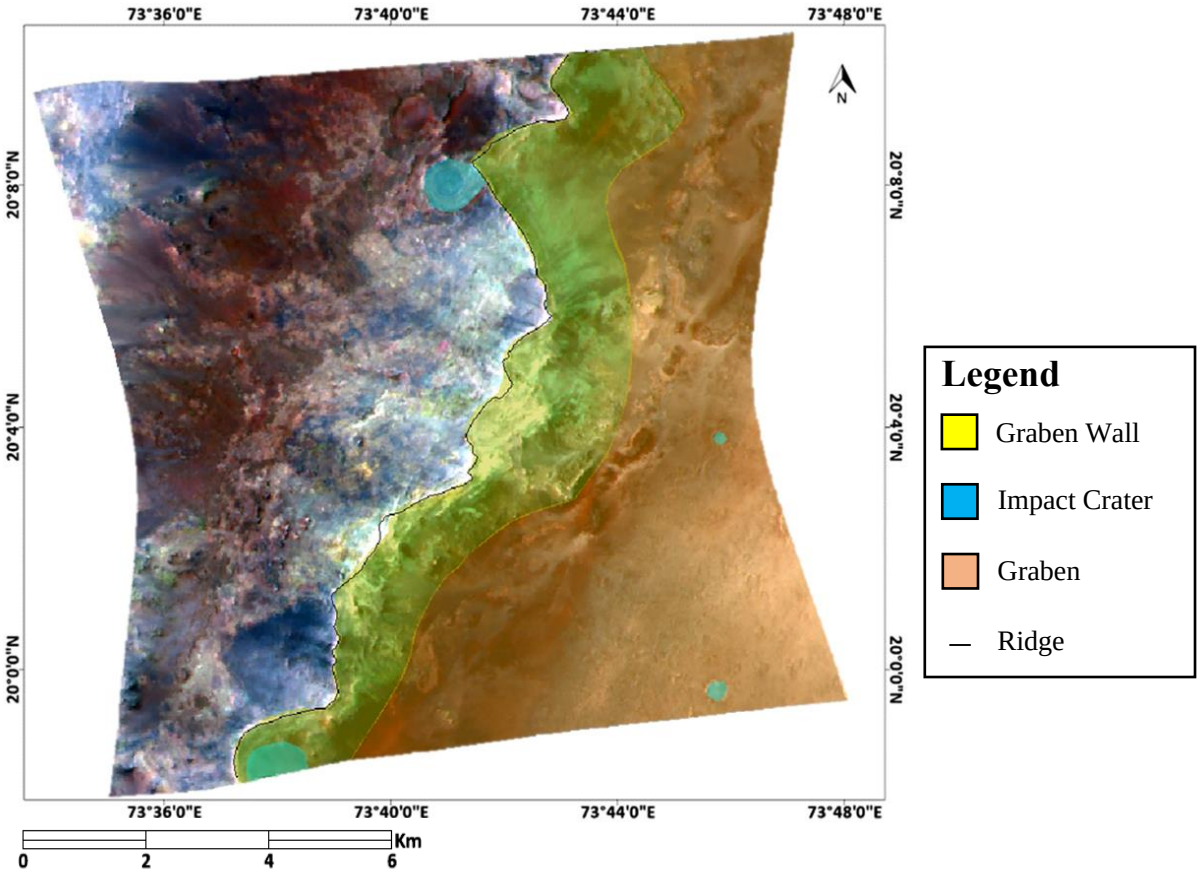

Figure 12. Geological structure outline of the area covered by the CRISM image, showing ridges in black line, impact craters in light blue, graben wall in yellow, and graben floor in orange.

3.3.1.2. Entropy Map

Entropy map of the Nili Fossae research area uses the MTRDR data that has been corrected by the CRISM team, created using the wavelength range of 1.0μm to 2.5μm. The low entropy value can be seen to be located along the graben walls, with few dark spots (low entropy value) in the surface of the horst. The map in Figure 13 is shown in a linear 1% stretch, which displays the top 1% of the entropy values as white, and the bottom 1% of the entropy values as black.

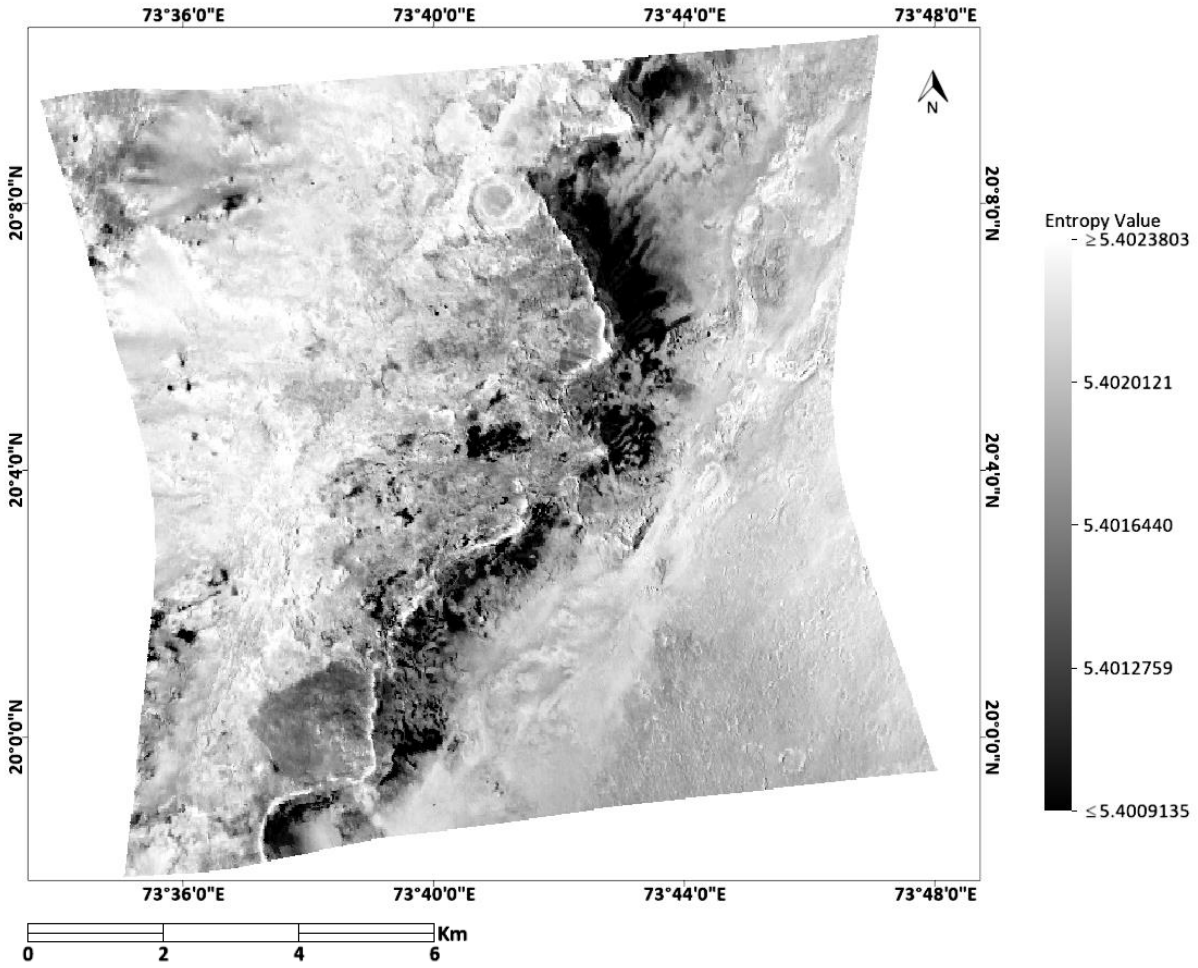

Figure 13. Entropy map of the Nili Fossae image (FRT00009D44) which shows entropy value ranging from 5.398967 to 5.402588.

The low entropy areas may represent different minerals as it is calculated from absorption features and not the wavelengths. To analyze the low entropy values, the low entropy values need to be separated into sections based on their location to see which minerals or occurences the low entropy values in that area represents. The low entropy areas are then separated by locations and calculated for its mean spectra. The result can be seen in Figure 14 where Figure 14a shows the entropy map overlain with the ROI of sections of the low entropy areas. Figure 14b shows the mean spectra of each section of the low entropy ROI. The color of the spectra represents the low entropy ROI corresponding to the color of the ROI.

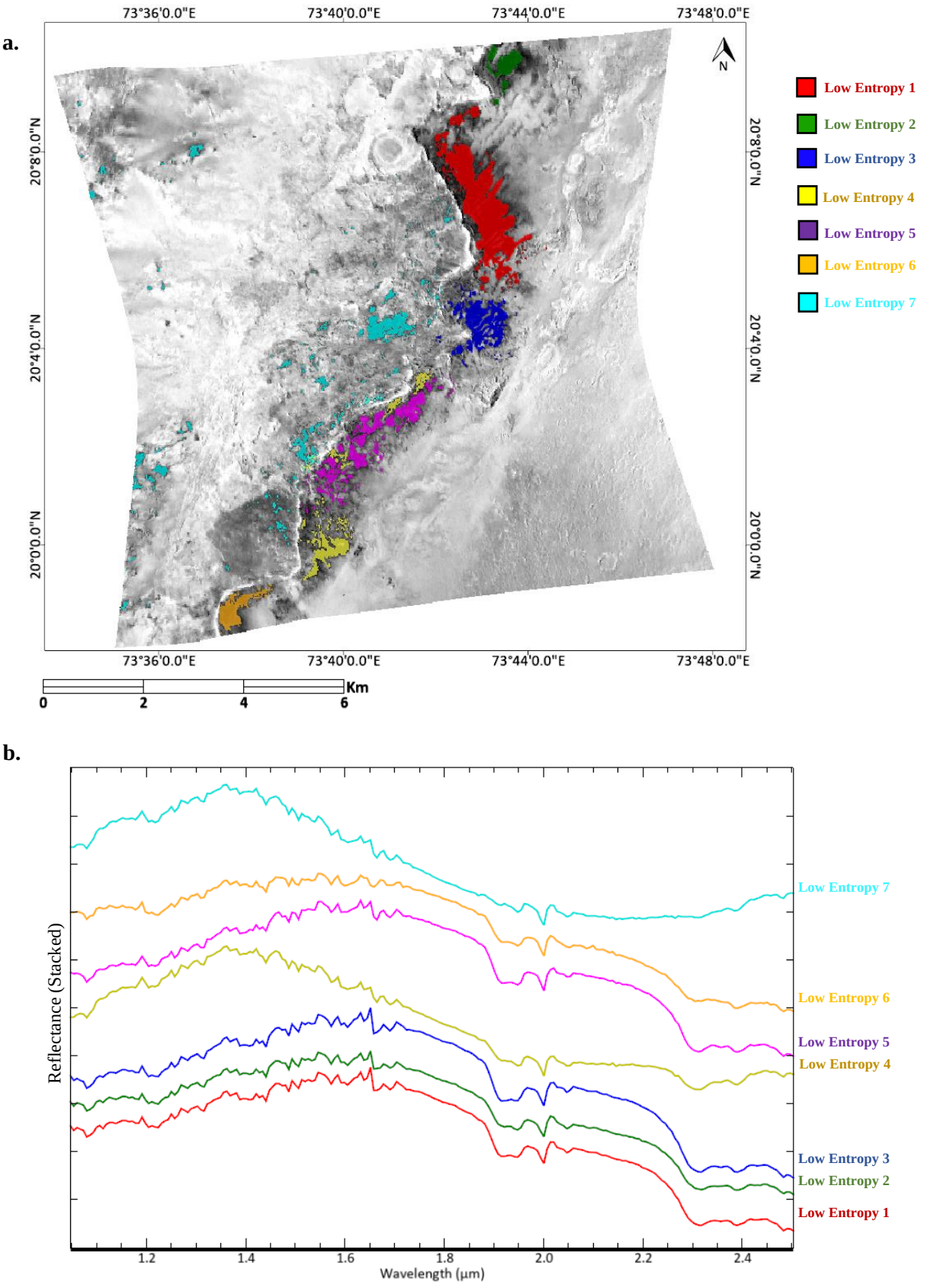

Figure 14. a.) Entropy map of the Nili Fossae research area with ROI sections of the low entropy and b.) the stacked mean spectra of each ROI corresponding with the colors.

Most of the low entropy value is located along the graben walls. Some low entropy patches are present in the surface of the horst. Based on the spectra in Figure 14b, it can be seen that the low entropy areas alongside the graben wall have similar absorption features (Low entropy 1 – Low entropy 6) located in the 2.30µm and 2.39µm which is an indication of Fe-Mg phyllosilicates. The low entropies in the graben walls also show absorption feature at 1.90µm which is a diagnostic feature of hydrated minerals.

Low entropy 7 has a broad absorption feature in the short-wave infrared, centered around the 2.00µm wavelength. The observed broad absorption feature may be an indication of low calcium pyroxene which has a broad absorption feature at 0.90µm and 2.00µm. There are also deep absorption features at 2.00µm which is caused by carbon dioxide in the atmosphere which has been already corrected and is the residue from the process of atmospheric correction.

3.3.1.3. Wavelength Map

From the spectra shown in Figure 14a, wavelength maps are then created to display the deepest absorption features throughout the image. Minerals can be identified by the wavelength location of absorption features. The wavelength map shown in Figure 15a uses the wavelength range of 2.10µm to 2.40µm to identify silicates in the short-wave infrared (SWIR) range due to the vibrational transitions, producing an absorption feature at 1.90µm (water) (Pontual, Merry, & Gamson, 1997). Digitization is done to map the minerals based on the color that represents the absorption feature. Figure 15a shows the orange color across the middle of the image. The orange color represents the deepest absorption feature that is located on the 2.30µm wavelength. Parts of the wavelength map also shows the color of cyan color, which represents the 2.20µm wavelength. The 2.30µm which is represented by the orange color could be a sign of the presence of carbonates or phyllosilicates, while the cyan color, located on the red circle in Figure 15a, represents the absorption feature of 2.20µm which may be an indication to the presence of kaolinite.

a.

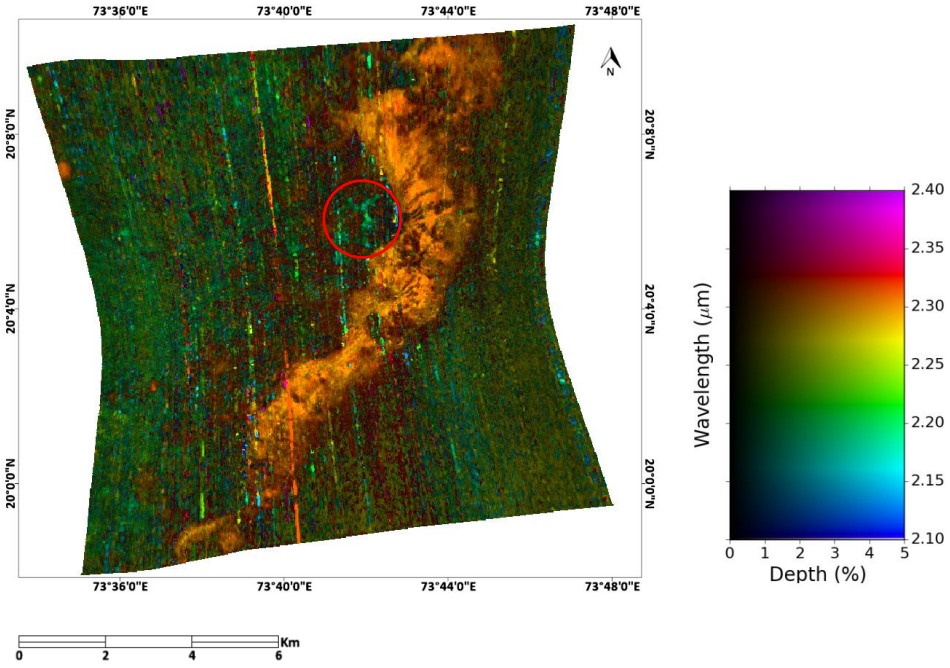

b.

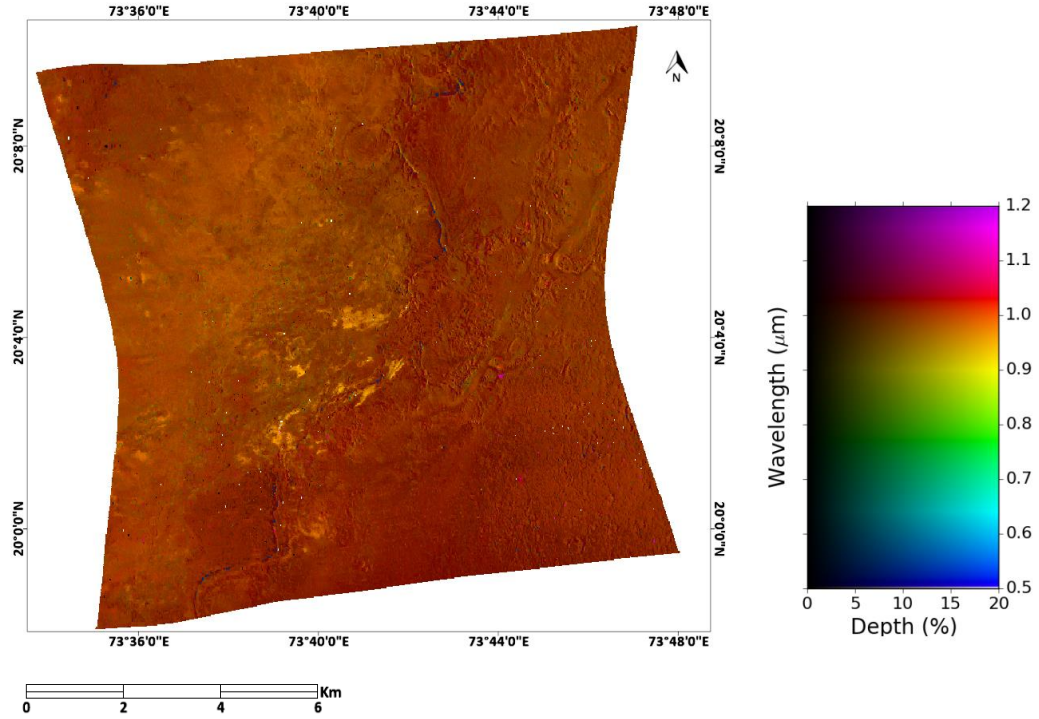

Figure 15. Wavelength map of the Nili Fossae research area showing; a) Wavelength map created using the wavelength range of 2.10µm to 2.40µm, highlighting areas with diagnostic features at the SWIR range and b) wavelength map created using wavelength range of 0.50µm to 1.20µm highlighting areas with diagnostic features at VNIR range.

Another wavelength map is created to identify rock-forming minerals occurring in the research area. A wavelength map with the wavelength range in the visible and near-infrared (VNIR), specifically using the range 0.50µm to 1.20µm with broad-feature fitting. Figure 15b shows the wavelength map created using the VNIR range. The wavelength map shows generally orange color, which represents the 1.0µm absorption feature. The 1.0µm absorption feature is a possible diagnostic feature of Olivine. Parts of the wavelength map shows a lighter orange color which represents the 0.9µm absorption feature and is an indication of iron. To further analyze the absorption features in the VNIR range, a broad-feature wavelength map is created using the wavelength range of 0.5µm to 2.5µm, to identify all the broad absorption features on the full wavelength range. The resulting broad-feature wavelength map is shown in Figure 16. Using the broad-feature wavelength map, the cyan color in Figure 16 represents the deepest absorption feature at around 0.90µm, which when compared with the wavelength map in the VNIR range shown in Figure 15b, shows similar locations of the 0.9µm absorption feature.

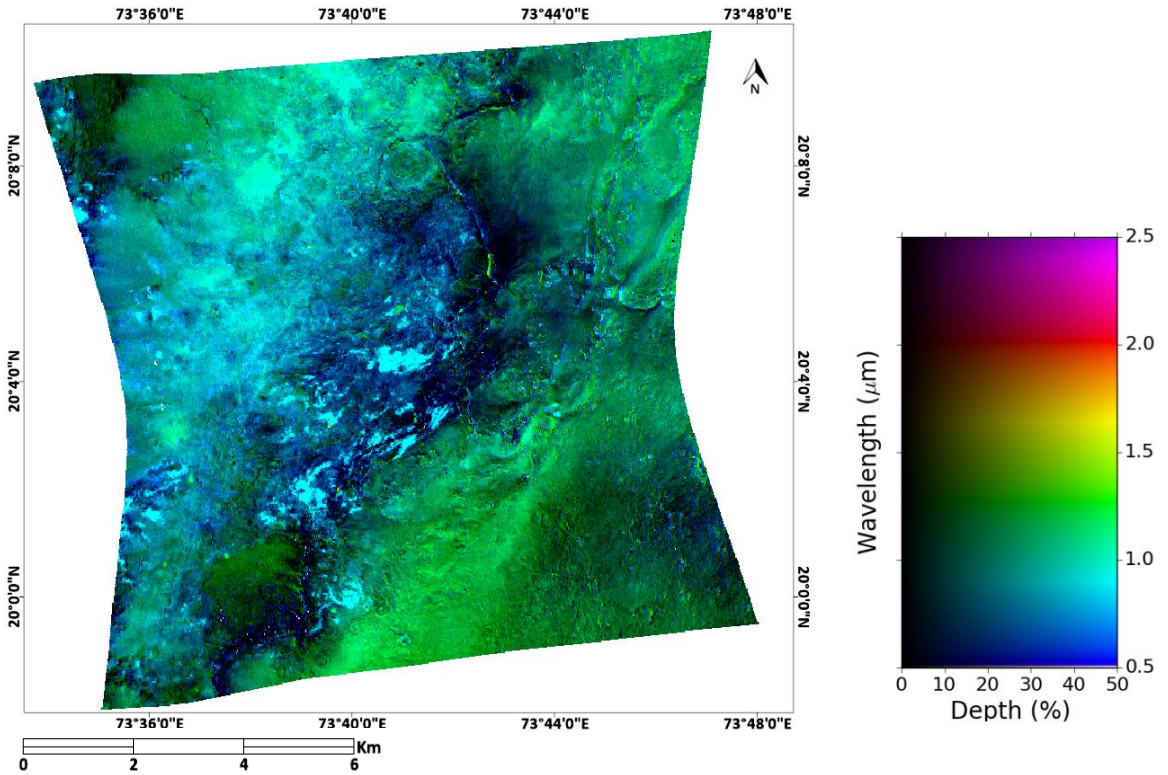

Figure 16. Wavelength map of the CRISM Nili Fossae image using broad-feature fitting and a wavelength range of 0.5µm to 2.5µm to identify broad absorption features.

3.3.1.4. Summary Product Maps

The summary product maps are created in this research to indicate areas that may show diagnostic features of certain minerals. The summary product maps are in an index format, showing high index values where there are spectral indication of certain minerals or mineral overtones. For the CRISM Nili Fossae image, the index created are the BD2290, BDCARB, and the LCPINDEX, based on mineral indications proposed from past studies (Mustard et al., 2009).

The research area has been shown to have absorption features at around 2.3µm which may be an indication of carbonates or phyllosilicates. Further analysis is needed to differentiate whether the 2.3µm is an indication of carbonates or phyllosilicates.

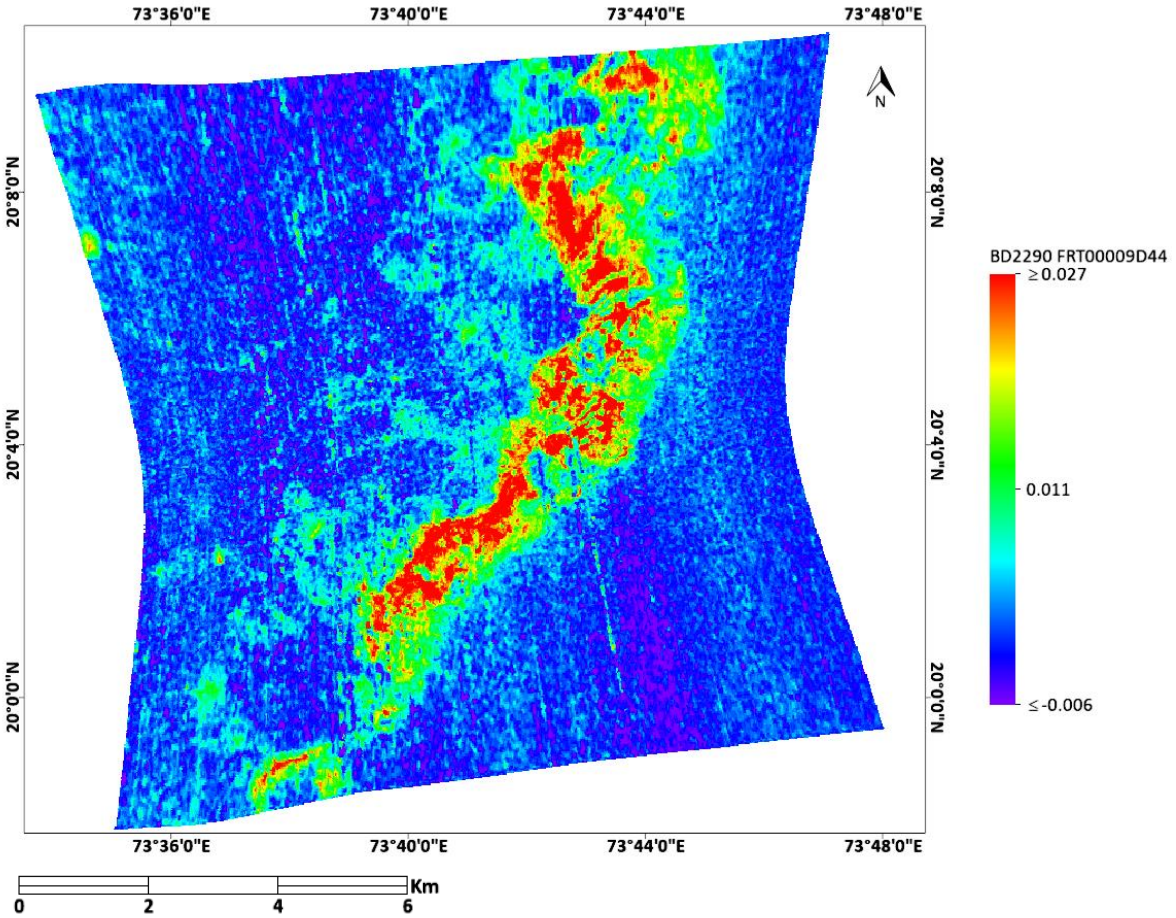

Figure 17. BD2290 summary product of the CRISM Nili Fossae image, which indicates Fe-Mg minerals, where the absorption features at the SWIR range is at 2.29µm (Pelkey et al., 2007a).

Figure 17 shows the locations where there are deep absorption features in the 2290nm wavelength range (BD2290) based on calculations from Pelkey et al., 2007. Figure 17 is created using the hyperspectral image of the CRISM Nili Fossae research area. The BD2290 summary product index shows areas where Mg Fe-OH minerals are present, where absorption features at 2290nm has a high index value and is represented by green to red color. The index is calculated with the formula as shown in Table 1.

The Mg Fe-OH minerals with a higher index value than 0.011 is located on the middle of the research area, following the graben walls. Along the graben walls, based on the wavelength map created from 2.10µm to 2.4µm (Figure 15a), it is evident that there is absorption feature at around 2.30µm which is a diagnostic feature of carbonate or Mg.Fe-OH minerals.

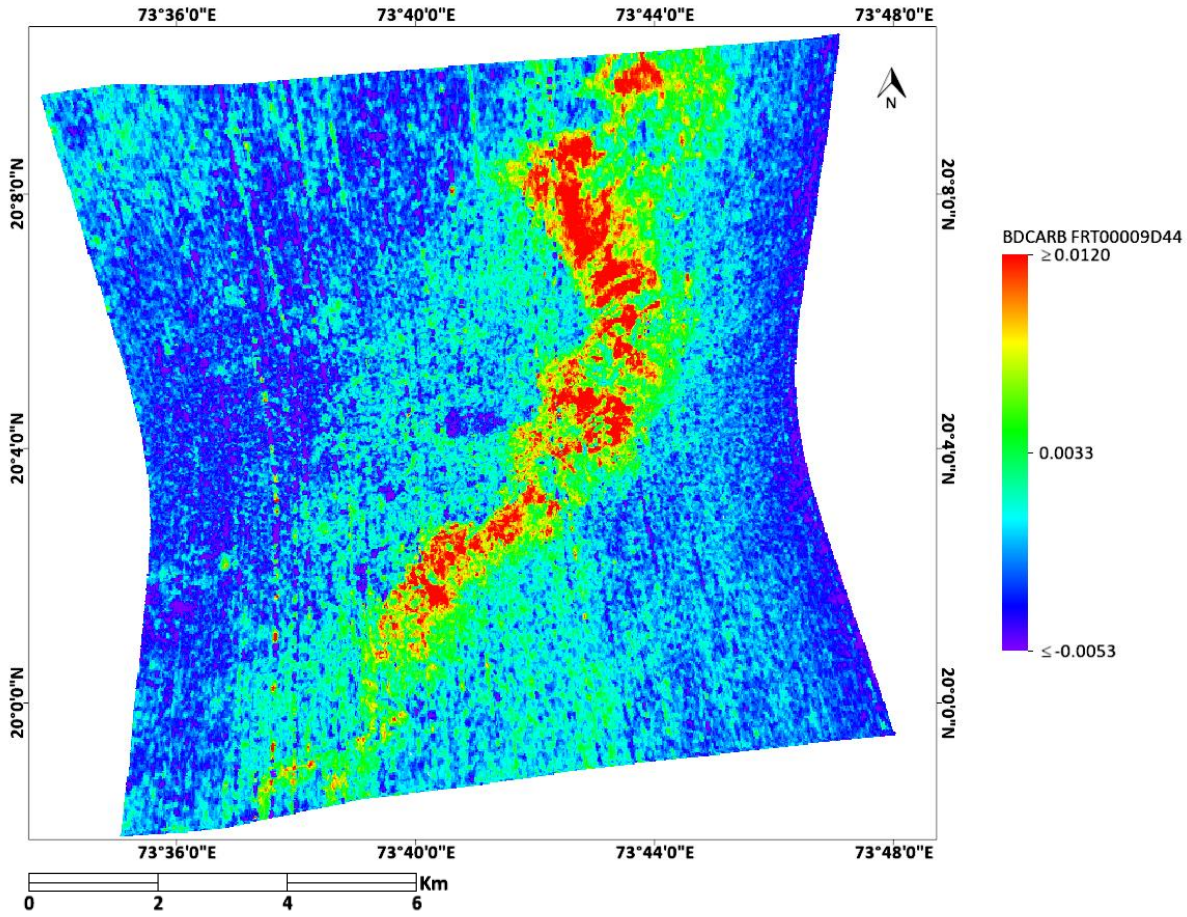

Figure 18. BDCARB summary product of the CRISM Nili Fossae image, which indicates carbonate overtones, highlighting locations where absorption features at the SWIR range is at 2.33μm (Pelkey et al., 2007a).

Figure *18* shows the locations of carbonate overtones based on the calculations from Pelkey et al., 2007 (BDCARB). The formula highlights the locations of carbonate overtones, where spectral features similar to when the vibrational spectrum of carbonate molecules transitions from a ground to an excited state (Gaffey, 1986), showing high index values. The index value is determined using the absorption feature at 2.33μm. Similar to the BD2290 index (Figure 17), the locations of the supposed carbonates are following the graben walls, in the middle of the research area. The BDCARB index formula is shown in Table 1.

The research area shows signs of low calcium pyroxene (LCP) appearing due to the broad absorption feature at the 900nm wavelength shown in Figure 15b and Figure 16. To further validate the claim of the presence of LCP in the Nili Fossae image, an LCP index map is created using the formula by Pelkey et al., 2007 (LCPINDEX). The index can be seen in Figure 19 where the location of the LCP is represented by the red color of the index. The location of the LCP matches with the broad feature wavelength map shown in Figure 15b and Figure 16 where it indicates the absorption feature at 900nm. The LCPINDEX summary product formula is shown in Table 1.

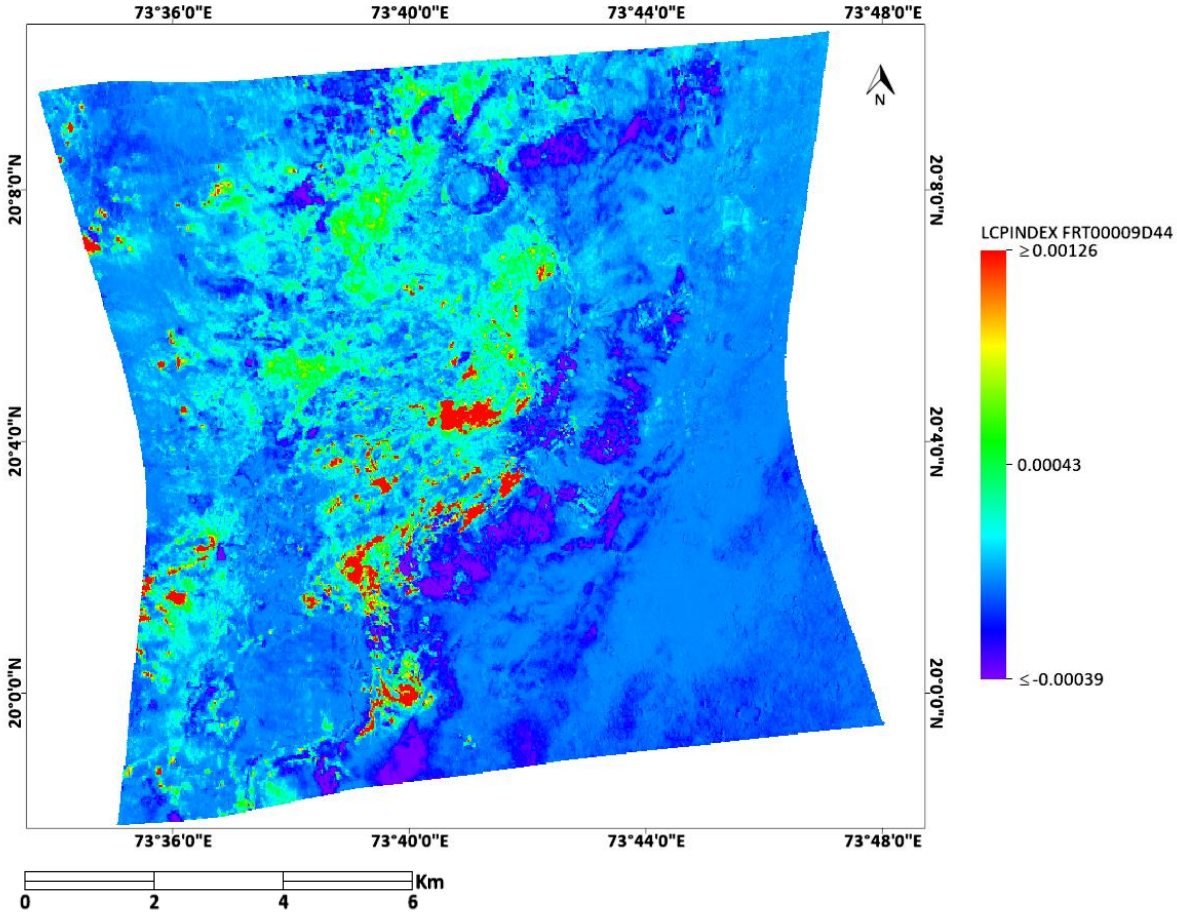

Figure 19. LCPINDEX summary product of the Nili Fossae CRISM image, which indicates the locations of low calcium pyroxene with a high index value (Pelkey et al., 2007a).

3.3.1.5. Log-residuals

The log-residual method is conducted to remove systematic errors from the image, which will help in identifying whether the 2.30µm absorption feature present in the Nili Fossae research area is carbonates or Fe-Mg phyllosilicates. If the 2.30µm absorption feature is indeed Fe-Mg phyllosilicate, then there will be a hydration feature at the 1.40µm. The 1.40µm is currently hidden in the systematic noises, with log-residuals, the 1.40µm absorption feature will be visible if it is present. The output of the log-residual method can be seen in the green spectra of Figure 20, where green spectra is created from the mean spectra of the red ROI on the map. The blue spectrum shows the mean spectrum of the red ROI without the log-residual method. Visually, we can already see the difference between the spectra.

The green spectrum shows reduced absorption at 2.00µm, which was caused by the presence of carbon dioxide in the research area. The green spectra now show a deeper absorption of the hydration band 1.90µm, which is further indication clay minerals present in the ROI. Both the blue and green spectra show absorption feature at the 2.31µm and a smaller absorption feature at the 2.40µm wavelength range.

The log-residual is conducted to combat the excessive noise in the wavelength range below 1.70µm, as can be seen in the blue spectrum. The resulting spectrum, which is the green spectrum, has reduced the noises below 1.70µm and shows a new feature that was hidden in the noise. The 1.40µm hydration band can now be seen in the green spectrum, which is an indication of clay minerals.

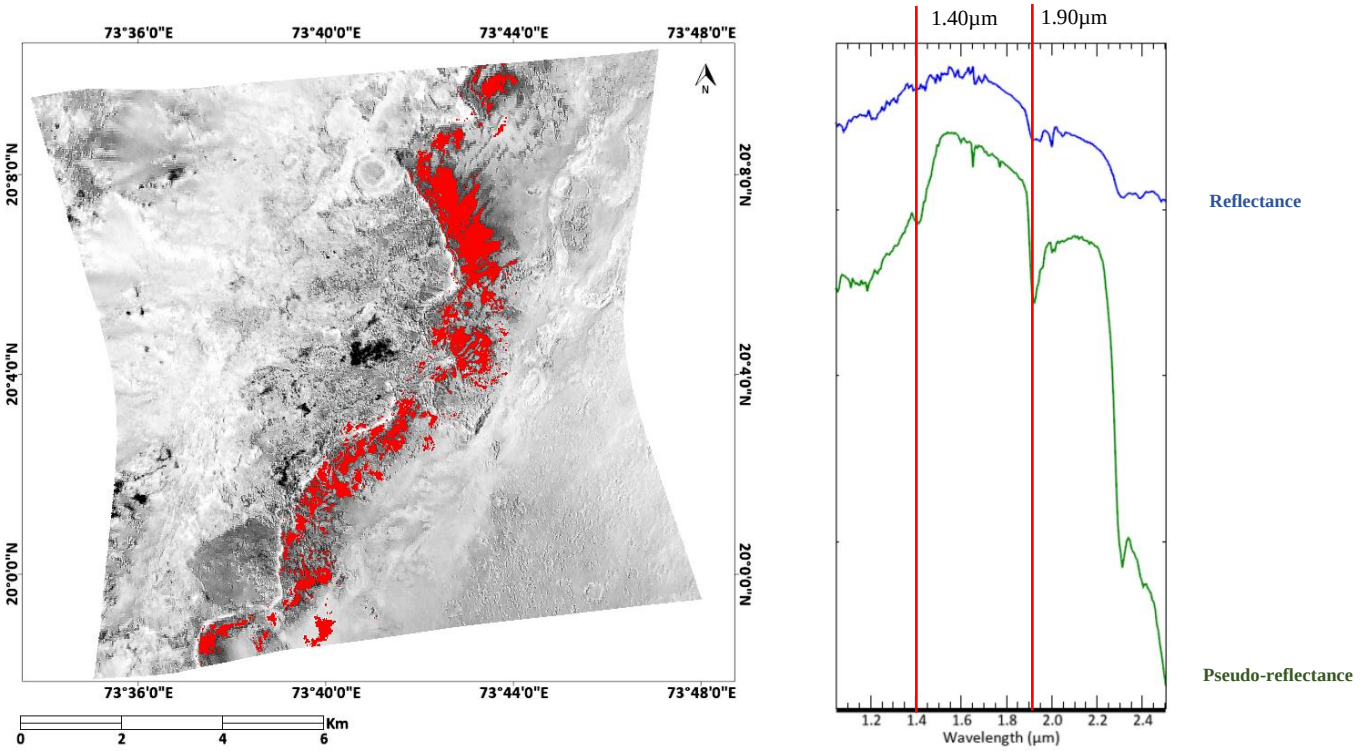

Figure 20. Mean spectra of the log-residual output across the graben wall of the CRISM Nili Fossae image. The spectra (right) show the mean spectrum of the ROI shown on the map (left). The blue spectrum shows the original spectrum with reflectance, the green spectrum shows the output of the log-residual method, creating a pseudo-reflectance with reduced systematic noise.

3.3.1.6. Mineral Map

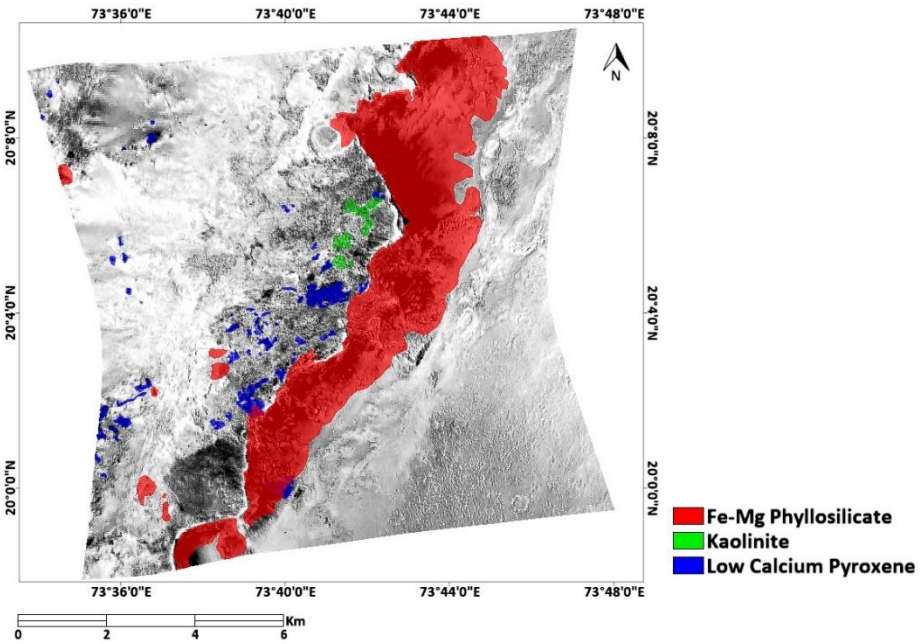

Figure 21. Mineral map of the CRISM Nili Fossae image, showing locations of the mineral Fe-Mg phyllosilicates (Red), kaolinite (Green), and low calcium pyroxene (Blue) overlain in the entropy map.

Using the wavelength map and the summary products map, the minerals present in the CRISM Nili Fossae image is mapped and is shown in Figure 21. Figure 22 shows the mean spectra of each mineral and is continuum removed, to compliment the absorption feature of the spectra.

The most prominent mineral in the research area is the Fe-Mg phyllosilicate which shows the absorption features at 2.30µm. The CRISM Spectral Library (Viviano-Beck et al., 2014) shows that the red areas in Figure 21, depicted to be Fe-Mg phyllosilicate, shows absorption features similar to saponite. The spectra show absorption features at 1.915µm which is the hydration band, and diagnostic saponite absorptions at 2.318µm and 2.390µm, which can be seen in Figure 22a. The 1.40µm feature is seen in the pseudo-reflectance spectra in Figure 20.

The 2.318µm feature shifts from 2.27µm to 2.32µm depending on the richness of Fe or Mg, where the absorption feature will shift to 2.27µm if it is Fe-rich, and shifts to the 2.32µm if it is more Mg-rich (Michalski et al., 2015). This suggests that the saponite present in the Nili Fossae research area has a richer Mg composition. From the wavelength map in Figure 15b and Figure 16, alongside the summary product of the LCP index (Figure 19), the locations of low calcium pyroxene of the Nili Fossae research area can be mapped. The broad diagnostic absorption feature of low calcium pyroxene can be seen in the 2.00µm wavelength range. Figure 22b shows the mean spectra of the low calcium pyroxene in the CRISM Nili Fossae research area, compared with the spectra taken from the CRISM spectral library (Viviano-Beck et al., 2014), coded C1SB01.

The 2.20µm absorption feature present in the Nili Fossae research area, shown in Figure 15, is an indication to the presence of kaolinite. The spectra of the indicated kaolinite mineral can be seen in Figure 22c, alongside the spectra of the kaolinite from the CRISM spectral library, coded CBJB25. The triple diagnostic feature of kaolinite at around 2.312µm, 2.350µm, and 2.380µm, which persists even in mixtures, shows in the spectra in Figure 22c. This indicates that the green area in the mineral map may represent kaolinite.

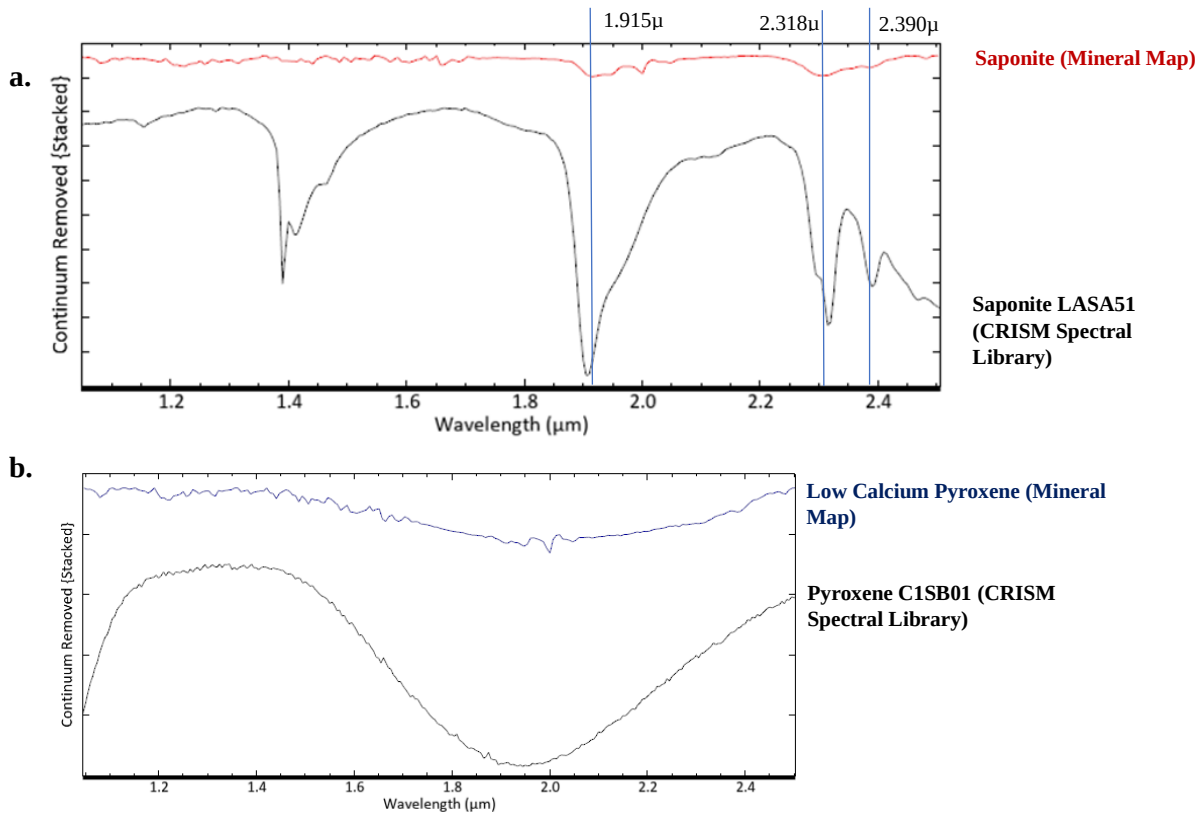

c.

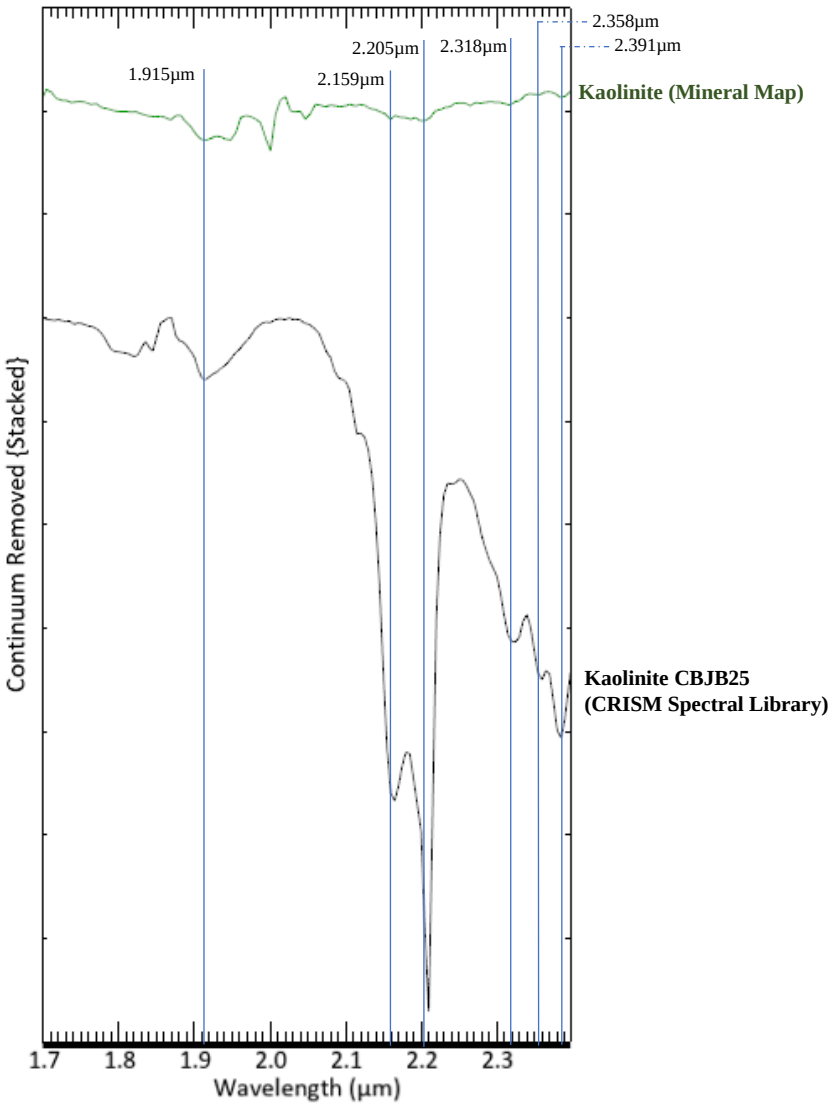

Figure 22. Mean spectra of the minerals indicated in the mineral map of the Nili Fossae research area, showing the spectra of the mineral Fe-Mg phyllosilicates (a.), low calcium pyroxene (b.), and kaolinite (c.). Each spectra is continuum removed and shown with comparison to the spectra from the CRISM spectral library.

3.3.2. Jezero Crater Research Area

The CRISM image of the Jezero Crater research area is labeled as FRT00005C5E, located South-East of the Nili Fossae research area, on the edge of the Isidis Basin. The center of the Jezero Crater research area is at The location of the Jezero Crater research area can be seen in Figure 23. Previous research (Goudge, Mustard, Head, Fassett, & Wiseman, 2015) suggested that the crater shows signs of Fe-Mg smectites, Mg-rich carbonates, and olivines. The red stripe on the CRISM Jezero Crater image is a mask used to exclude the area due to systematic error.

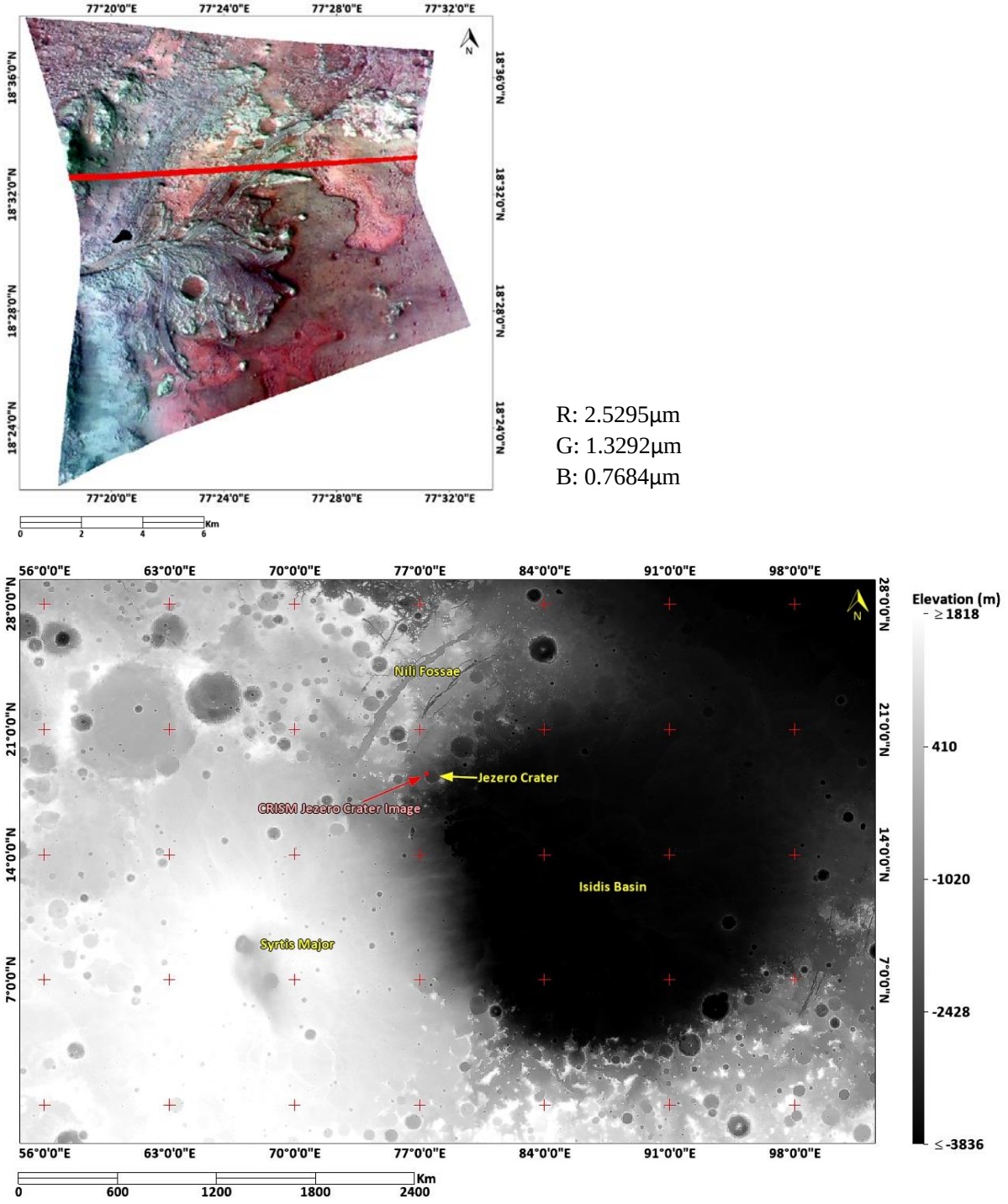

Figure 23. The CRISM Jezero Crater image, located on the edge of the Isidis Basin.

3.3.2.1. Geological Structure

The prominent geological structure of the Jezero Crater research area is the delta fan (Goudge, Milliken, Head, Mustard, & Fassett, 2017) located on the center to west side of the CRISM Jezero Crater image. The delta fan has been impacted by a crater named the Belva Crater (Sun & Stack, 2020), alongside many other small impact crater sites in throughout the image. Figure 24 shows the CRISM Jezero Crater image with the outlined geological structure. The research area also shows part of the fluvial channel which was the source of the delta fan deposits of the West part of the image, connecting with the delta fan.

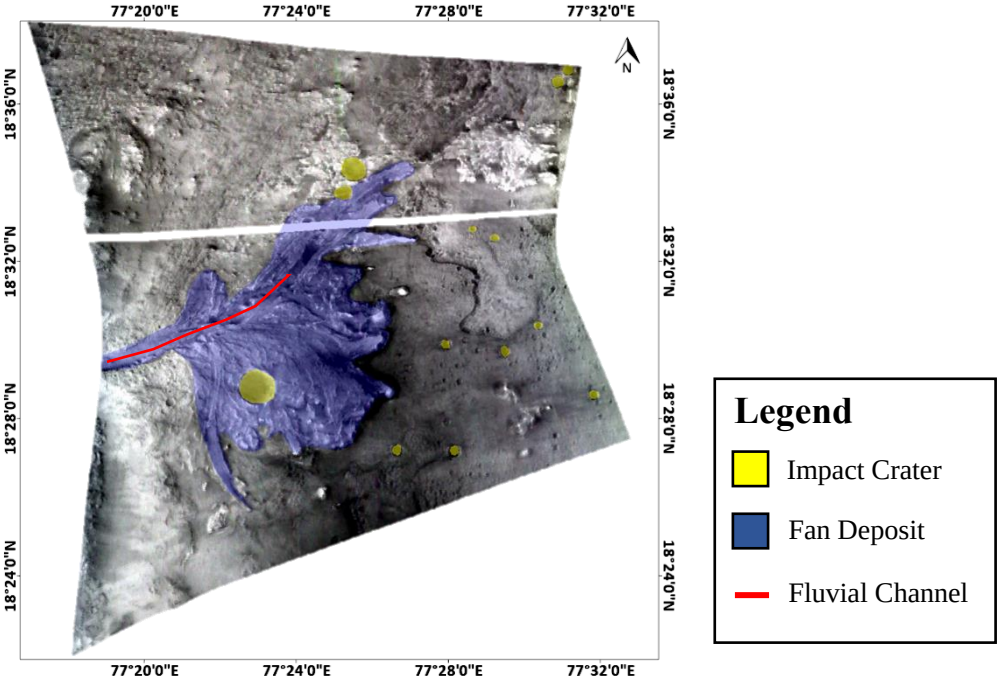

Figure 24. The geological structure of the CRISM Jezero Crater image

3.3.2.2. Entropy Map

The entropy map of the CRISM Jezero Crater image was created using the wavelength range of 1.0μm to 2.5μm. The entropy map of the image can be seen in Figure 25 and has an entropy value ranging from 5.400989 to 5.402593 and a mean of 5.402309. The entropy map uses the Linear 5% stretch which sets the color of the bottom 5% of the histogram as 0 and the top 5% of the histogram as white. There are multiple areas with low entropy values, the most prominent one is the low entropy patch in the west side of the image, shown as low entropy ROI 1 in Figure 26.

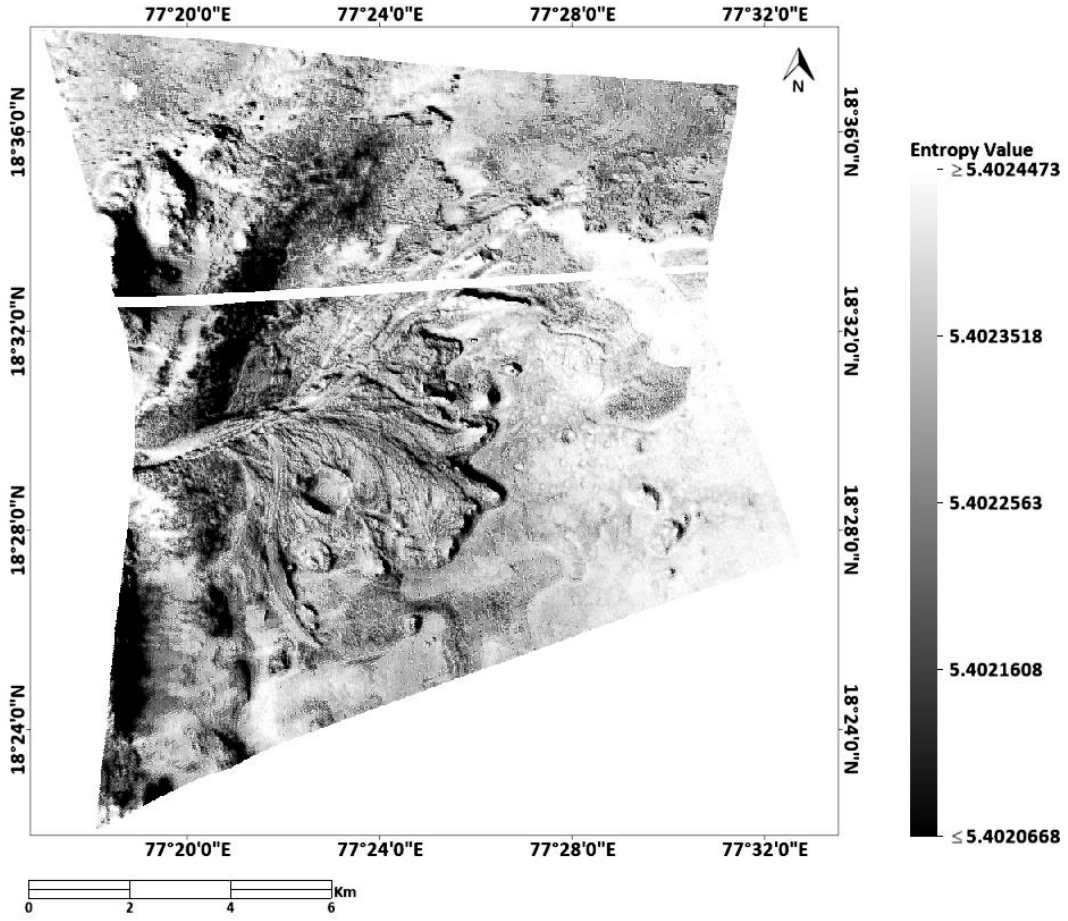

Figure 25. CRISM instrument entropy map of the CRISM Jezero Crater image with entropy values ranging from 5.400989 to 5.402593 using a linear 5% stretch.

The low entropy values are divided, based on their location, into areas which can be seen in Figure 26 alongside the mean spectra of each area. The spectra show absorption features in the 1.90μm and 2.05μm which are spread out throughout the research area. The 2.05μm is caused by the carbon dioxide in the atmosphere that has already been reduced during atmospheric correction.

The delta fan low entropy areas are represented by the ROI low entropy 2. Figure 26 also shows that the low entropy 1 ROI shows a deeper absorption feature at the 2.30μm range, which is an indication of either carbonate or Fe-Mg Phyllosilicate. Low entropy 1 ROI also shows a deeper broad absorption feature near the 1.00μm which is a possible indication of olivine.

Figure 26b also shows the high entropy ROI spectra which is sampled from the Eastern side of the research area, to be used as a comparison. The high entropy spectra, compared to the low entropy spectra, shows a more invariant absorption features, which caused the high entropy value. Compared with the high entropy value ROI, the low entropy ROIs have a steeper slope from the 2.10μm and beyond, shown in Figure 26b.

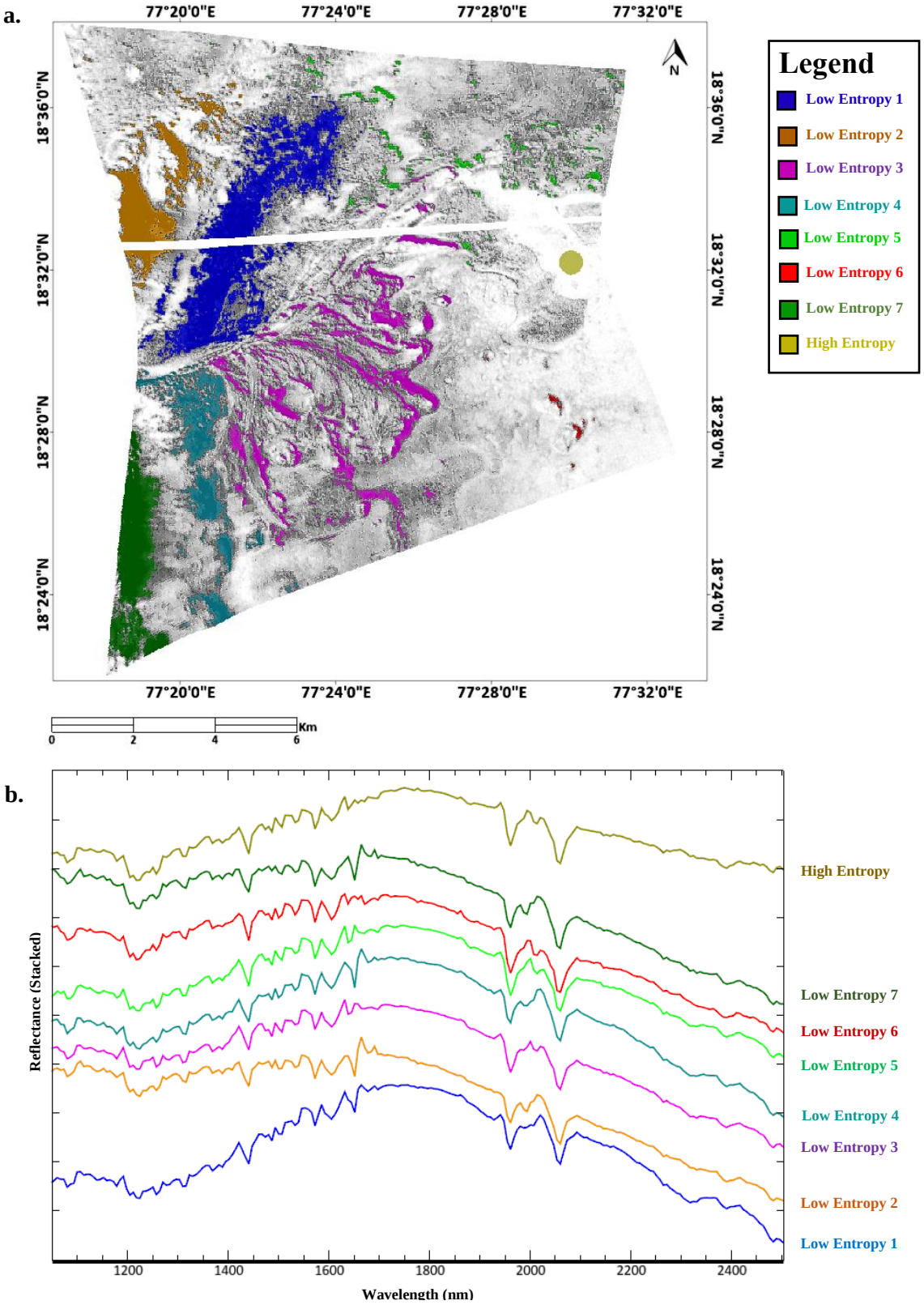

Figure 26. a.) Entropy map of the CRISM Jezero Crater image with ROI sections of the low entropy and b.) the stacked mean spectra of each ROI corresponding with the colours.

3.3.2.3. Wavelength Map

The wavelength map shows the deepest absorption feature of the spectra represented by the color. The orange color in Figure 27 shows the deepest absorption feature at around 2.30µm, which is an indication of either carbonates or Fe-Mg phyllosilicates. The wavelength map shows that the delta fan of the research area is covered by orange colors that represents absorption at 2.30µm, alongside the noticeable large area of orange color North of the delta fan. This suggests that there are deposits of Fe-Mg phyllosilicate or carbonates in the delta fan of the research area. The green color of the wavelength map represents the deepest absorption feature at 2.20µm. The wavelength map also shows heavy striping spread throughout the image, caused by non-uniformities among input and output characteristics of matrix sensors (Ceamanos & Douté, 2010).

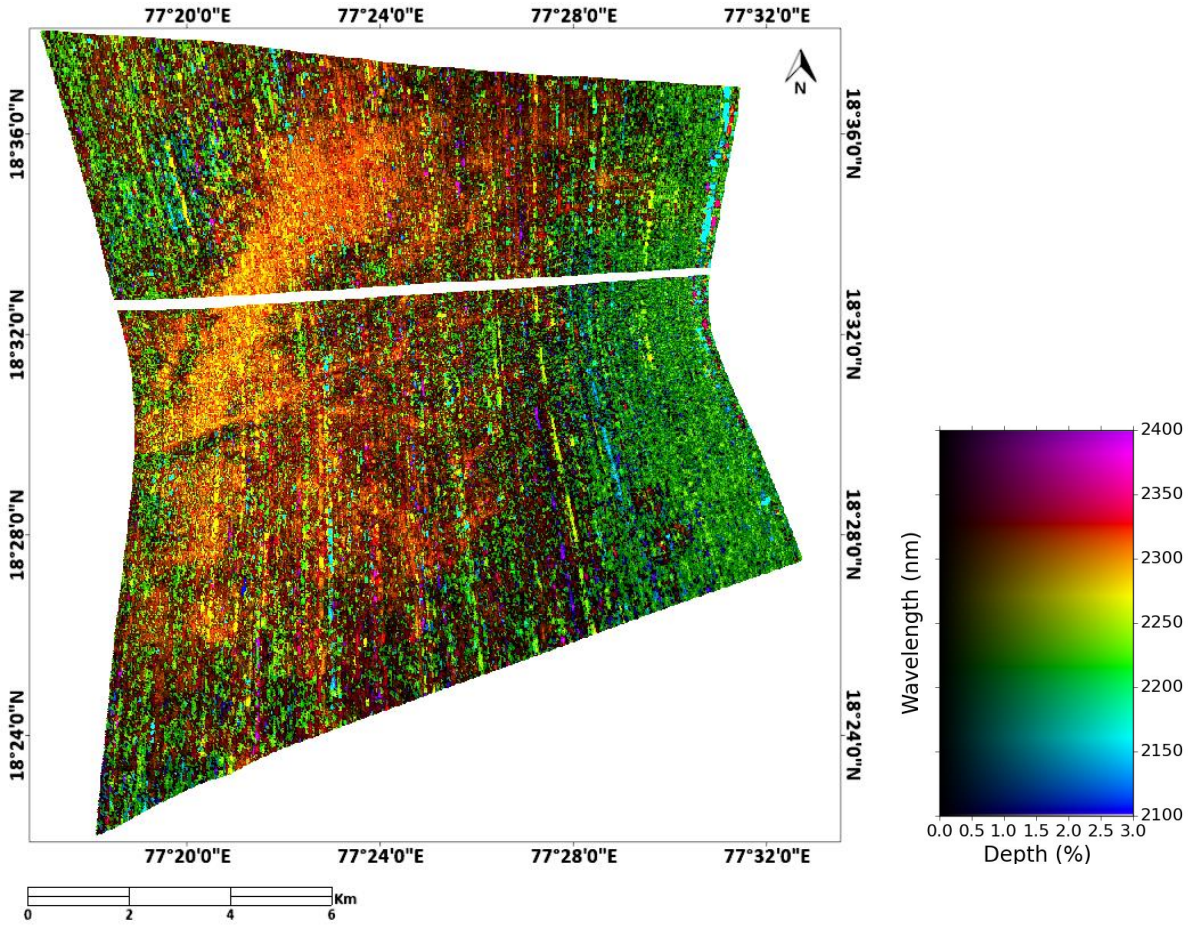

Figure 27. Wavelength map of the CRISM Jezero Crater image showing the deepest absorption features with the wavelength range of 2.10µm to 2.40µm.

3.3.2.4. Summary Product Maps

The summary product maps are created to indicate areas that shows certain types of minerals. Past studies (Horgan, Anderson, Dromart, Amador, & Rice, 2020) have shown that in the Jezero Crater, there are indication of the presence of carbonates, Fe-Mg phyllosilicates, and olivine. Hence the summary product maps created are the BD2290, BDCARB, and OLINDEX index.

Based on the wavelength map, which indicates that there may be Fe-Mg phyllosilicates or carbonates in the area, a BD2290 summary product is created by me to identify areas that shows features of Fe-Mg phyllosilicates. Similar to the wavelength map in Figure 27, the BD2290 (Figure 28) shows the highest index value is located north of the delta fan. The BD2290 summary product is shown in a linear 5% stretch, which shows the top 5% of the histogram as red, and bottom 5% of the histogram as purple. Red-colored patches are also present in the delta fan as well as east of the delta fan. The index is calculated with the formula as shown in Table 1.

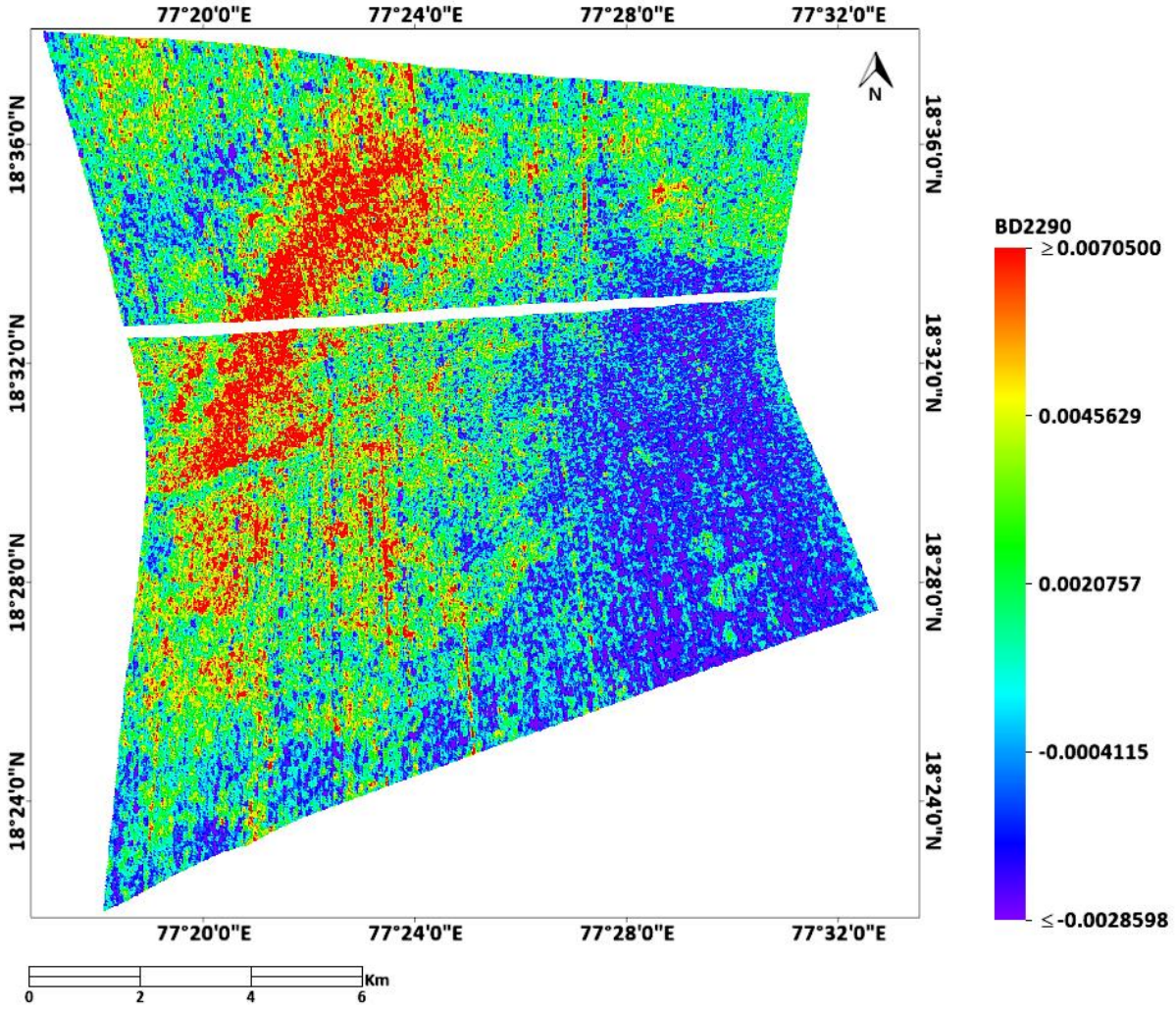

Figure 28. BD2290 summary product of the Jezero Crater research area, which indicates Mg. Fe-OH minerals, where the absorption features at the SWIR range is at 2.29μm (Pelkey et al., 2007a).

Previous researchers (Horgan et al., 2020) have indicated that there are signs of carbonates in the research area, which is backed by the large areas of orange colour in the wavelength map (Figure 27) that represents absorption features at 2.30μm. The BDCARB index, which is shown in Figure 29, shows areas with absorption features at 2.33μm that indicates the presence of carbonates. The BDCARB index map shown in Figure 29, is displayed in a linear 5% stretch. The BDCARB index shows similar pattern

as the BD2290 index map in Figure 28, where most of the high value is located north of the delta fan. Similar to the BD2290 index map, the BDCARB index map also shows red-colored patches in the delta fan and east of the delta fan. The BDCARB index uses the formula shown in Table 1.

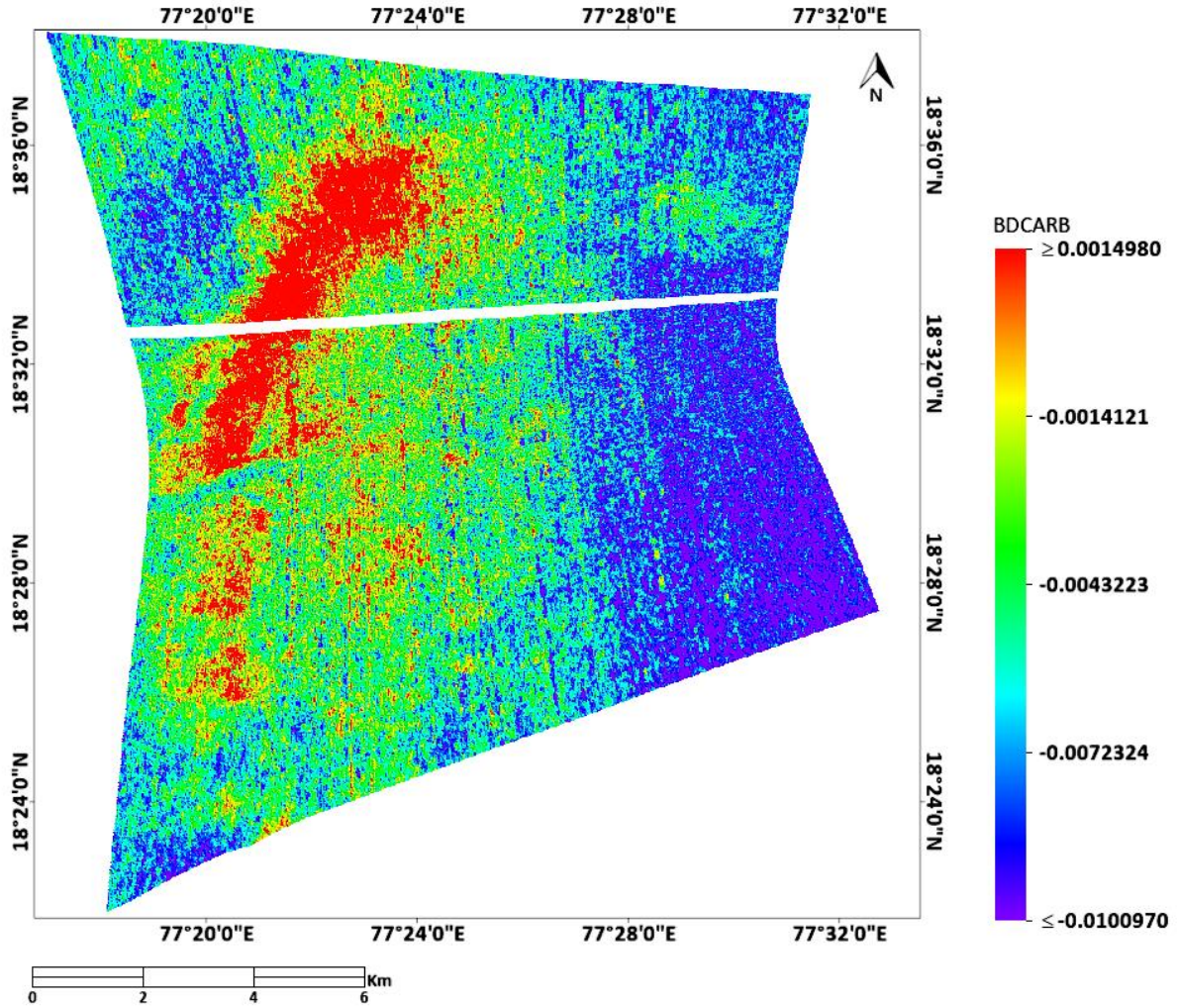

Figure 29. BDCARB summary product of the CRISM Jezero Crater image, which indicates carbonate overtones, highlighting locations where the absorption features at the SWIR range is at 2.33μm and 2.53μm (Pelkey et al., 2007a).

Past researchers (Horgan et al., 2020) also suggested that there are indications of olivine present in the area, specifically in the areas north, east, and south of the delta fan. The locations that indicate the presence of olivine can be seen in Figure 30. The OLINDEX index map is shown in a linear 1% stretch, because based on Pelkey et al., 2007b, indications of olivine will yield a high index value. From comparing Figure 29 and Figure 30, some of the olivine is located in similar locations with the high BDCARB index value. There are also high value patches of the OLINDEX index south of the delta fan. The delta fan itself shows little to no signs of high value index of the OLINDEX index. The OLINDEX index uses the formula shown in Table 1.

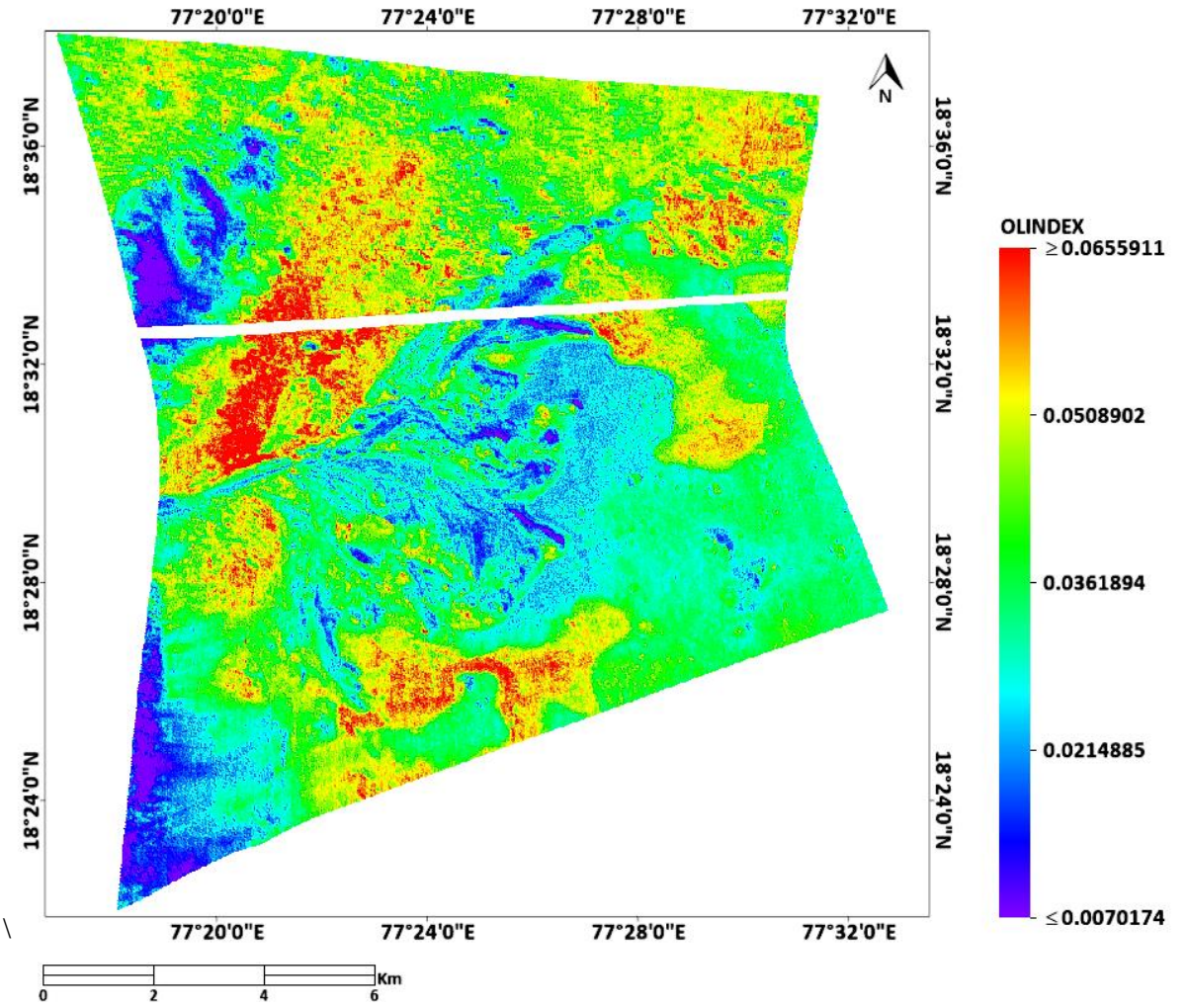

Figure 30. OLINDEX summary product of the CRISM Jezero Crater image, which high index value indicates the presence of olivine.

3.3.2.5. Log-residuals

Fe-Mg phyllosilicates will show absorption features at the 1.40µm, because of hydration band in clay minerals. Log-residual is conducted to apply normalization of the image, helping to analyse the spectra below 1.70µm. Figure 31 shows the ROI created where the deepest absorption feature is at 2.30µm, which may be an indication of Fe-Mg phyllosilicates. The mean spectra of the ROI can be seen in Figure 31, represented by the red spectrum. The spectra show absorption features at 2.30µm and also an absorption feature at around 2.40µm, which may be an indication of Fe-Mg phyllosilicates. Through log-residual, systematic noise in the wavelength range below 1.70µm is reduced. The output spectra of the 2.30µm deepest absorption feature ROI of the log-residual method can be seen in Figure 31, represented by the black-coloured spectra. The pseudo-reflectance spectra created through log-residual does not show 1.40µm absorption feature, and the feature at 2.40µm feature is also gone. The absence of the hydration band absorption feature at 1.40µm suggests that the deep absorption feature at 2.30µm, represented by the orange colour in the wavelength map shown in Figure 27, is an indication of carbonates and not Fe-Mg phyllosilicates. From the pseudo-reflectance spectrum in Figure 31, absorption feature at 1.30µm is seen, which is an Fe^{2+} bands. The RLUB of the CRISM Jezero Crater image can be seen in Appendix 2.

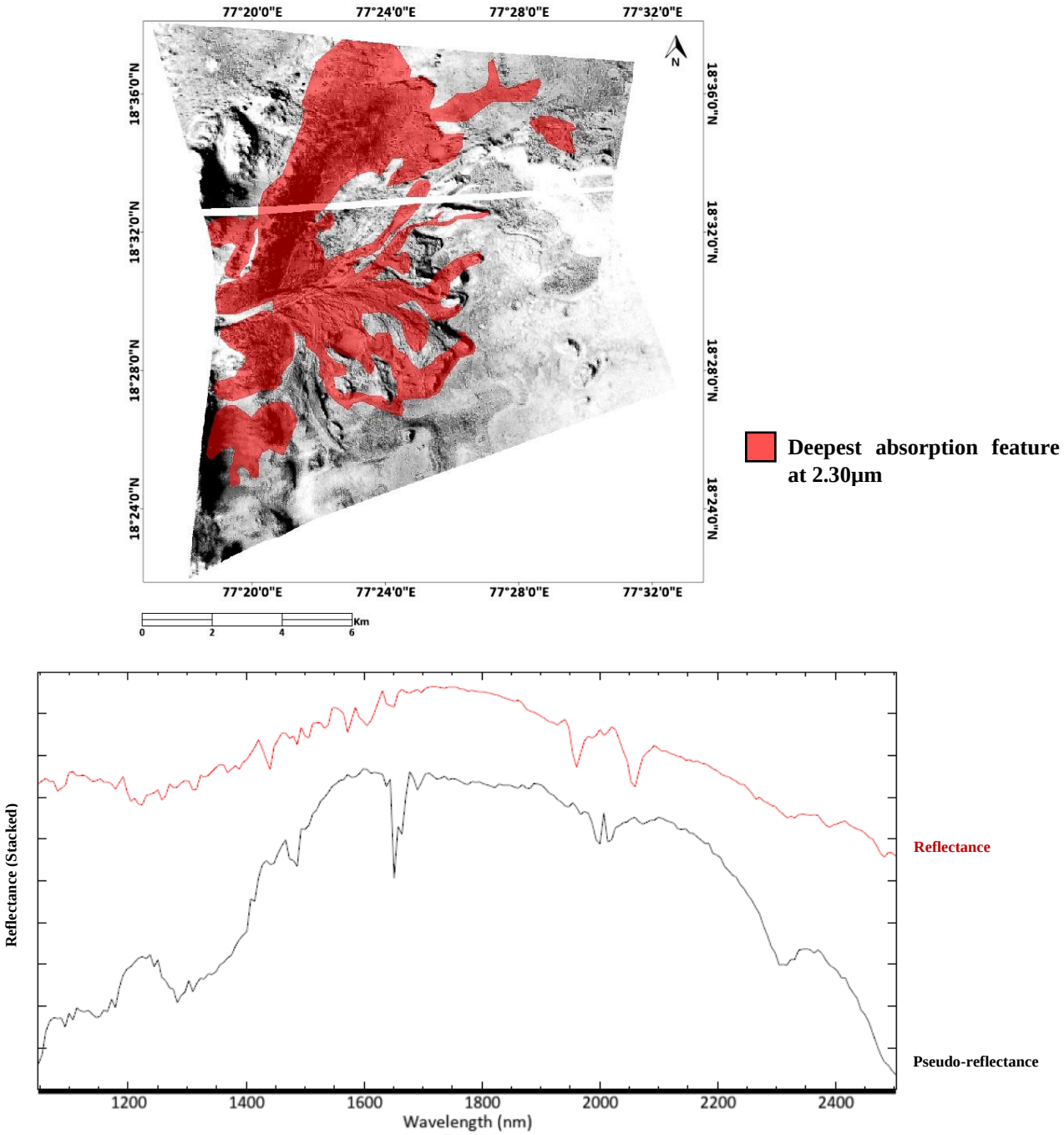

Figure 31. ROI of the 2.30µm absorption feature from the wavelength map overlain on the entropy map of the CRISM Jezero Crater image. The red spectra show the mean spectrum of the red ROI shown on the entropy map. The black spectrum shows the mean spectral output of the log-residual method of the red ROI.

3.3.2.6. Mineral Map

The minerals present in the Jezero Crater area is mostly mapped from the absorption feature at 2.30µm that is an indication of carbonates, and from the OLINDEX summary product. The mineral map of the Jezero crater research area can be seen in Figure 32, where the locations of carbonates can be seen through the blue ROI. The mineral map is based on the wavelength map in Figure 27 that shows the locations where the deepest absorption features is located at the wavelength of 2.30µm. The summary product map, specifically the BDCARB index, also supports the mineral map as it shows similar locations of the carbonate overtones. The BDCARB index can be seen in Figure 29. The spectra of the

carbonates in the Jezero Crater research area can be seen in Figure 31, alongside the pseudo-reflectance spectra. The pseudo-reflectance spectra in Figure 31 shows that there is absence of 1.40µm absorption feature, which would distinguish the carbonates from the Fe-Mg phyllosilicates. The olivine in the mineral map is mapped by creating a threshold for the highest index value of the OLINDEX summary product in Figure 30. In Figure 32, parts of the image show a mixture of olivine and carbonates.

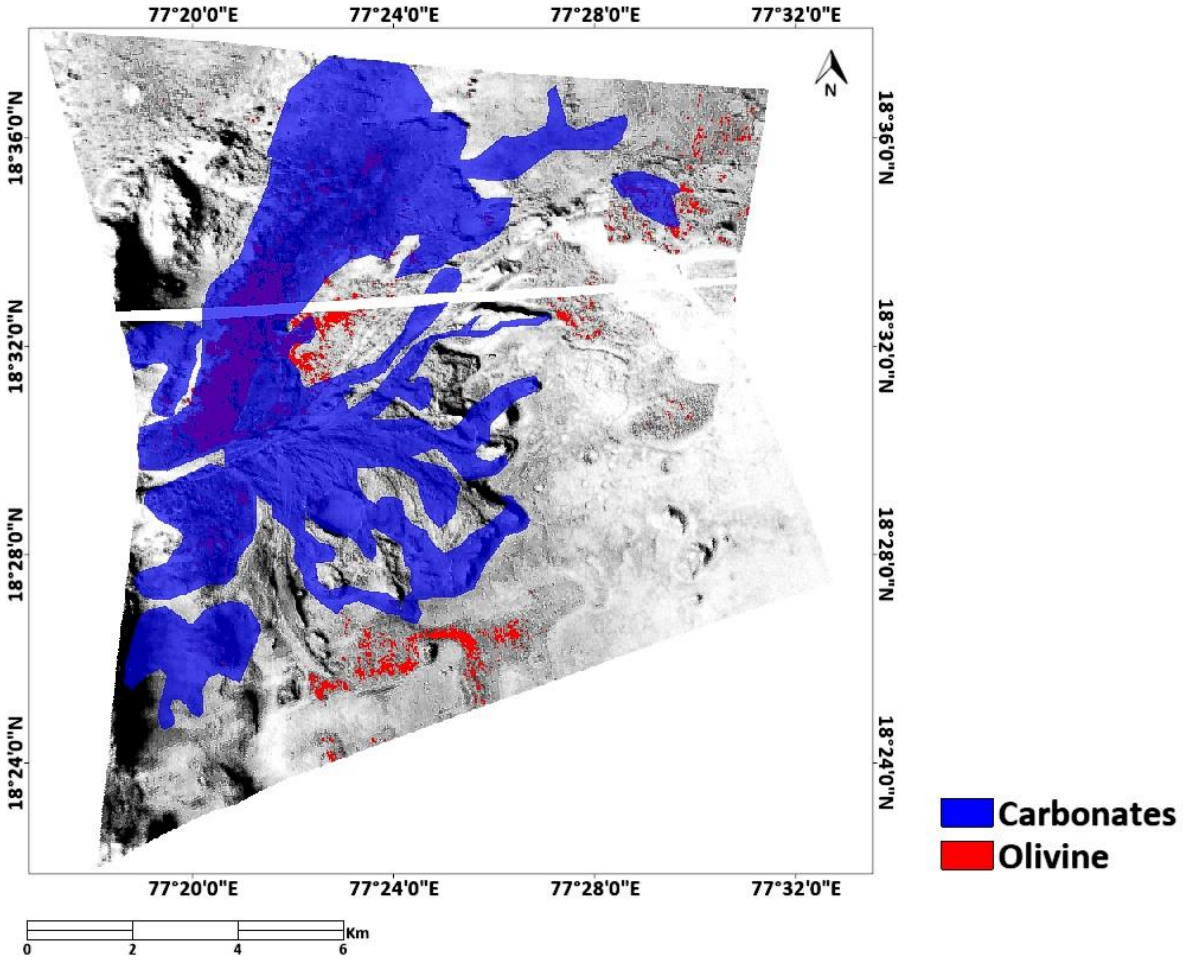

Figure 32. Mineral map of the CRISM Nili Fossae image, showing locations of carbonates (blue) based on wavelength map, BDCARB index, and olivine (red) based on the OLINDEX index.

3.4. OMEGA Images

3.4.1. Nili Fossae Research Area

The OMEGA image of the Nili Fossae research area covers the Nili Fossae region. The image is located west of the Isidis Basin. The location of the image can be seen in Figure 33, where the ROI of the OMEGA Nili Fossae image is overlain on a MOLA image that shows the elevation of the research area.

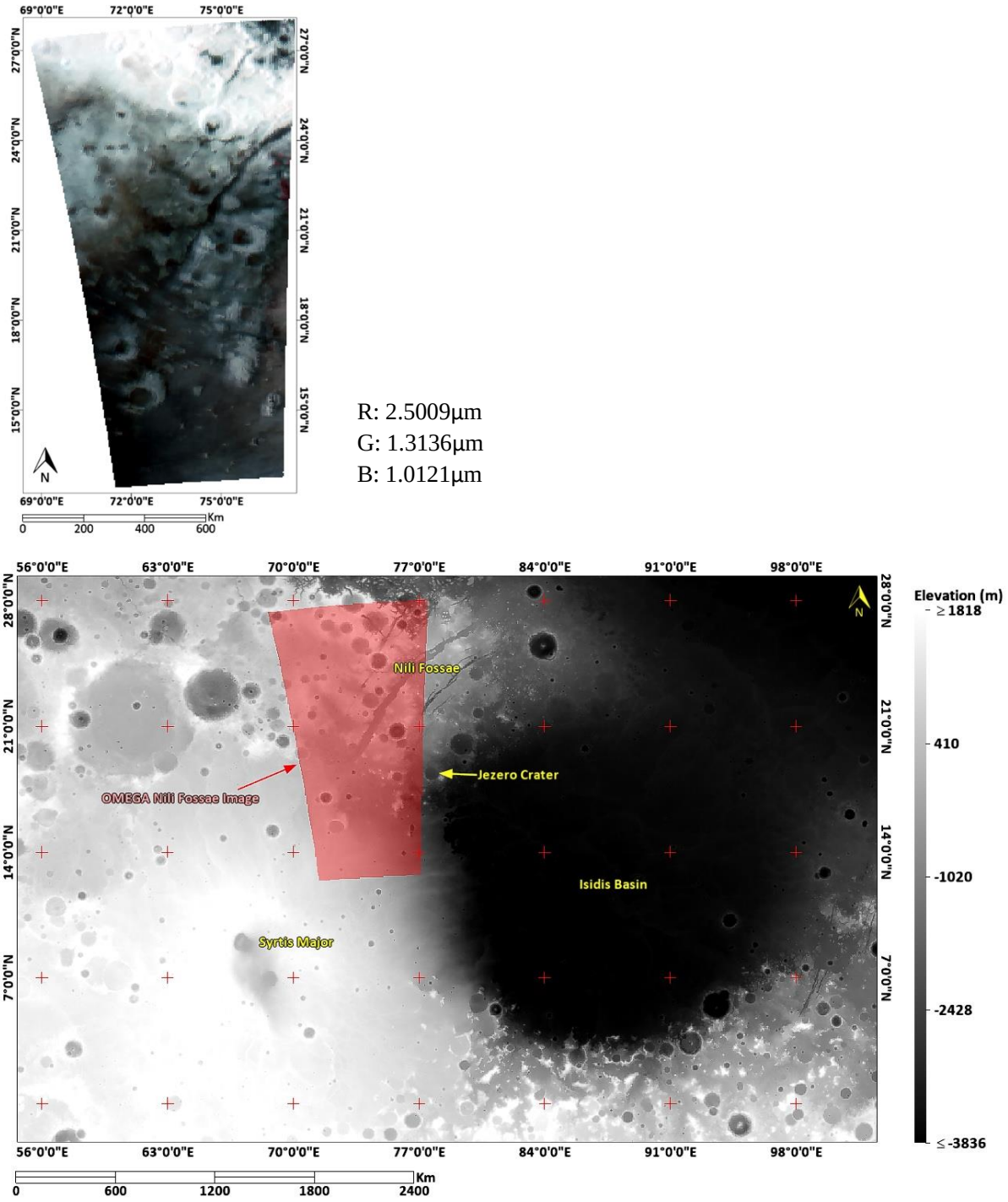

Figure 33. Location of the OMEGA image of the Nili Fossae research area.

3.4.1.1. Entropy Map

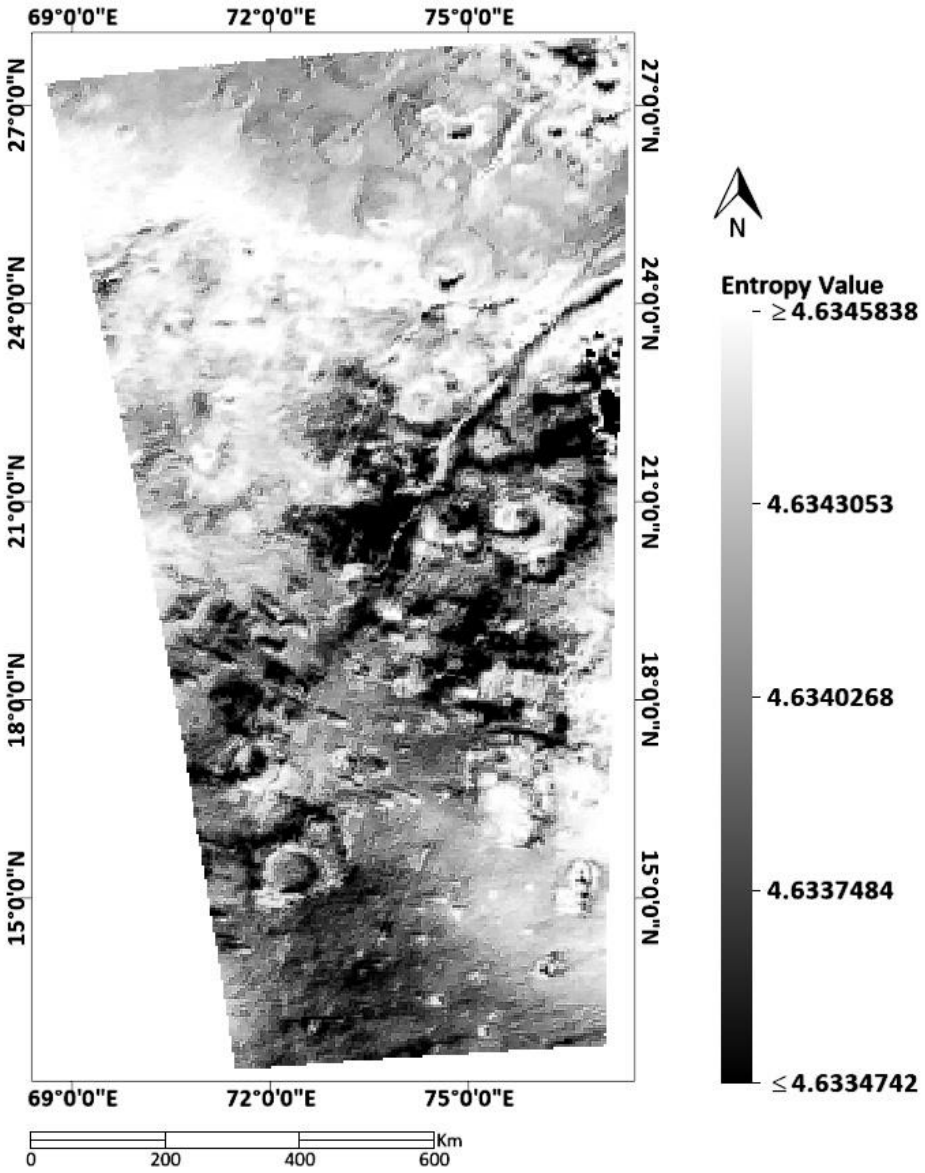

Figure 34. Entropy map of the OMEGA Nili Fossae image with entropy values ranging from 4.626537 to 4.634666, with an average entropy value of 4.634159, shown in a linear 5% stretch.

The entropy map of the OMEGA Nili Fossae image created using wavelength range from 1.0μm to 2.5μm, showing entropy values ranging from 4.626537 to 4.634666, with an average entropy value of 4.634159. The large graben, located in the Nili Fossae area shows low entropy values. Most of the low entropy values are located in the Nili Fossae region, which indicates that the Nili Fossae region yields spectra that have deeper or more distinguishable absorption features.

An ROI is then created by using a threshold based on the entropy values, to show areas that has low entropy values. The ROI is then divided based on the location of the low entropy values. The ROI indicating the locations of the low entropy value, alongside a high entropy sample ROI can be seen in Figure 35. Figure 36 shows the mean spectra of each ROI. The difference can already be seen from the high entropy sample ROI and the low entropy ROIs, where the low entropy ROIs has a more downward slope after the 1.60μm.

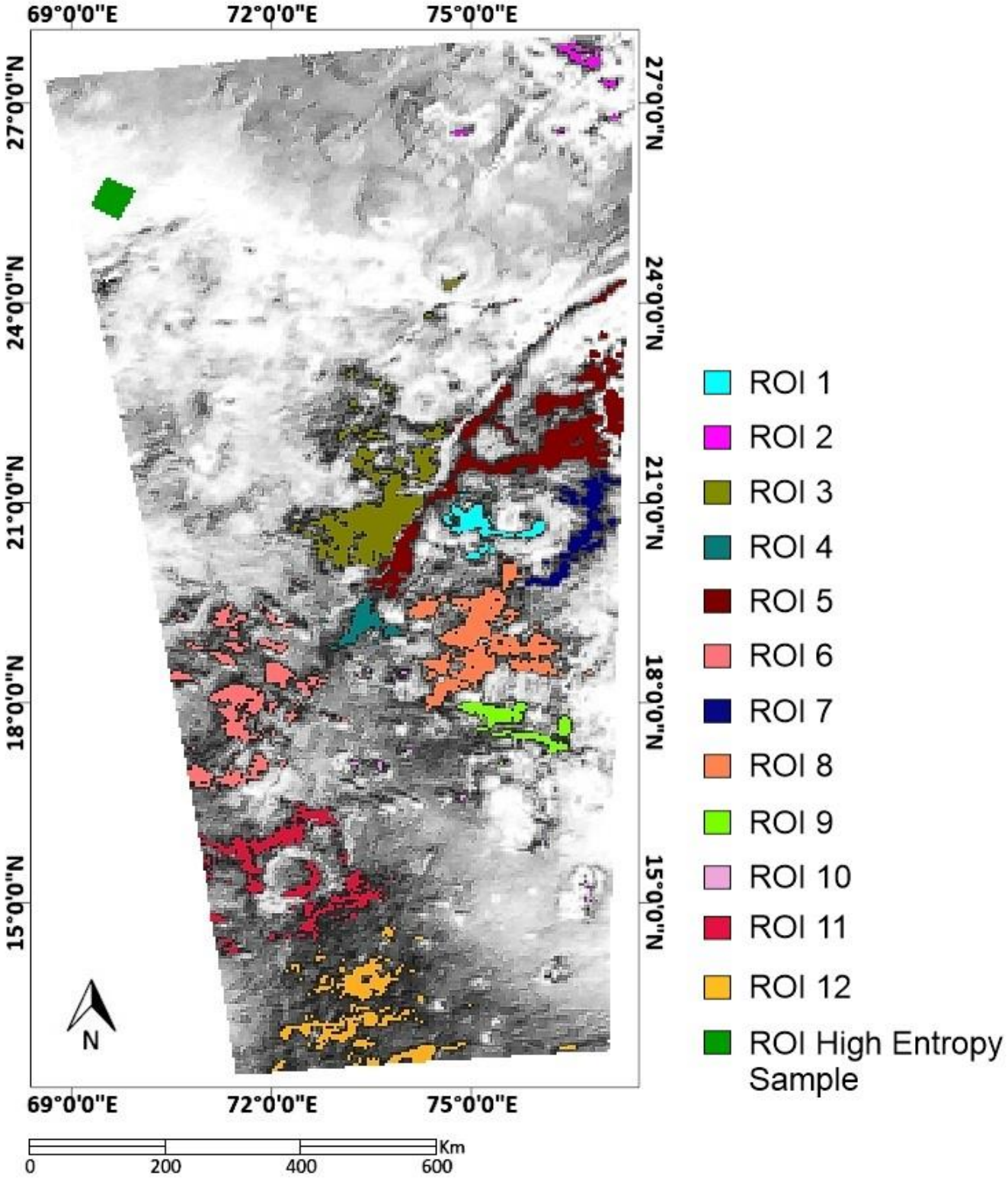

Figure 35. Low entropy ROIs of the OMEGA Nili Fossae image and a high entropy sample ROI for comparison.

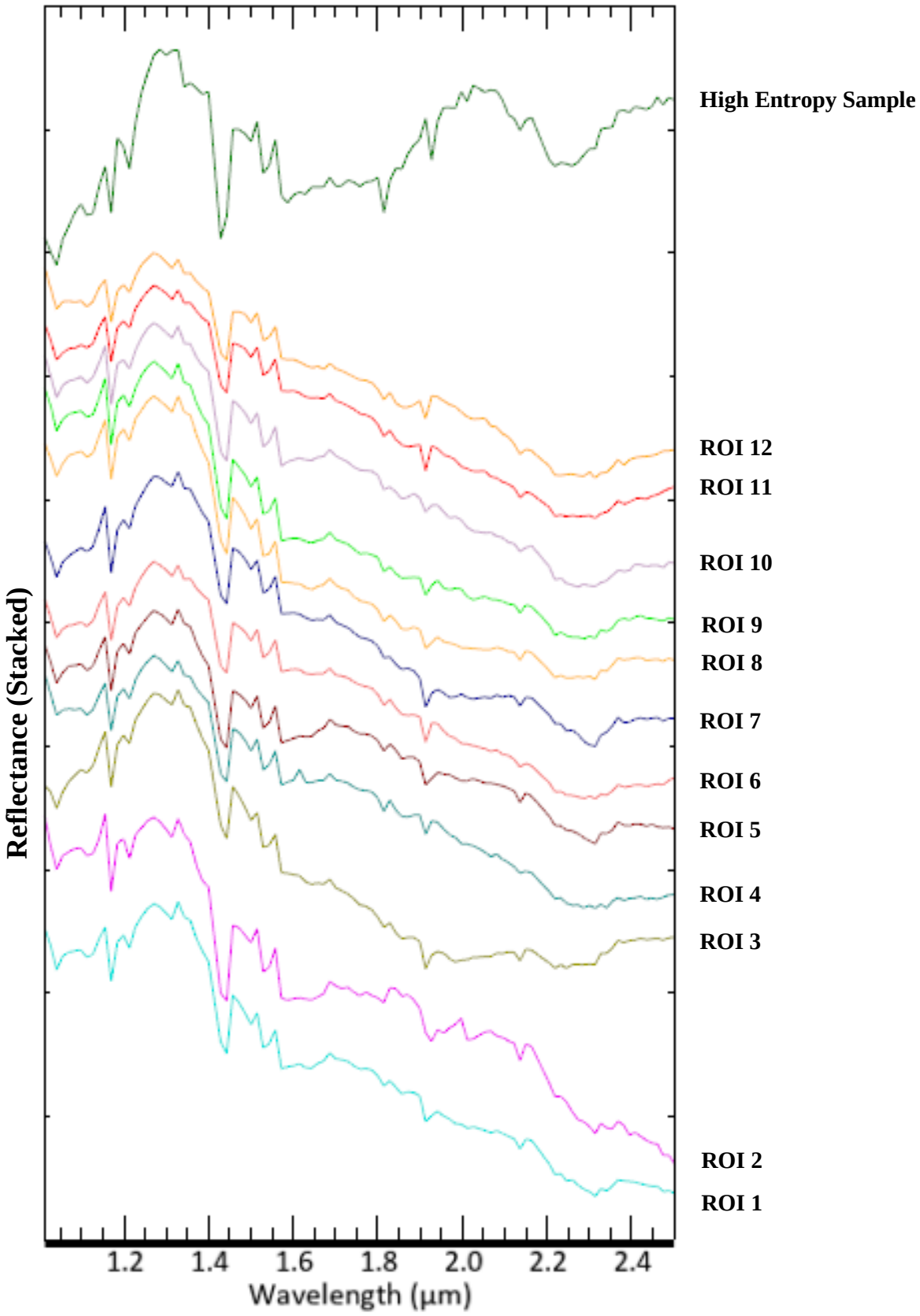

Figure 36. Mean spectra of the ROI low entropy values and ROI of a high entropy value sample.

3.4.1.2. Wavelength Map

The wavelength map of the OMEGA Nili Fossae image is created from the wavelength range of 2.10µm to 2.40µm, done to identify absorption features at the SWIR range. The research area shows the deepest absorption features mostly in the 2.20µm – 2.30µm range, as can be seen in Figure 37.

The 2.20µm deepest absorption feature is represented by the green colour in the wavelength map. The 2.20µm deepest absorption feature mostly covers the south part of the research area. The research area also shows deep absorption feature at the 2.30µm wavelength range, represented by orange colours. The Nili Fossae region shows both deep absorption features at 2.20µm and 2.30µm, which may be an indication of Fe-Mg phyllosilicates, carbonates, or Al-OH minerals. Parts of the research area shows yellow colour, which represents the deepest absorption features at the area to be around 2.27µm. The black coloured area of the wavelength map are areas that have shallow or no absorption features in the SWIR range.

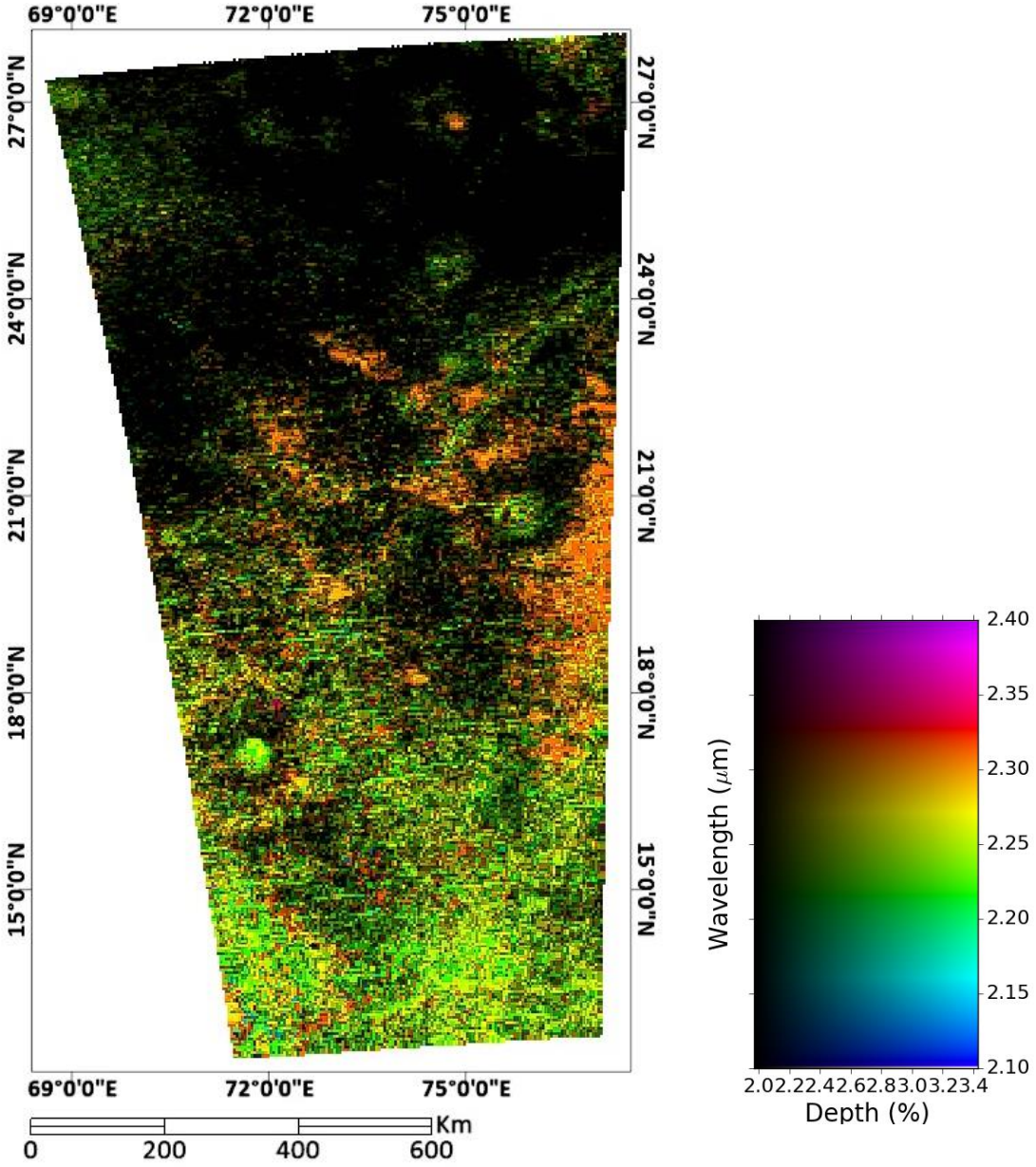

Figure 37. Wavelength map of the OMEGA Nili Fossae image, showing the deepest absorption features from 2.10µm to 2.40µm.

3.4.1.3. Summary Product Maps

The BDCARB index shows locations that show spectral features of carbonate overtones, specifically by the 2.30µm absorption feature. Figure 38 shows the areas that show these carbonate overtones, represented by the red color. The BDCARB index of the OMEGA Nili Fossae research area shows values ranging from -0.014721 to 0.017839 with an average index value of 0.000463. The area that shows carbonate overtones are located in the central-east section of the research area, at and below the Nili Fossae region covered by the research area. The BDCARB index uses the formula in Table 1. The BDCARB index map is shown in a linear 2% stretch, to emphasize the top and bottom 2% of the values, which is represented by the red color and purple color respectively.

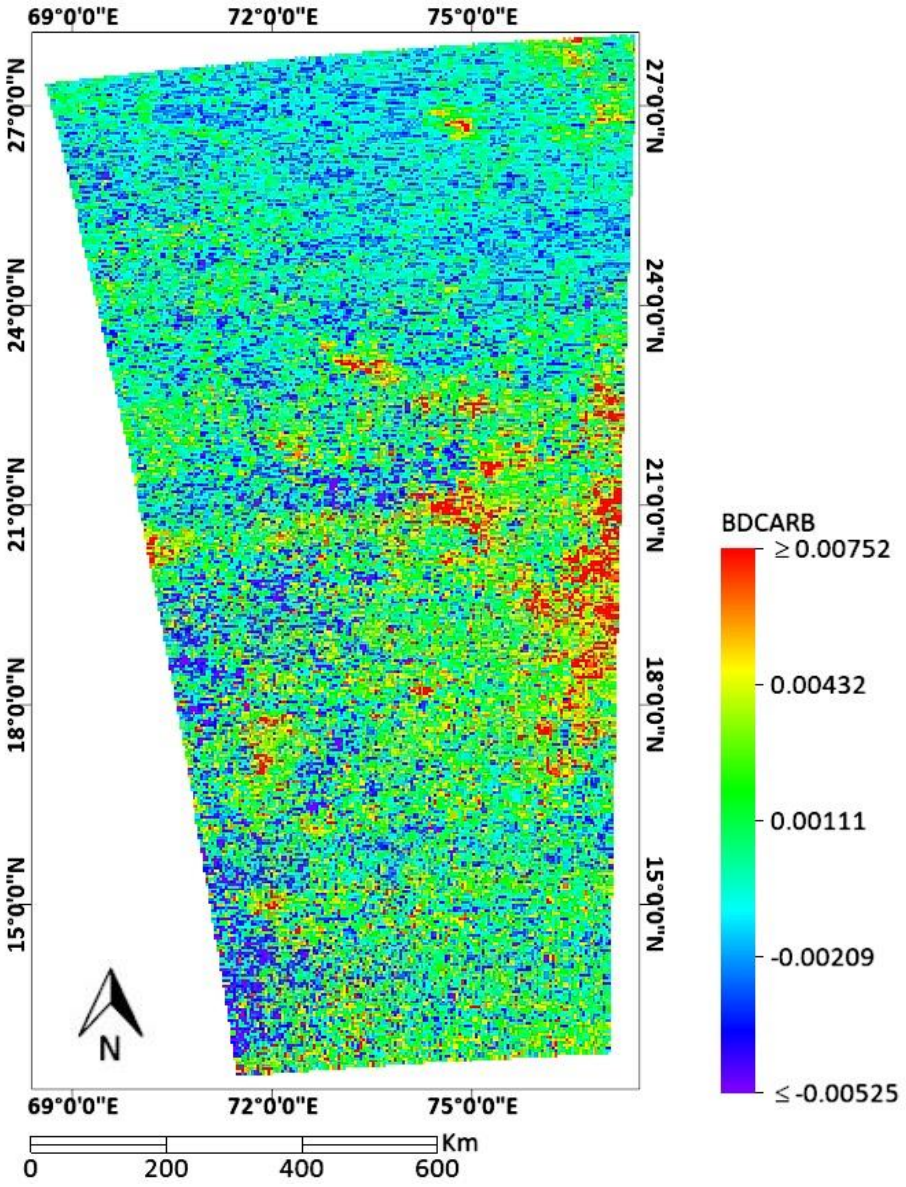

Figure 38. BDCARB index of the OMEGA Nili Fossae image indicating locations showing areas with carbonate overtones, with an index value ranging from -0.014721 to 0.017839 and an average index value of 0.000463.

The BD2290 index summary product, which can be seen in Figure 39 shows the locations where Fe-Mg minerals are possibly located. The index uses the absorption feature at 2.29µm as an indicator. The BD2290 index of the research area has an index value ranging from -0.040046 to 0.035870 and an average index value of 0.003194. The index is calculated with the formula as shown in Table 1.

Similar to the BDCARB index, the red area, which indicates the possible locations of Fe-Mg minerals, are mostly located on the central-east section of the research area, below the Nili Fossae region. Different from the BDCARB index, the BD2290 index shows more high index values located throughout the image as patches, which can be seen in Figure 39, in the central to south east side of the image.

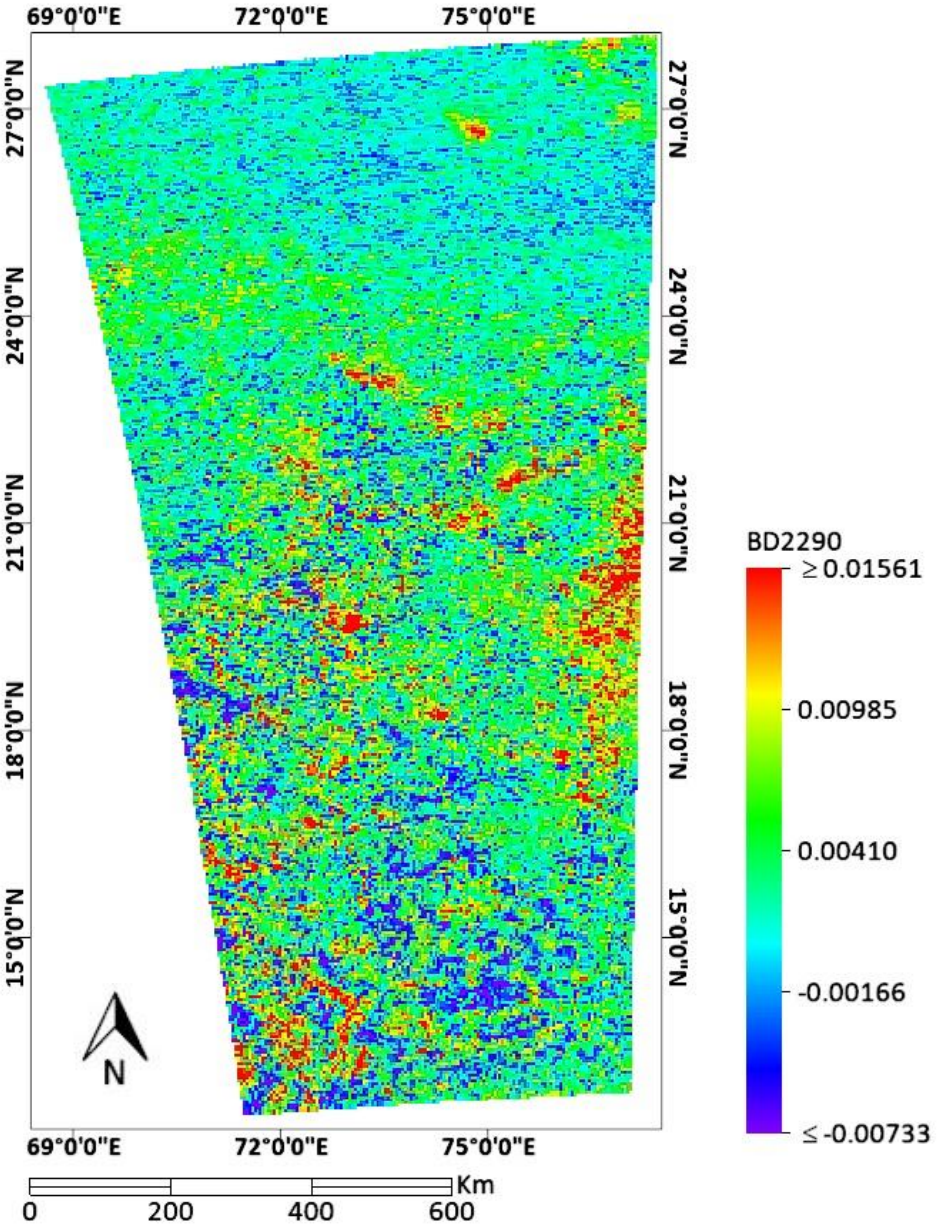

Figure 39. BD2290 index of the OMEGA Nili Fossae image indicating locations showing spectral features of Fe-Mg minerals, with an index value ranging from -0.040046 to 0.035870 and an average index value of 0.003194.

The OLINDEX index summary product, which can be seen in Figure 40 shows the locations where olivine is possibly located. The OLINDEX index of the research area has an index value ranging from

-0.118603 to 0.267489 and an average index value of -0.034629. The OLINDEX index uses the formula shown in Table 1.

The OLINDEX index is shown in a linear 1% stretch, because in this index, only the strongly positive index value will show the location of olivine (Pelkey et al., 2007a). Therefore, only the red color of the research area shows the locations of olivine, as it is the top 1% of the OLINDEX index value. The location of olivine can be seen to be in the central east side of the research area, alongside the east of the Nili Fossae region. There are also patches of red colored areas indicating the presence of olivine throughout the research area, such as in the lower east section of the research area.

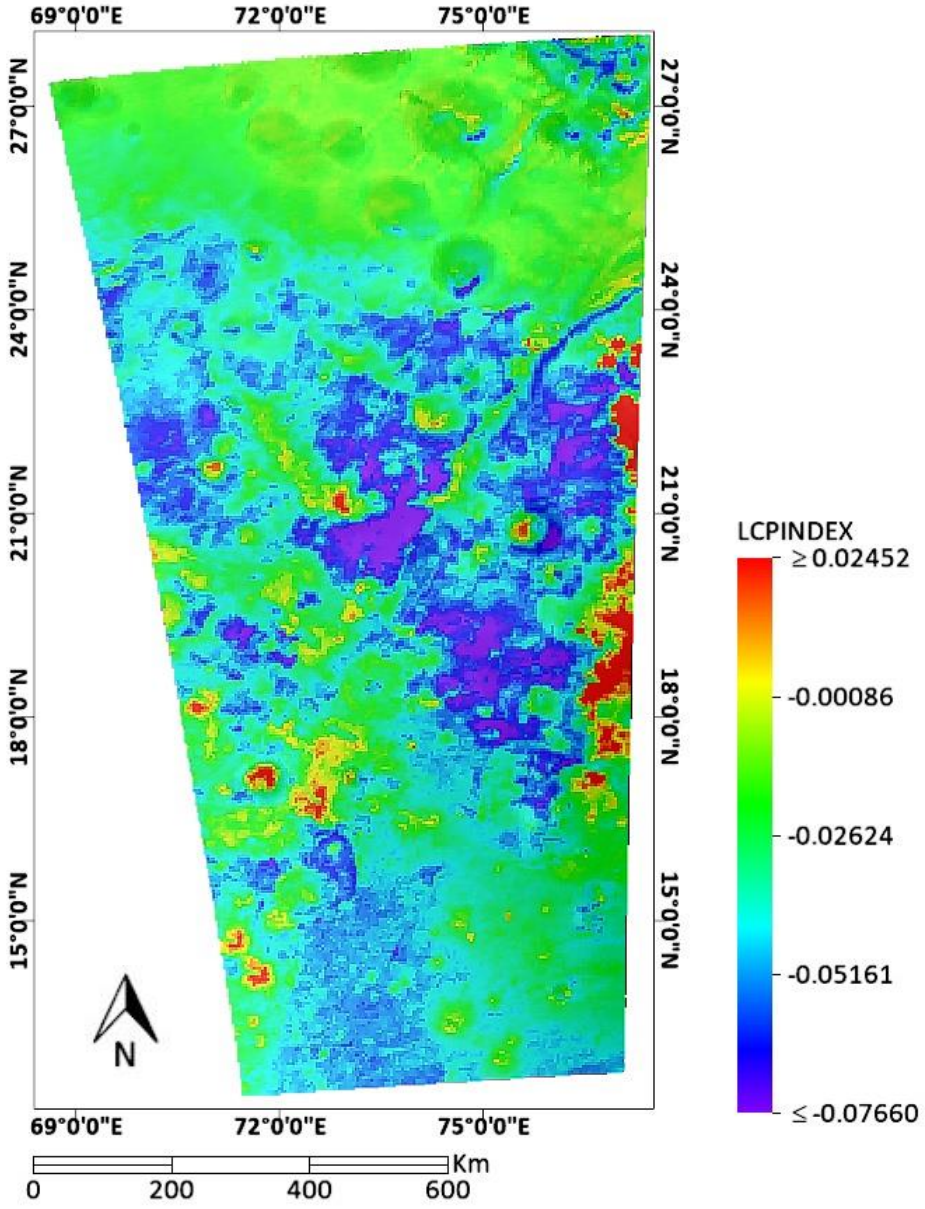

Figure 40. OLINDEX index of the OMEGA Nili Fossae image indicating locations showing spectral features of olivine, with an index value ranging from -0.118603 to 0.267489 and an average index value of -0.034629. Olivine will be indicated by a strongly positive index value.

The LCPINDEX index summary product, which can be seen in Figure 41 shows the locations where low calcium pyroxene may be located. The LCPINDEX index of the research area has an index value

ranging from -0.002264 to 0.005087 and an average index value of 0.000811. The LCPINDEX summary product uses the formula shown in Table 1.

The LCPINDEX index is shown in a linear 2% stretch. The location of LCP can be seen to be in the central side of the research area, on and west of the Nili Fossae region. There are also patches of red colored areas throughout the research area, such as in the east and lower west section of the research area.

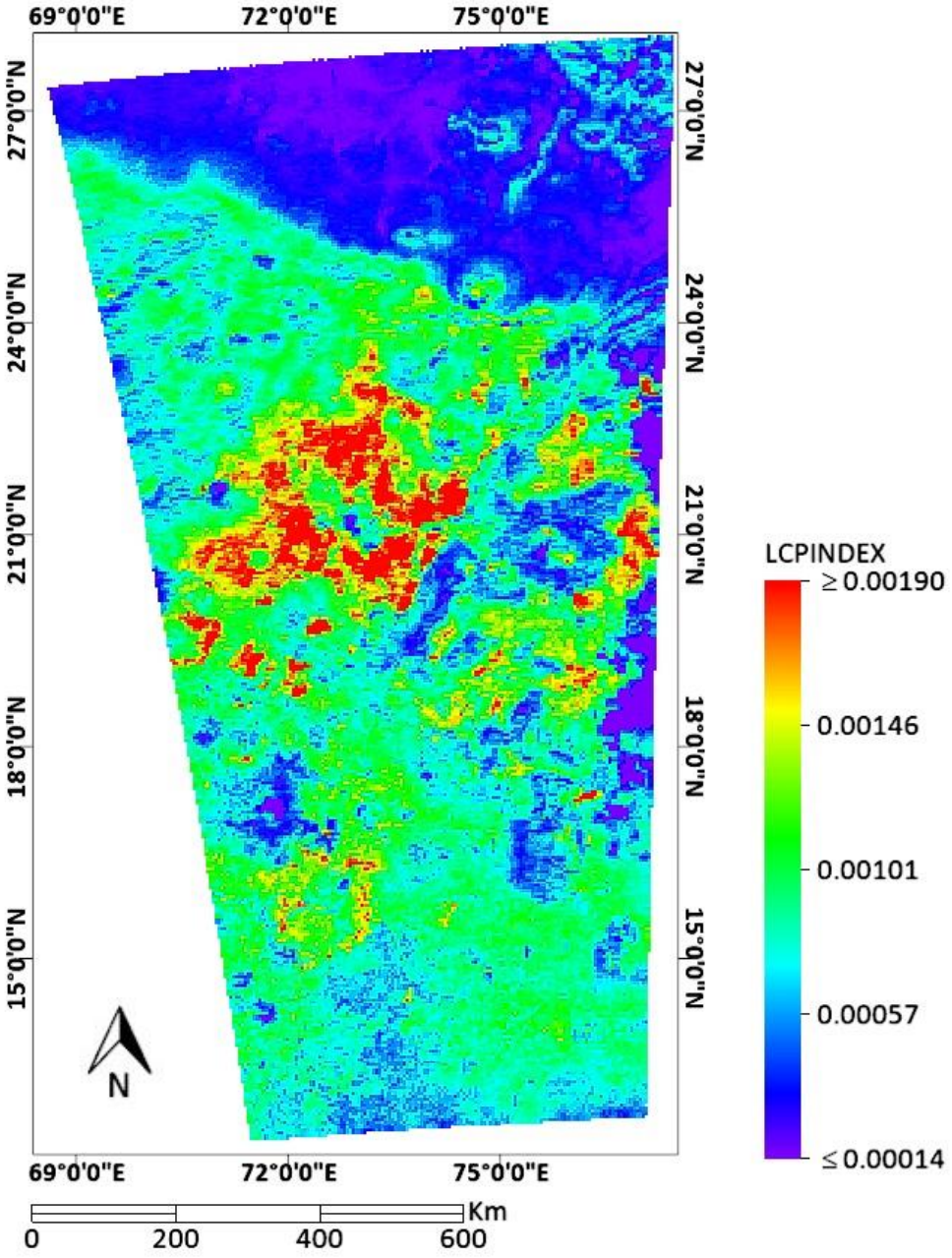

Figure 41. LCPINDEX index of the OMEGA Nili Fossae image indicating locations showing spectral features of low calcium pyroxene, with an index value ranging from -0.002264 to 0.005087 and an average index value of 0.000811.

3.4.2. Jezero Crater Research Area

The location of the OMEGA Jezero Crater image can be seen in Figure 42, where the ROI of the image is overlain on a MOLA map that shows the elevation of the research area. The OMEGA Jezero Crater image comprises of parts of Nili Fossae and a part of the Jezero Crater. The OMEGA Jezero Crater image, similar to the OMEGA Nili Fossae image, is located west of the Isidis Basin. Parts of the OMEGA Jezero Crater image overlap with the OMEGA Nili Fossae image, specifically in the Nili Fossae region.

R: 2.4877µm
G: 1.3136µm
B: 1.124µm

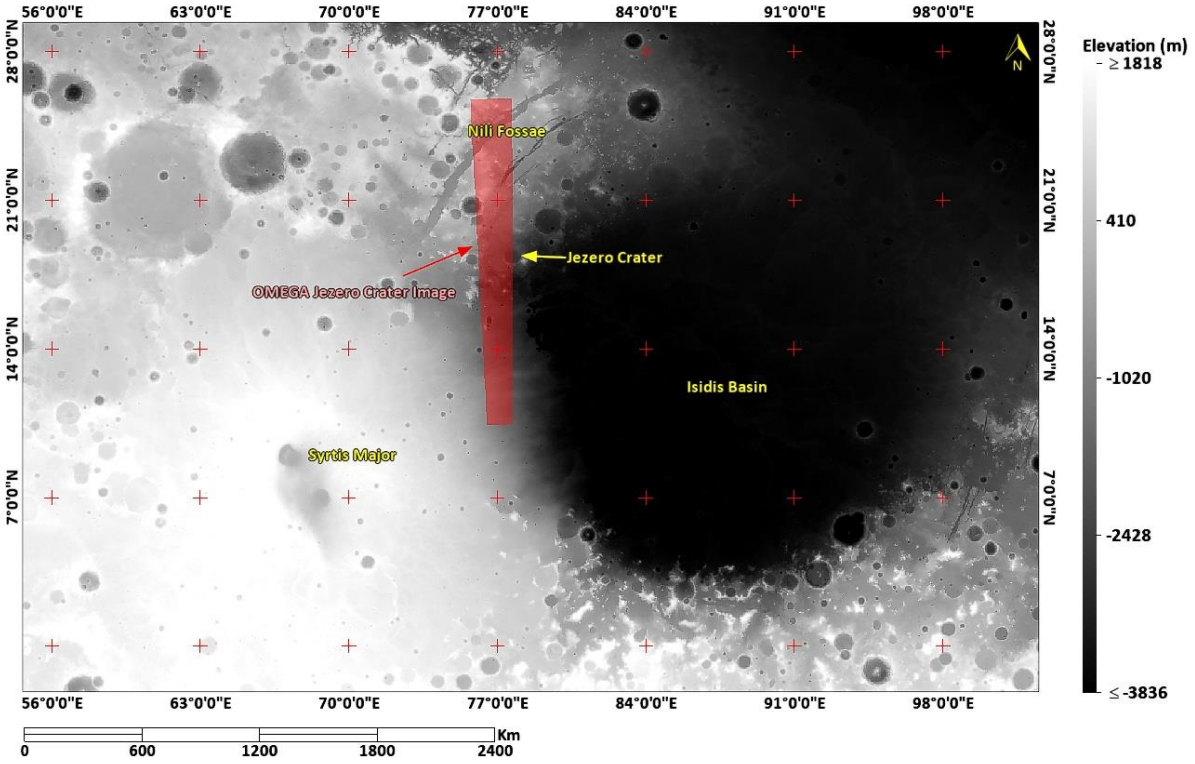

Figure 42. Location and Mars Orbiter Laser Altimeter (MOLA) map of the OMEGA instrument Jezero Crater research area, showing altitudes ranging from -3517m to 1497m, with an average altitude of -1195m.

3.4.2.1. Entropy Map

The entropy map of the OMEGA Jezero Crater research area, shown in Figure 43, shows entropy value ranging from 4.556987 to 4.564284, with an average entropy value of 4.562708. The entropy map is created from wavelength range 1.0µm to 2.5µm, shown with a linear 5% stretch which highlights the bottom 5% of the entropy value. The entropy map shows that the OMEGA Jezero Crater research area has low entropy values in the graben of the Nili Fossae region.

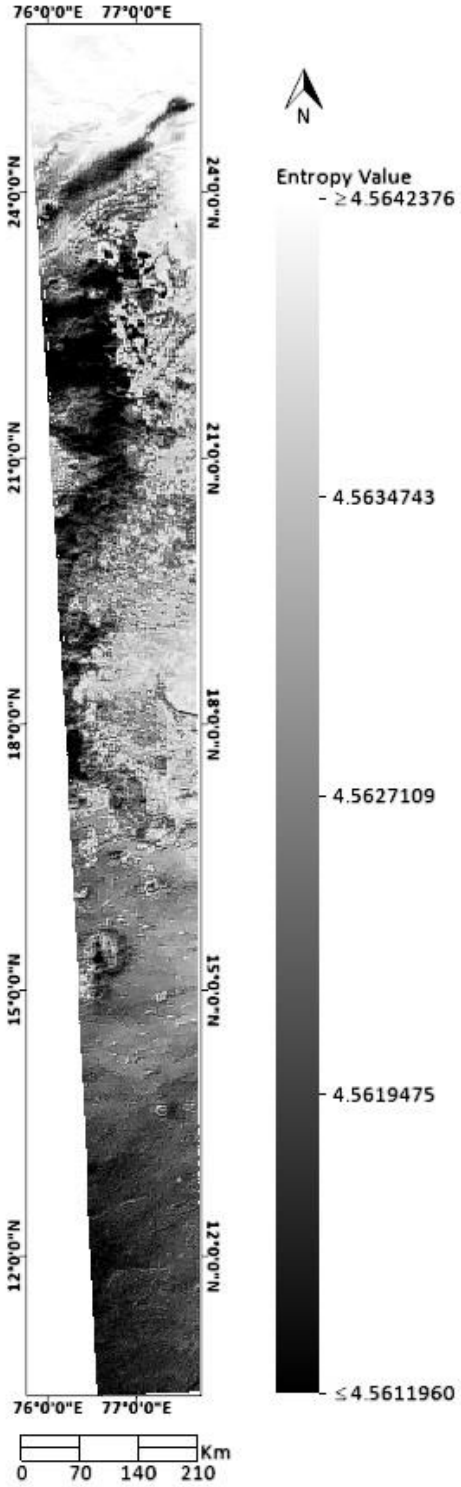

Figure 43. Entropy map of the OMEGA Jezero Crater image with entropy values ranging from 4.556987 to 4.564284, with an average entropy value of 4.562708, shown in a linear 5% stretch.

Figure 44 shows the ROIs of the low entropy values created using a threshold based on entropy values present in the research area, split based on its location. Figure 44 also shows the mean spectra of each ROI. From the spectra, we can see that the high entropy sample spectra differ from the low entropy spectra. The high entropy sample spectra show a more invariant spectra with little differences in its reflectance values, which causes it to have the high entropy value in the entropy map.

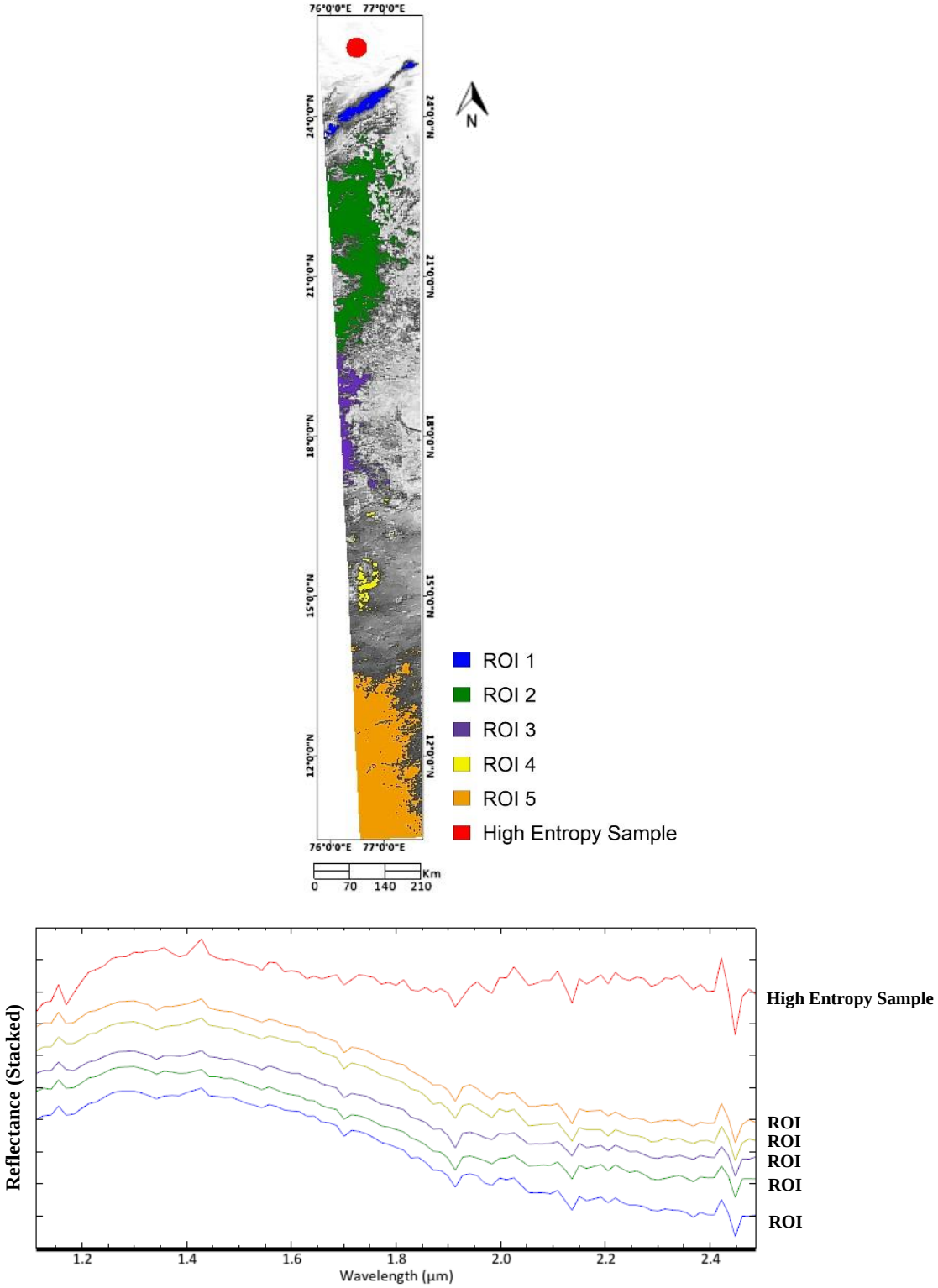

Figure 44. Low entropy ROIs of the OMEGA Jezero Crater image and a high entropy sample ROI for comparison, alongside the mean spectra of each ROI.

3.4.2.2. Wavelength Map

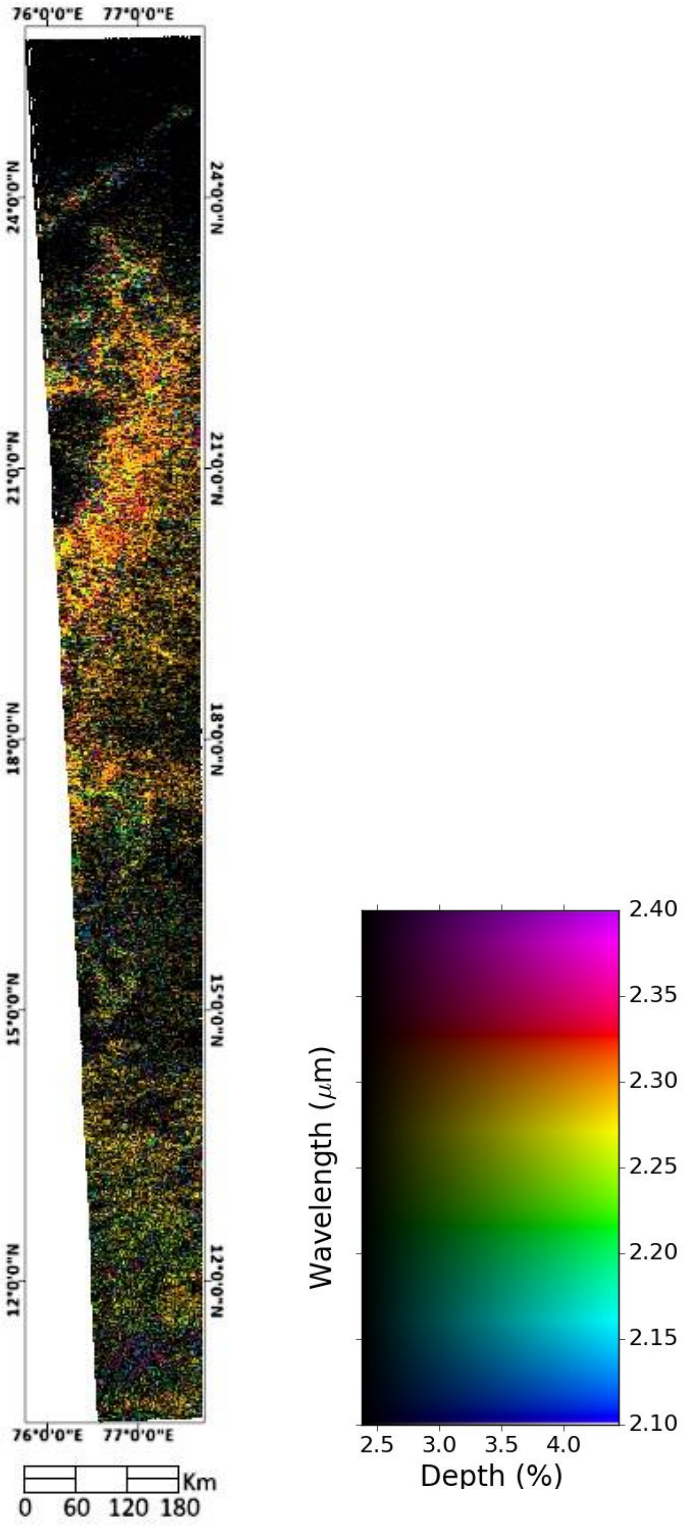

Figure 45. Wavelength map of the OMEGA Jezero Crater image, showing the deepest absorption features from 2.10µm to 2.40µm.

3.4.2.3. Summary Product Maps

The BDCARB index shows locations that show spectral features of carbonate overtones, specifically by the 2.30µm absorption feature. Figure 46 shows the areas that show these carbonate overtones, represented by the red color. The BDCARB index of the OMEGA Jezero Crater research area shows values ranging from -0.025693 to 0.029373 and an average index value of 0.001652. The area that shows carbonate overtones are located in the central section of the OMEGA Jezero Crater research area, at and below the Nili Fossae region covered by the research area. The BDCARB index uses the formula shown in Table 1. The BDCARB index map is shown in a linear 2% stretch, to emphasize the top and bottom 2% of the values, which is represented by the red color and purple color respectively.

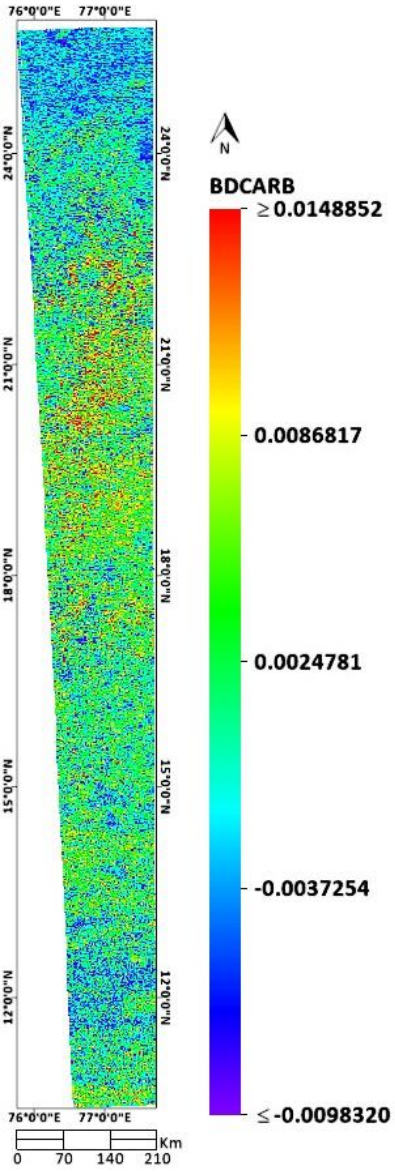

Figure 46. BDCARB index of the OMEGA Jezero Crater image indicating locations showing areas with carbonate overtones, with an index value ranging from -0.025693 to 0.029373 and an average index value of 0.001652.

The BD2290 index summary product, which can be seen in Figure 47Figure 39 shows the locations where Fe-Mg minerals are located. The index uses the absorption feature at 2.29μm as an indicator. The BD2290 index of the research area has an index value ranging from -0.035449 to 0.060659 and an average index value of 0.007257. The index is calculated with the formula as shown in Table 1.

Similar to the BDCARB index, the red area, which indicates the possible locations of Fe-Mg minerals, are mostly located on the central section of the research area, below the Nili Fossae region. Different from the BDCARB index, the BD2290 index shows more high index values located throughout the research area as patches, which can be seen in the central to south side of the research area.

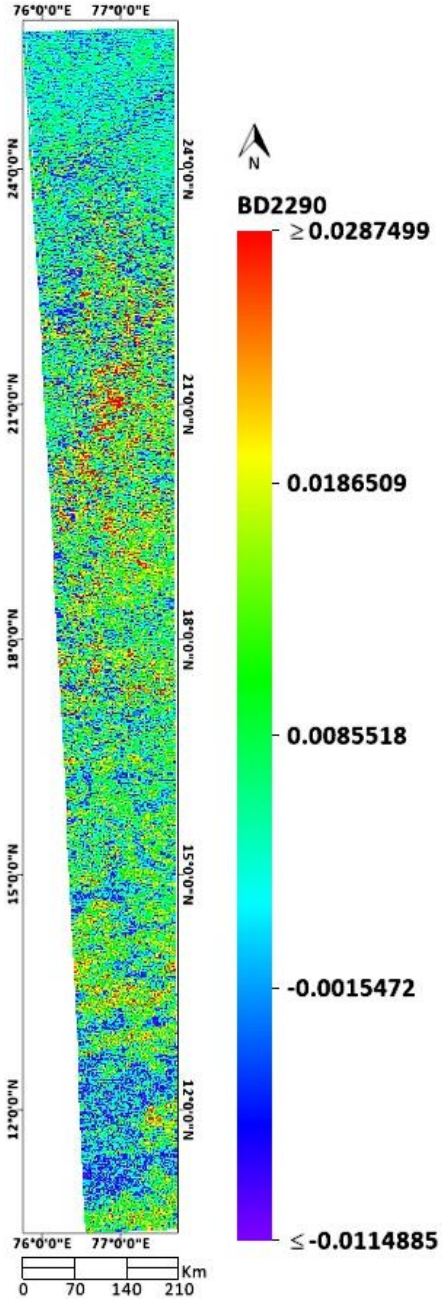

Figure 47. BD2290 index of the OMEGA Jezero Crater image indicating locations showing spectral features of Fe-Mg minerals, with an index value ranging from -0.040046 to 0.035870 and an average index value of 0.003194.

The OLINDEX index summary product, which can be seen in Figure 48 shows the locations where olivine is located. The OLINDEX index of the research area has an index value ranging -0.149045 to 0.301734 and an average index value of -0.032738. The OLINDEX index uses the formula shown in Table 1.

The OLINDEX index is shown in a linear 1% stretch, because in this index, only the strongly positive index value will show the location of olivine (Pelkey et al., 2007a). Therefore, only the red color of the research area shows the locations of olivine, as it is the top 1% of the OLINDEX index value. The location of olivine can be seen to be in the top east side of the research area.

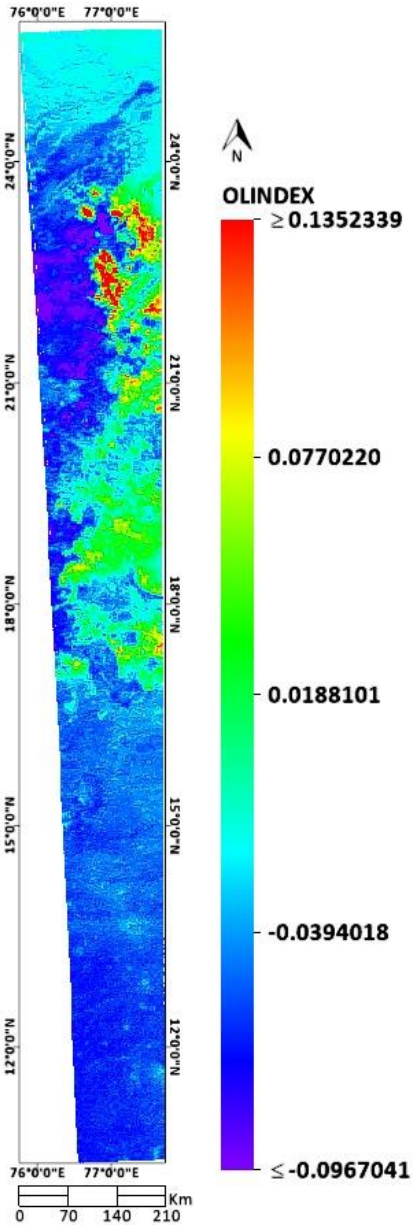

Figure 48. OLINDEX index of the OMEGA Jezero Crater image indicating locations showing spectral features of olivine, with an index value ranging from -0.149045 to 0.301734 and an average index value of -0.032738. Olivine will be indicated by a strongly positive index value.

The LCPINDEX index summary product, which can be seen in Figure 49 shows the locations where low calcium pyroxene is located. The OLINDEX index of the research area has an index value ranging from -0.002622 to 0.004504 and an average index value of 0.000541. The LCPINDEX summary product uses the formula shown in Table 1

The LCPINDEX index is shown in a linear 2% stretch. The location of LCP can be seen to be in the top west side of the research area where the Nili Fossae region is located. There are also patches of red colored areas in the south section of the research area.

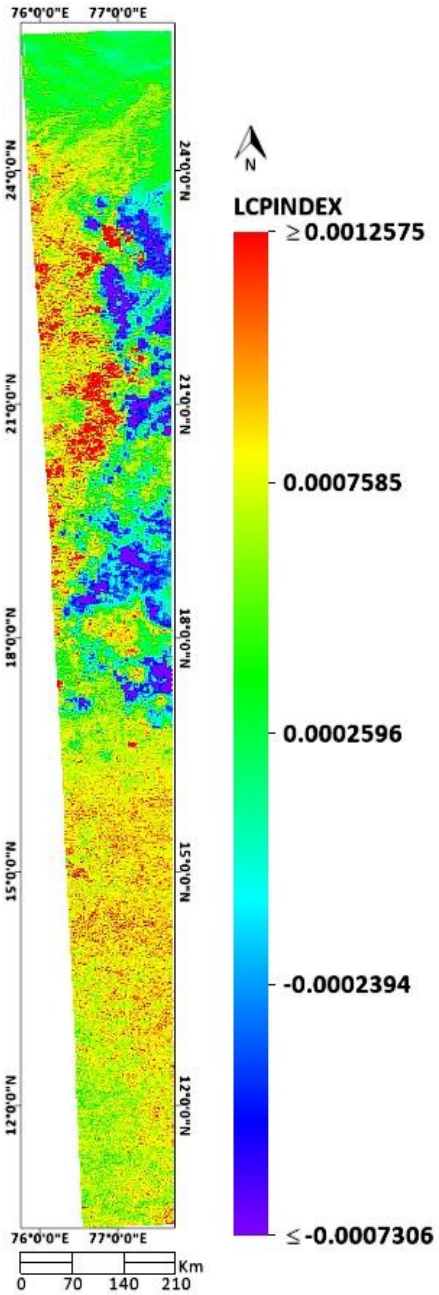

Figure 49. LCPINDEX index of the OMEGA Jezero Crater image indicating locations showing spectral features of low calcium pyroxene, with an index value ranging from -0.002622 to 0.004504 and an average index value of 0.000541.

4. Discussion

The discussion chapter of the research discusses the result of the research and how it relates with each other. The first section of the discussion will discuss the processing step of the CRISM data, and the comparison between the raw TRDR, processed TRDR, and MTRDR CRISM Nili Fossae image. The processing section will also discuss the interpretation of the regression analysis conducted on the relationship of each data.

The second section of the discussion chapter discusses the spectra variation of the different levels of entropy values. The entropy variation section will also discuss how the spectra of the different levels of entropy values affect the calculations of the entropy value. The comparison of spectra uses the mean ROI of the different level of entropy values, created using a threshold of entropy values depending of the level of entropy value.

The third section of the discussion chapter discusses the interpretation of the low entropy values by comparing the location of the low entropy value with the wavelength maps and summary products created in the result chapter of the research. The section discusses the relationship between the low entropy values relates to the wavelength and summary product maps, and if the low entropy values does indeed show areas indicating the presence of minerals.

The last section of the discussion chapter discusses how the more detailed CRISM images relates to the regional scale OMEGA images. The comparison is conducted by overlaying the entropy maps of the CRISM images with the entropy maps of the OMEGA images. This section discusses how the entropy values of the CRISM images relates to the entropy values of the OMEGA images.

4.1. Processing & Entropy Comparison

The result shows similarities spectrally, between the TRDR data that has been corrected by me and the MTRDR which has been corrected by the CRISM team. This highly differs from the raw TRDR data that show the absorption features caused by atmospheric transmission and noise. Both spectra showing the remnants of the carbon dioxide absorption feature after processing at the 2.0μm wavelength, which can be seen in the mean spectra of both Figure 8a and Figure 8b. There are also small differences such as the spikes in the maximum spectra of the MTRDR data (Figure 8b) around the 1.93μm and 1.15μm wavelength. There is also a relatively small difference in the reflectance values on both of the mean spectra in Figure 8a and Figure 8b.

Figure 9 shows that the MTRDR data has very similar entropy values as the processed TRDR data, while the raw TRDR data is seen to have lower entropy values than the other two CRISM data. The TRDR data that has been only geometrically corrected has lower entropy values which is caused by the absorption features of carbon dioxide that is still present due to the absence of atmospheric correction. The absorption caused by the carbon dioxide causes differences between the average reflectance value and the reflectance value causing lower entropy values. The spectral similarities between the TRDR data that has been corrected with the MTRDR data results in similar entropy values between the 2 entropy maps.

Figure 10a shows that the relationship between the MTRDR and the corrected TRDR entropy maps yields a value of 94.2% which means that the MTRDR and the corrected TRDR entropy maps has very similar entropy values. The comparison between the MTRDR and the TRDR raw entropy map (Figure 10b) only yields 58.8% while the comparison between the TRDR corrected entropy map and the TRDR raw entropy map (Figure 10c) yields 73.0%. From Figure 10 it can be seen that the relationship between the MTRDR and the TRDR corrected entropy maps yields the lowest standard error, as can be seen in the regression model in Figure 10a.

4.2. Entropy Variation

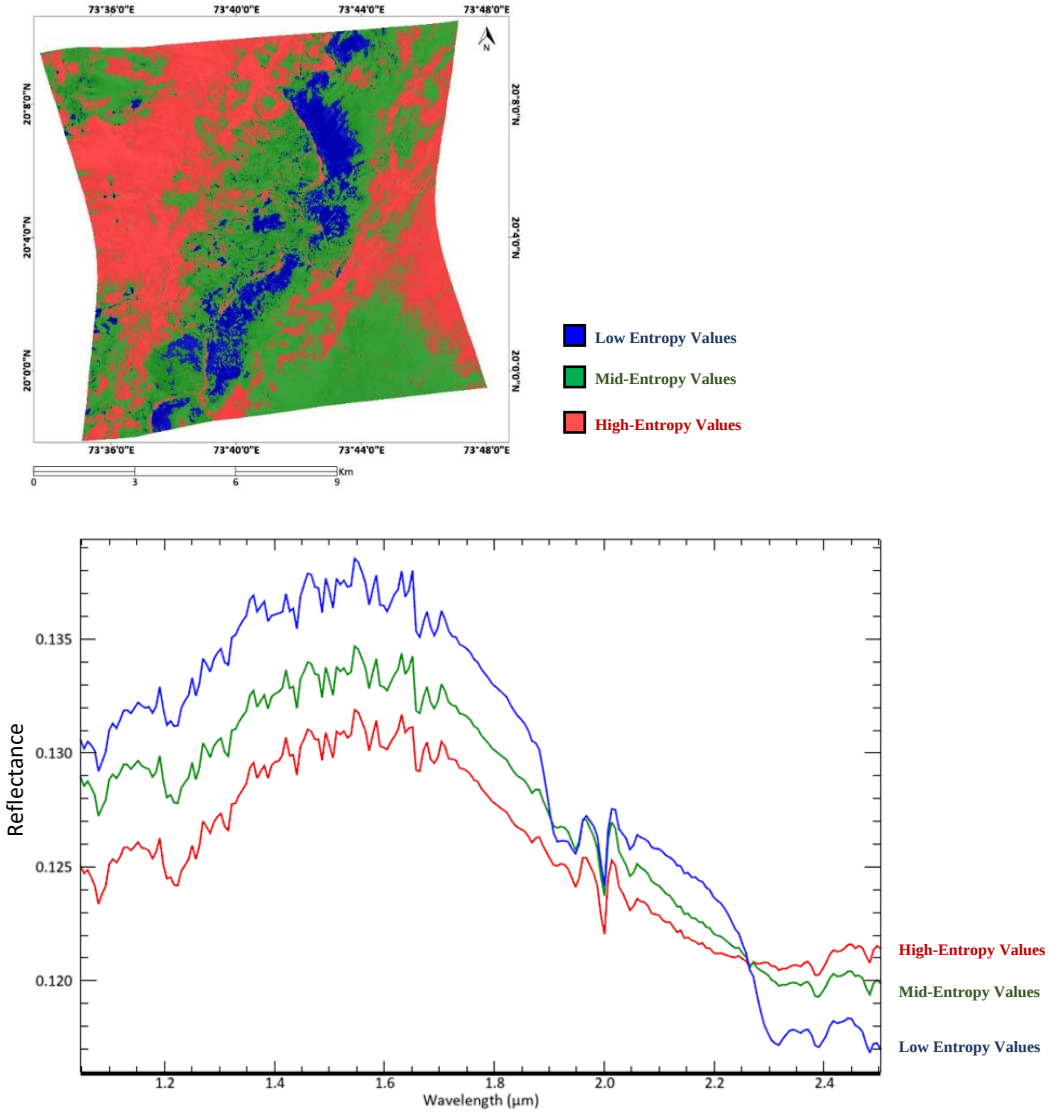

Figure 50. Entropy value variation of the Nili Fossae CRISM image, showing ROIs of areas with low, middle, and high entropy values, alongside the mean spectra of each ROI.

The entropy map of the Nili Fossae CRISM image in Figure 13, which was created using wavelength range from 1.0µm to 2.5µm, has shown that the entropy values range from 5.398967 to 5.402588 with an average of 5.401969. The spread of the entropy values can be seen in Figure 50. The ROI of the low, middle, and high entropy value is created using a threshold. The low entropy value ROI is taken from areas that has entropy values ranging from 5.398967 to 5.401500, while the mid-entropy value is taken from the entropy values ranging from 5.401500 to 5.402100. The high entropy value ROI is taken from entropy values above 5.402100.

It can be seen those spectra with a higher variety of reflectance values, have lower entropy values. High entropy values, represented by the red colored ROI, show more invariant reflectance and do not show deep absorption feature when compared to the spectra of the low entropy zones. The mid-entropy values, which can be assumed as the average spectra of the research area, show a more deeper absorption features than the high-entropy spectra.

The low entropy value spectra show a higher difference in reflectance in the wavelength range from 1.00µm to 1.90µm, and a steeper slope of the spectra after the 2.00µm band. The low entropy value also shows a deeper absorption feature at the wavelength 2.30µm and 2.40µm, which is caused by the Fe-Mg phyllosilicates located in the CRISM Nili Fossae research area. This differences in reflectance values caused the spectra to show a low entropy value.

Figure 50 shows that the absorption features at wavelength range from 1.00µm to 1.70µm shows no differences in depth and wavelength. The 1.00µm to 1.70µm are caused by systematic noise of the instrument from the infrared filter transmission. Similarly, the 2.00µm absorption feature also does not affect the entropy value, because it is caused by atmospheric absorption feature of carbon dioxide, but should be removed during atmospheric correction.

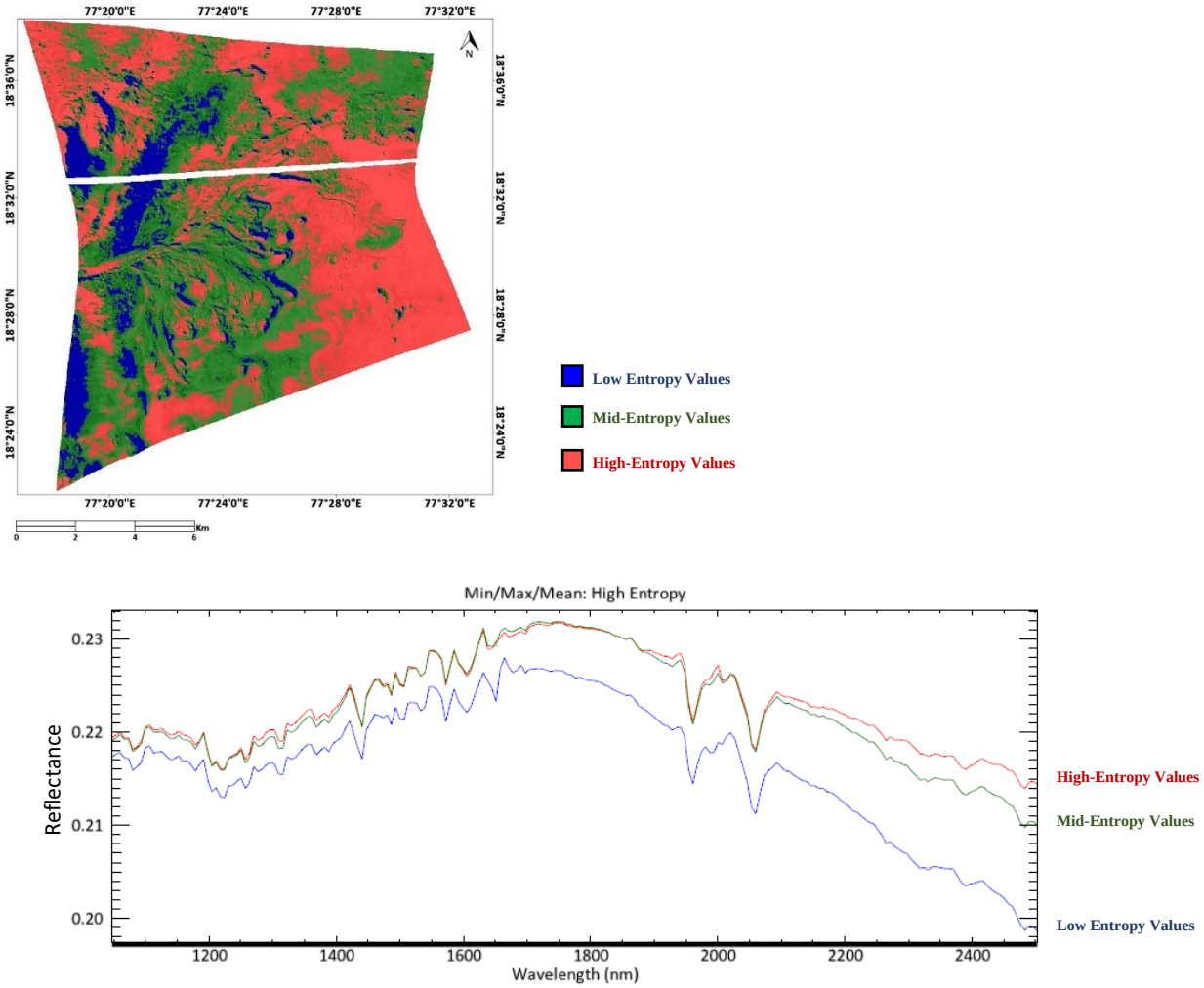

Figure 51. Entropy value variation of the Jezero Crater CRISM image. a) Shows ROIs of areas with low, middle, and high entropy values, and b) the mean spectra of each ROI.

Different from the Nili Fossae CRISM research area, the Jezero Crater CRISM research area has higher entropy values, ranging from 5.400989 to 5.402593 and a mean of 5.402309, due to more invariance in the reflectance of the image. The low entropy ROI of the Jezero Crater CRISM image is below 5.402150. The mid-entropy value ROI is taken from entropy values 5.402150 to 5.402350, and above 5.402350 is used as the entropy value for the high entropy value ROI. Figure 51 shows the ROI of low, middle, and high entropy values. Figure 51 also shows the mean spectra of each ROI.

The Jezero Crater CRISM image shows that the high and the mid-entropy spectra are somewhat similar, with differences in reflectance value above the 2.10µm wavelength. The high entropy spectrum has a more invariant reflectance compared to the mid-entropy spectrum. The low entropy spectrum shows a lower reflectance values when compared with the mid and high entropy value ROI, with a steeper slope of reflectance values above the 1.70µm. This steeper slope of reflectance resulted in lower entropy values, as can be seen in Figure 51 where the spectra of different levels of entropy value are shown. The invariance of reflectance values of the high and mid entropy spectra are what caused the higher entropy value.

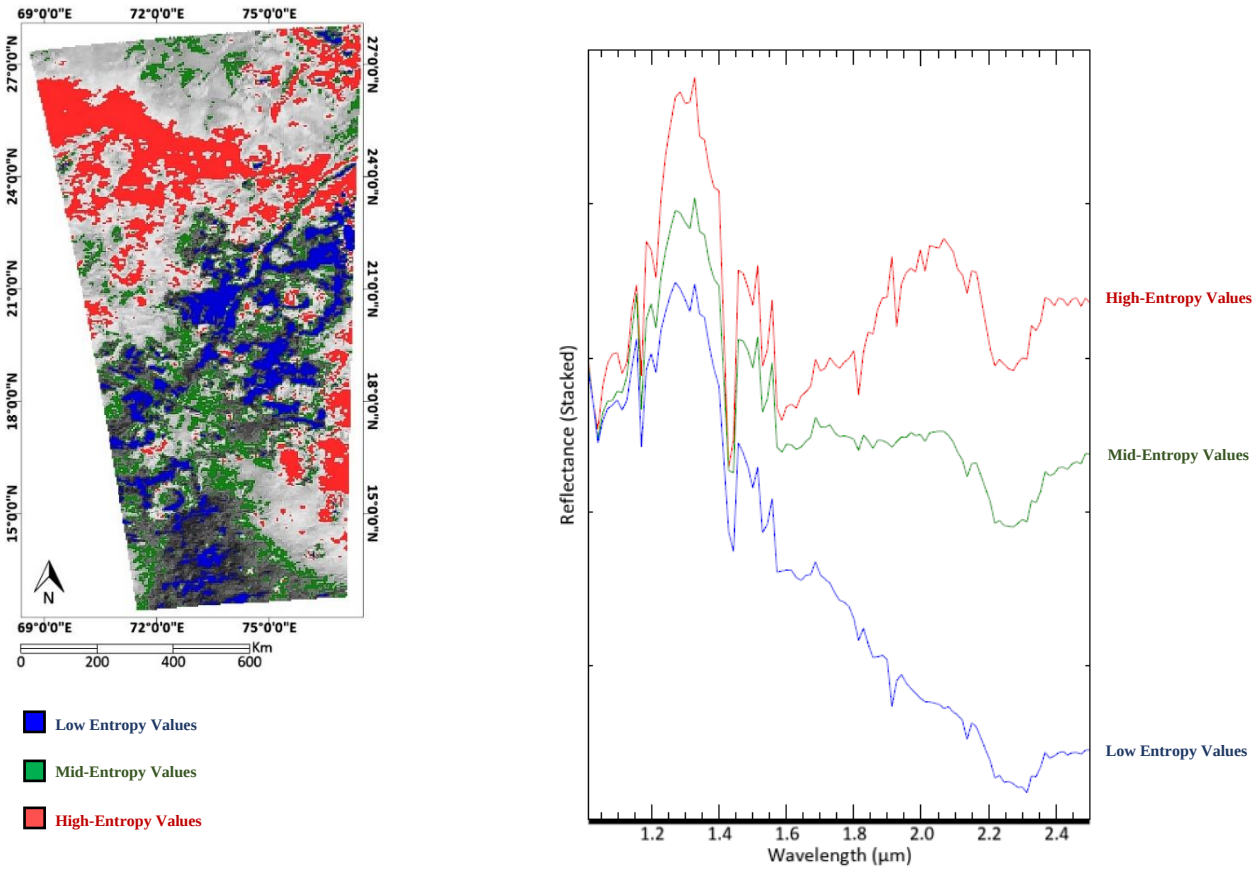

Figure 52. Entropy value variation of the OMEGA Nili Fossae image, showing ROIs of areas with low, mid, and high entropy values, alongside the mean spectra of each ROI in a stacked reflectance y-axis (0 stack offset).

Moving towards the OMEGA images, Figure 52 shows the ROI for the low, mid, and high entropy values of the OMEGA Nili Fossae research area. Figure 52 also shows the spectra as stacked reflectance. The OMEGA Nili Fossae research area yields entropy values ranging from 4.626537 to 4.634666, with an average entropy value of 4.634159. The low entropy value ROI is created from entropy value of below 4.63360 while the high entropy value ROI is created from the entropy values above 4.63450. The mid entropy ROI is created using entropy values from 4.634000 to 4.634150.

The cause of the lower entropy value than the CRISM research areas are due to the more noticeable noise absorption features in the range before 1.60µm. Similar to the CRISM research areas, the low entropy value spectra show a steeper slope, which may be caused by a broad absorption feature, at the

wavelength range after 1.60µm, which is not present in the high entropy spectra. The mid entropy spectra also show a faint broad absorption feature in the SWIR range, which is what caused the mid entropy value, as can be seen in Figure 52.

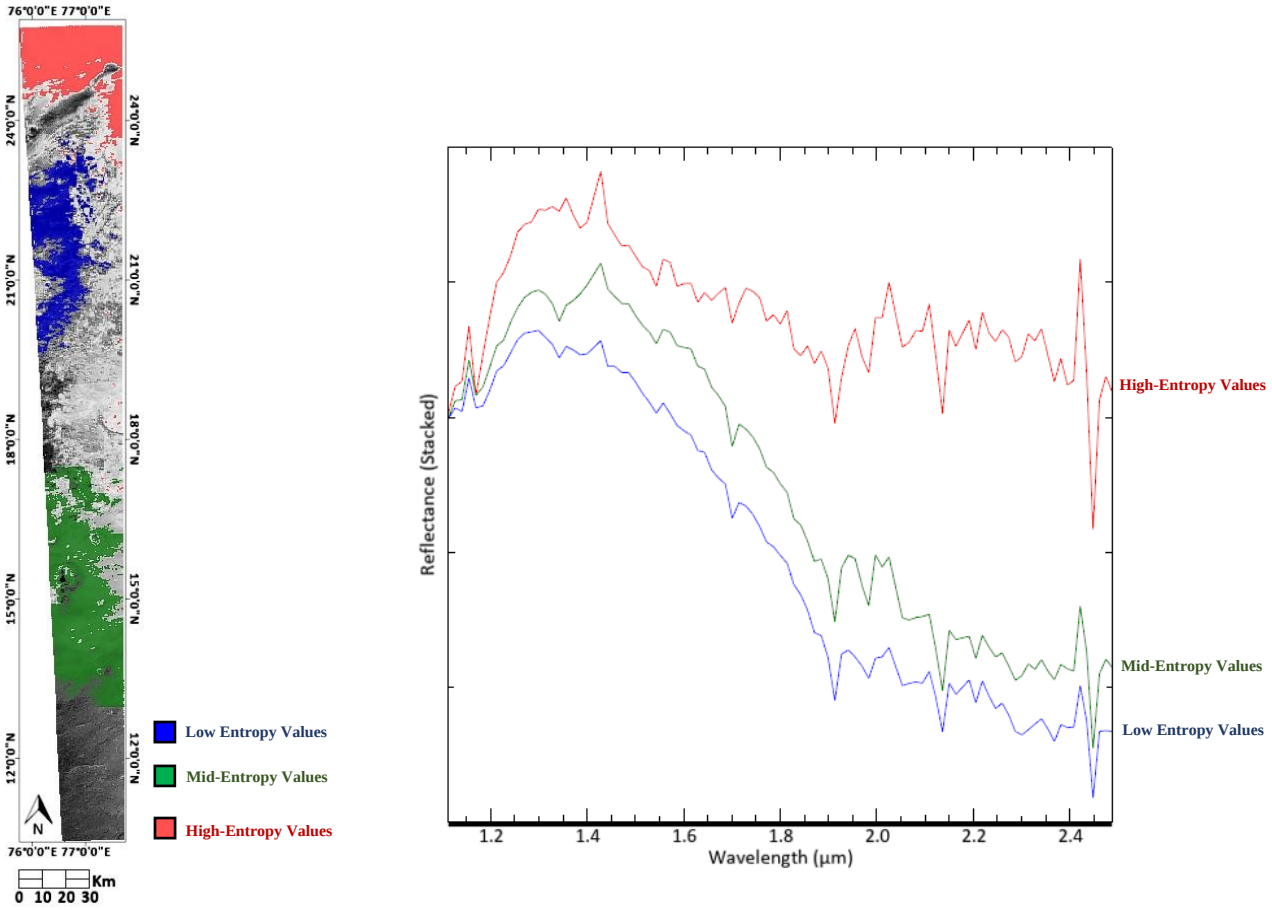

Figure 53. Entropy value variation of the OMEGA Jezero Crater image, showing ROIs of areas with low, mid, and high entropy values, alongside the mean spectra of each ROI in a stacked reflectance y-axis (0 stack offset).

Similar to the OMEGA Nili Fossae research area, the ROIs used for the entropy variation comparison in the OMEGA Jezero Crater research area are representing low and high entropy values. The mean spectra shown in Figure 53, shows the reflectance value stacked. The OMEGA Jezero Crater image has entropy values ranging from 4.556987 to 4.564284, with an average entropy value of 4.562708, lower than the entropy values in the OMEGA Nili Fossae research area. The low entropy ROI is taken from entropy value below 4.562000, while the high entropy ROI is taken from entropy values above 4.564000, and the mid entropy ROI is taken from entropy value 4.562000 to 4.563000. The threshold is then spatially subsetted so that it does not represent different minerals. The spectra in Figure 53 shows that the low entropy spectra show a steeper curve after the 1.50µm, which causes the low entropy value. Comparing the mid and low entropy value ROI, there is little difference between the spectra, where it shows that the steepness of the curve is almost identical. The difference between the low and mid entropy value spectra is that the low entropy spectra have a deeper broad absorption feature in the SWIR range. In contrast, the high entropy spectra show a more invariant reflectance value range but with deeper absorption features.

4.3. Entropy Interpretation

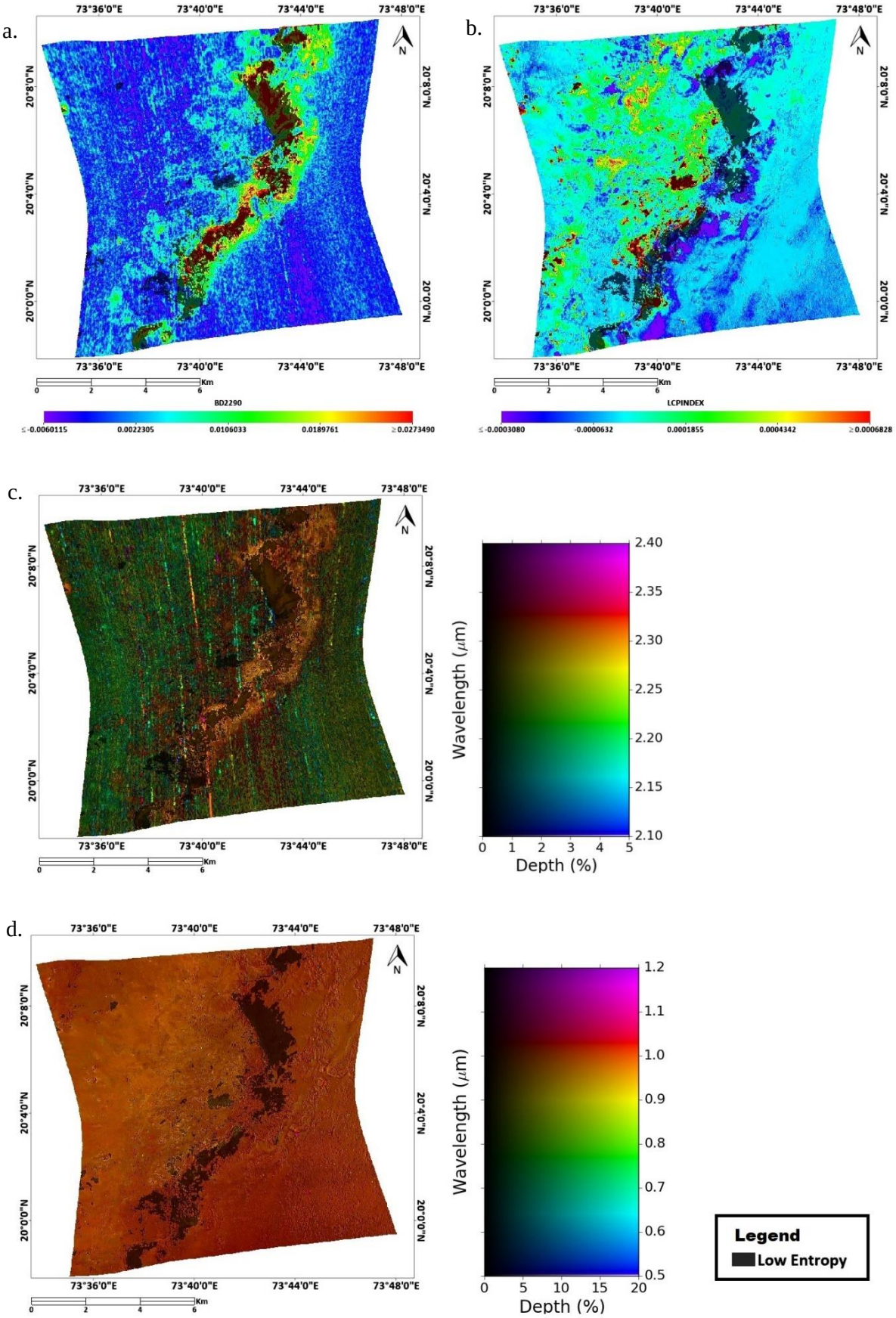

Figure 54. Low entropy ROI (Black) of the CRISM Nili Fossae image overlain with the a.) BD2290 index, b.) LCPINDEX, c.) 2.10μm – 2.40μm wavelength map, and d.) 0.5μm – 1.2μm wavelength map.

Figure 54 shows the low entropy values ROI, created by using a threshold of entropy values ranging from 5.398967 to 5.401500, overlain with the wavelength maps and summary products maps of the CRISM Nili Fossae image in the result section. The summary product map of BDCARB index is not shown in Figure 54 as the 2.30µm absorption feature was analyzed to be Fe-Mg phyllosilicates (Section 3.3.1.6). Figure 21, which is the mineral map of the CRISM Nili Fossae research area, shows the ROI of the minerals present in the CRISM Nili Fossae research area overlain in the entropy map created in Figure 13. The low entropy value in the graben wall were an indication of the presence of Fe-Mg phyllosilicates. When comparing with the BD2290 index shown in Figure 54a, which indicates the location of Fe-Mg minerals, the low entropy values in the graben wall matches with the high index value. This shows that the low entropy value in the graben wall represents the Fe-Mg phyllosilicates of the CRISM Nili Fossae research area. When compared with the wavelength map shown in Figure 54c, the location of the low entropy value in the graben wall matches with the orange colour representing the 2.30µm absorption feature. The low entropy shows the area with the deepest absorption feature, which means that the area around the low entropy value of the graben wall that also shows 2.30µm as the deepest absorption feature has a shallower absorption feature than the areas with low entropy value.

The low entropy values in the surface of the horst matches with the wavelength maps shown in Figure 15b and Figure 16, where it shows indication of LCP in the 0.90µm, which can also be seen in Figure 54d. The low entropy values in the surface of the horst also shows similarities with the high index value areas of the LCPINDEX, shown in Figure 54b. The entropy maps are created from the wavelength range of 1.00µm to 2.50µm. The low entropy value of the LCP present in the CRISM Nili Fossae research area is due to the broad absorption feature of LCP in the SWIR range.

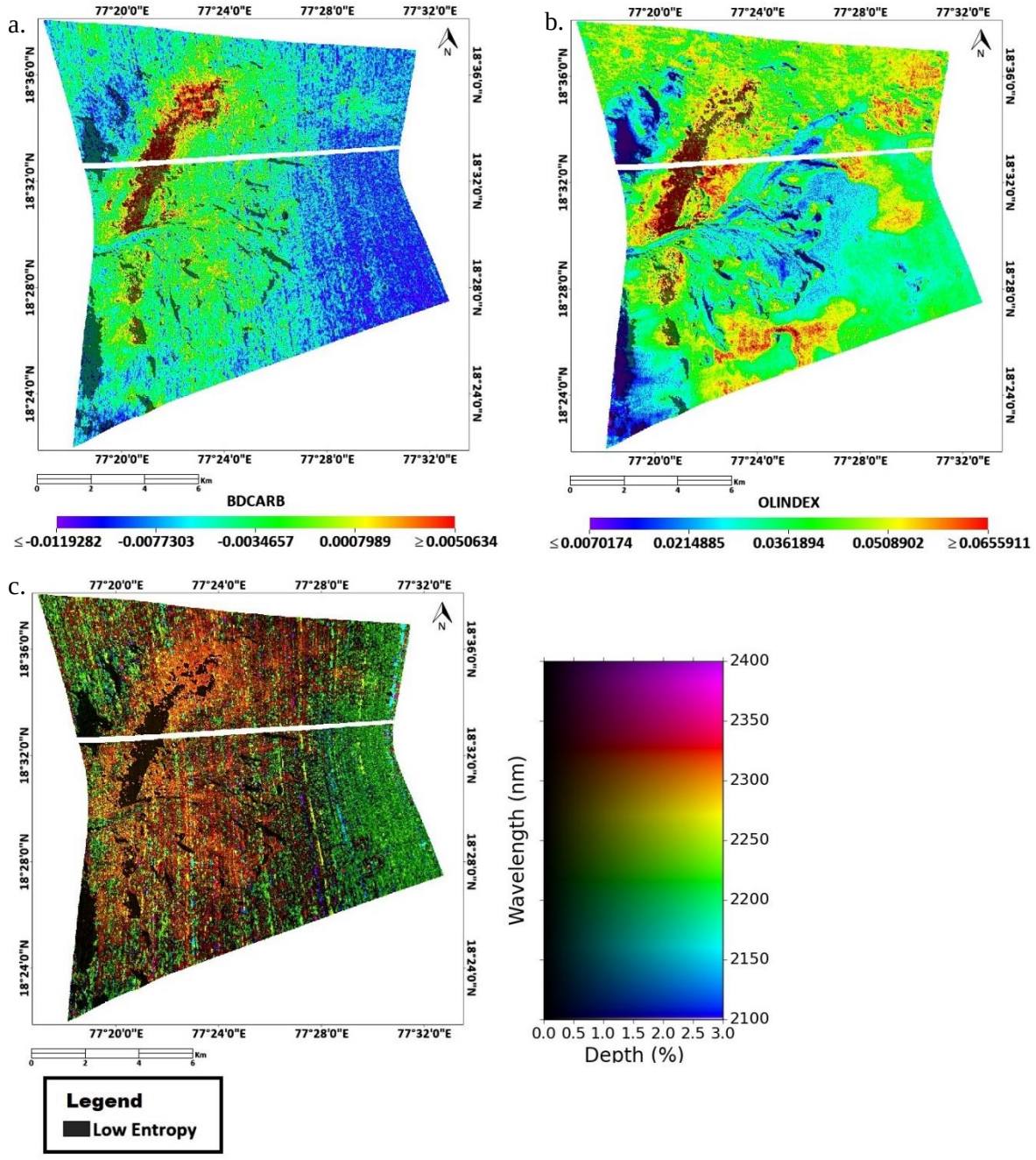

Figure 55. Low entropy ROI (Black) of the CRISM Jezero Crater image overlain with the a.) BDCARB index, b.) OLINDEX, and c.) 2.10µm – 2.40µm wavelength map.

Figure 55 shows the low entropy ROI in black colour, overlain with the wavelength map and the summary product maps created in the results chapter. The BD2290 summary product map, which indicates the location of Fe-Mg phyllosilicates, is not shown, because the analysis in section 3.3.2.6, the 2.30µm absorption feature is analysed to be carbonates. The CRISM Jezero Crater research area also show similarities between the areas with low entropy values with the wavelength map and the summary product maps. Figure 55a shows that parts of the low entropy ROI match well with the high BDCARB index. The matching low entropy ROI is the low entropy ROI 1 and 4 (Figure 26). The same entropy value ROIs also matches well with the OLINDEX in Figure 55b. Figure 55c shows the low entropy value ROI overlain with the wavelength map created in Figure 27. Figure 55c shows that most

of the low entropy value represents 2.30µm as the deepest absorption feature, which is an indication of carbonates.

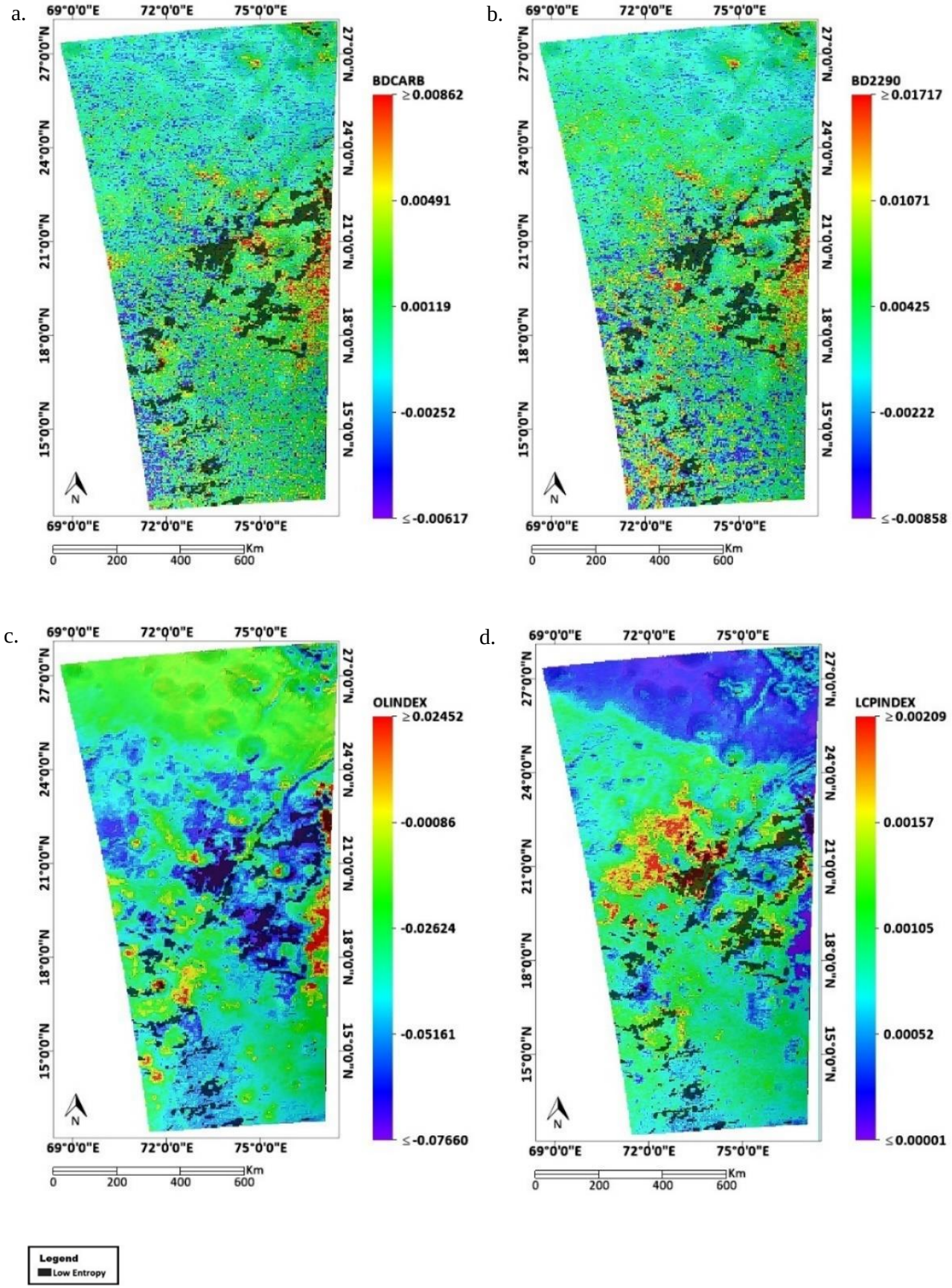

e.

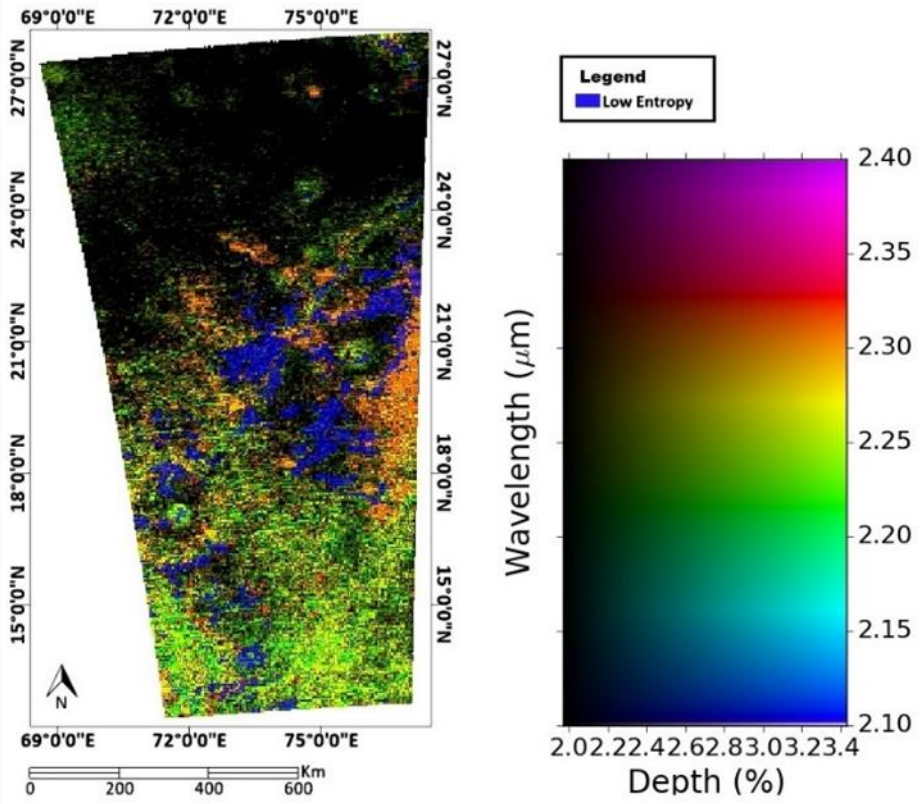

Figure 56. Low entropy ROI (Black) of the OMEGA Nili Fossae image overlain with the a.) BDCARB index, b.) BD2290 index, c.) OLINDEX index, d.) LCPINDEX index, and e.) 2.10μm – 2.40μm wavelength map.

The low entropy values of the OMEGA Nili Fossae research area are more likely to represent deeper broad absorption features rather than a single band deep absorption feature, as can be seen in Figure 52. Figure 56 shows the ROI of the low entropy values overlain in the wavelength map and summary products of the OMEGA Nili Fossae research area.

The comparison between the low entropy value ROI and the LCPINDEX summary product, which can be seen in Figure 56d, shows that in the Nili Fossae region, some the locations of highly positive LCPINDEX index value are represented by the low entropy values (ROI 3 and ROI 7 in Figure 35). ROI 7 and ROI 1 in Figure 35 may also indicate the presence of carbonate, as it overlays on the high BDCARB index in Figure 56a. Further investigation is needed to analyze the mineral indication in ROI 7 as it also shows indication of Fe-Mg phyllosilicate, as seen in Figure 56b. Parts of the low entropy values, specifically the east section of the low entropy value ROI (East section of low entropy value ROI 5 in Figure 35), represent the mineral olivine, which can be seen in Figure 56c.

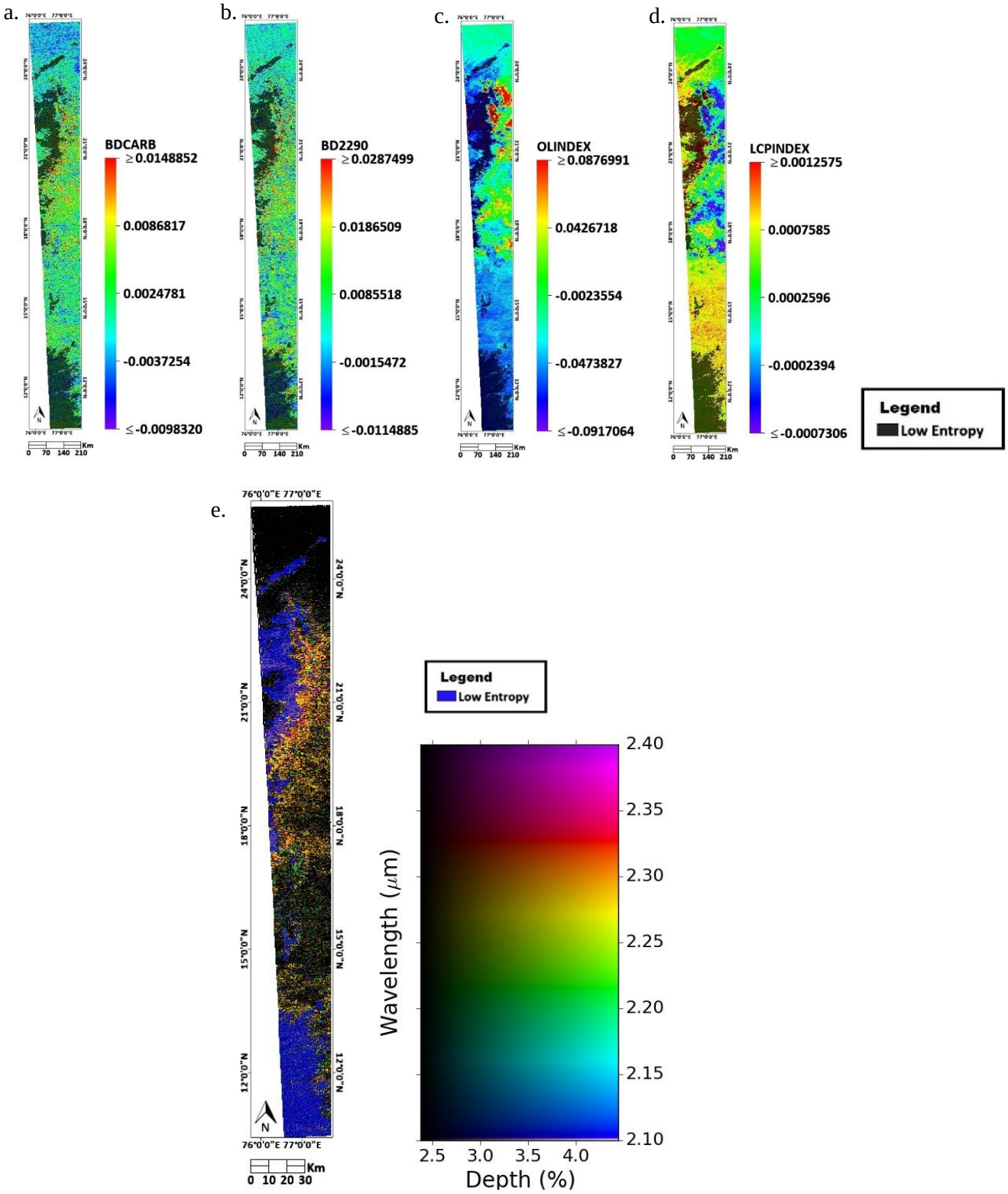

Figure 57. Low entropy ROI (Black) of the OMEGA Jezero Crater image overlain with the a.) BDCARB index, b.) BD2290 index, c.) OLINDEX index, d.) LCPINDEX index, and e.) 2.10μm – 2.40μm wavelength map.

Figure 57a shows the low entropy value ROI of the OMEGA Jezero Crater image overlain on the BDCARB summary product map. Parts of the low entropy ROI covers the high index value of the BDCARB summary product map, specifically on ROI 2 (Figure 47). Figure 57b shows similar locations of high index value of the BD2290 summary product map. Figure 57c shows the low entropy value ROI overlain in the OLINDEX summary product map. The low entropy value does not cover any part of the high index value of the OLINDEX summary product map, which meant the low entropy value in the OMEGA Jezero Crater image does not indicate presence of olivine, though it is present in the image based on the OLINDEX summary product map. From Figure 57d, it can be seen that most of the low entropy value in the north part of the research area represents the LCP. The pattern of the low entropy value matches with the highly positive index value of the LCPINDEX index map. The low entropy values at the south part of the research area does not show any similar patters with any of the summary products and may be caused by systematic noise. Figure 57e shows the low entropy value ROI overlain with the wavelength map of the OMEGA Jezero Crater image. Figure 57e shows that locations where the low entropy ROI overlaps with the 2.30µm deepest absorption feature is shown as high index value in the BDCARB and BD2290 summary product maps.

4.4. Comparison of entropy derived from the CRISM and the OMEGA instrument data.

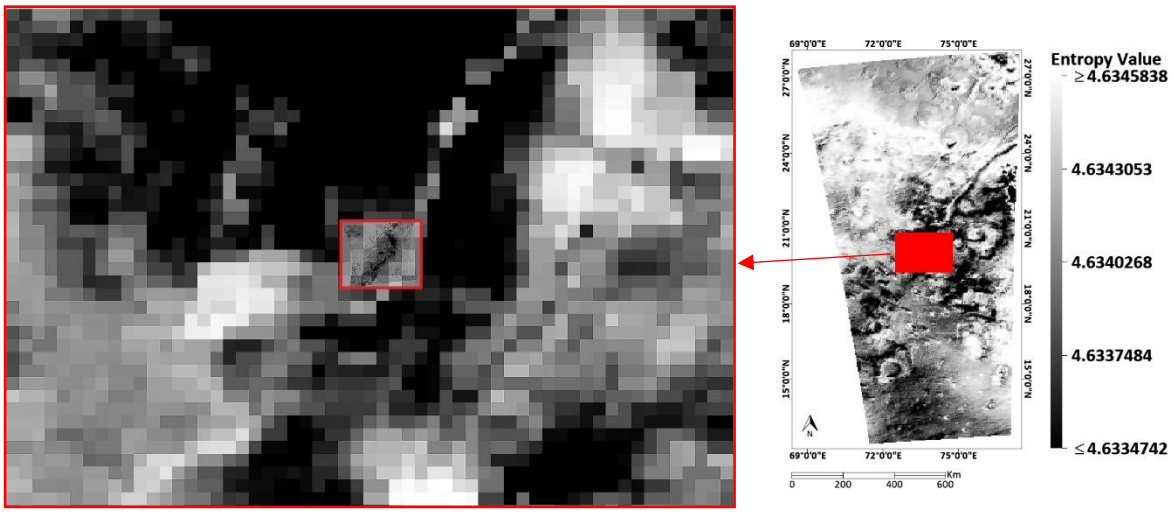

Figure 58. Entropy map of the CRISM Nili Fossae image overlain with the entropy map of the OMEGA Nili Fossae image.

Looking at Figure 58, areas with low entropy values between the OMEGA and CRISM Nili Fossae research areas shows similarities. As can be seen in Figure 58, the low entropy value of the graben wall can be seen in both the OMEGA and CRISM Nili Fossae research area. Due to the larger pixel size of the OMEGA dataset, the low entropy values in the graben wall are shown as the mineral LCP. From the comparison between the summary products in Figure 56, it also shows that the low entropy value of where the CRISM Nili Fossae research area is does show positive index value in the BD2290 of the OMEGA Nili Fossae research area.

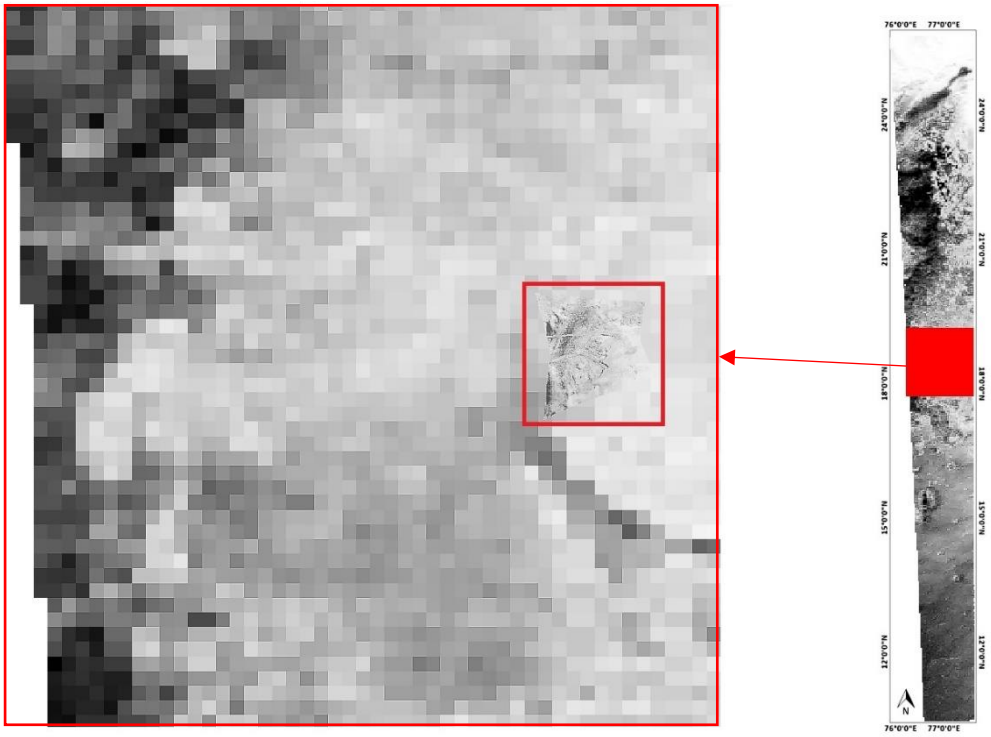

Figure 59. Entropy map of the CRISM Jezero Crater image overlain with the entropy map of the OMEGA Jezero Crater image.

Figure 59 shows the entropy map and summary products of the OMEGA Jezero crater research area overlain with the CRISM Jezero Crater research area to be used as comparison. From the entropy map comparison, it can be seen in Figure 59 that the area where the CRISM Jezero Crater research area is located shows a mid to high entropy value. The low entropy value of the CRISM Jezero Crater research area does not show in the OMEGA Jezero Crater research area. This is caused by the averaging of the entropy values in a regional scale. The OMEGA Jezero Crater research area shows that there are places with lower entropy values than the area where the CRISM Jezero Crater research area is located, causing the entropy value of the CRISM Jezero Crater research area to be perceived as having mid to high entropy values. The effect can also be seen in Figure 59, where the low entropy values of the CRISM Jezero Crater research area shows mid entropy value in the OMEGA Jezero Crater research area.

5. Conclusion

Based on the result and discussion conducted in this research, conclusions can be made. The conclusions are made from analyzing the spectral representation of the range of entropy values and comparison between small (CRISM) and large (OMEGA) scale research areas. The conclusions made are:

- Section 4.1 discusses the effect of processing on the CRISM Nili Fossae image. The resulting processed image by me (Corrected TRDR CRISM image) shows very little difference with the processed image by the CRISM team (MTRDR image) in reflectance and absorption features. Through regression analysis conducted in section 3.1, the corrected TRDR image by me and the MTRDR image corrected by the CRISM team shows a very strong relationship and therefore shows very little difference. This concludes that the use of the either the processed TRDR and the MTRDR image in this research will show little to no difference.

- Broad wavelength features affect the entropy value calculation. In the CRISM Nili Fossae research area, the mineral LCP is represented by low entropy values. LCP, which has broad diagnostic features, is shown to have low entropy values. Similar to the CRISM Nili Fossae research area, low entropy values in the OMEGA Nili Fossae research area also shows a steeper spectral curve compared to the high entropy value spectra. The mean spectra of the high entropy sample ROI show more variety and deeper absorption feature, but it has high entropy value. The high entropy value differs from the low entropy value by the steeper curve of the spectra, which is caused by the presence of a broad absorption feature. The difference in the high and low entropy spectra can be seen in section 4.2. This concludes that broad absorption features have a higher effect in the calculation of entropy values than single bands absorption feature.

- Based on the interpretation in section 4.3, the minerals indicated by the low entropy values is not limited to hydrothermal alterations, but also minerals that show broad absorption features. In the CRISM Nili Fossae results section, the entropy map also indicates locations where low calcium pyroxene is present. In the CRISM Jezero Crater image results section, the low entropy value indicates locations where olivine, which has broad absorption features, may be present. A conclusion can be made that low entropy values will show areas that indicates a strong presence of minerals that has broad absorption features.

- The entropy method is used as an exploratory tool in a regional scale by using OMEGA images. The resulting low entropy values indicates areas that shows a deeper absorption feature and may be an indication of the presence of certain minerals. The variety of summary product maps in this research are created based on past studies that shows the general minerals that is located throughout mars. Based on the discussion in section 4.3, in the OMEGA images, the low entropy values do indicate areas where minerals may be present, but faint absorption features may cause a mineral to not be indicated as low entropy value.

- Entropy values can be interpreted by using wavelength and summary product maps, as seen in section 4.3. The low entropy values will indicate locations where minerals may be present. By creating an ROI using threshold of low entropy values and overlaying it in wavelength and summary product maps, we can identify the minerals present in the research area. A conclusion can be made that by using only entropy maps, we cannot indicate which minerals the low entropy value represents, unless we do further interpretation by using wavelength and summary product maps.

- The wavelength map shows the deepest absorption feature wavelength location. The comparison between the entropy map and the wavelength map in section 4.3 shows that the entropy value does not cover all the locations of the deepest absorption feature of the wavelength map. This is because the areas covered by the entropy value shows locations where

the spectra have deeper absorption features, or deeper broad absorption feature, than the rest of the research area.

- Based on the discussion in section 4.4, by comparing the OMEGA and CRISM research area, it can be concluded that the entropy exploration method will be more effective when conducted in a more detailed image. When using the entropy method in a regional scale, places that may show low entropy values may be shown to have higher entropy values in a more detailed image, due to the effect of mixed pixels. Therefore, the entropy method can be used to indicate areas that has deeper absorption features compared to other areas within the same research area.

From the conclusions, it can be said that the entropy method can be used as a space exploration tool. The entropy method would work on a large scale, but would be more effective when conducted in a more detailed image. The entropy method does show areas that has deeper absorption features and would be a great method to indicate areas where minerals may be present.

6. Recommendations

The entropy method would benefit greatly if more extensive analysis is conducted to analyze the viability of the entropy method as a space exploration tool. Due to the time limitation, some of these analyses cannot be conducted in this research. For future researchers, the recommendations for further analysis of the entropy method as a space exploration tool is as such:

- A more extensive quantitative analysis of the spectra would be effective in analyzing how the spectra affect the calculation of the entropy values.
- Do a quantitative analysis of the entropy validation step, to calculate the accuracy of the low entropy values and the mineral representation of the low entropy values. For example, by creating vectors of the low entropy values of different mineral representation and calculate the area difference between the low entropy values vector and the mineral spread vector.
- Conduct the entropy method using a wider spectral subset, specifically areas that may show broad absorption features, such as employing a spectral subset of 0.45µm to 2.65µm. This spectral subset will indicate areas that show deeper absorption features in the VNIR range.

References

Bakker, W. H., Van Ruitenbeek, F. J. A., Van Der Werff, H. M. A., Zegers, T. E., Oosthoek, J. H. P., Marsh, S. H., & Van Der Meer, F. D. (2014). Processing OMEGA/Mars Express hyperspectral imagery from radiance-at-sensor to surface reflectance. Planetary and Space Science, 90, 1–9. https://doi.org/10.1016/j.pss.2013.11.007

Bibring, J. P., Langevin, Y., Mustard, J. F., Poulet, F., Arvidson, R., Gendrin, A., … Neukum, G. (2006). Global mineralogical and aqueous Mars history derived from OMEGA/Mars express data. Science, 312(5772), 400–404. https://doi.org/10.1126/science.1122659

Bibring, J. P., Soufflot, A., Berthé, M., Langevin, Y., Gondet, B., Drossart, P., … Forget, & F. (2004). OMEGA: Observatoire pour la Minéralogie, l'Eau, les Glaces et l'Activité. Mars Express: The Scientific Payload, SP-1240, 37–49. Retrieved from https://sci.esa.int/s/WEyq9YW

Brown, A. J., & Storrie-Lombardi, M. (2014). MR PRISM-Spectral Analysis Tool for the CRISM. Retrieved from https://arxiv.org/abs/1401.7089v1

Carr, M. H. (1987). Water on Mars. Nature, 326(6108), 30–35. https://doi.org/10.1038/326030a0

Carr, M. H., & Head, J. W. (2010). Geologic history of Mars. Earth and Planetary Science Letters, 294(3–4), 185–203. https://doi.org/10.1016/j.epsl.2009.06.042

Ceamanos, X., & Douté, S. (2010). Spectral smile correction of CRISM/MRO hyperspectral images. IEEE Transactions on Geoscience and Remote Sensing, 48(11), 3951–3959. https://doi.org/10.1109/TGRS.2010.2064326

Cover, T. M., & Thomas, J. A. (2005). Elements of Information Theory. In Elements of Information Theory. https://doi.org/10.1002/047174882X

Data Design Working Group. (2020). PDS4 Concepts. Retrieved from https://pds.nasa.gov/datastandards/documents/

El Maarry, M. R. (2011). Detection of Hydrothermal Systems on Mars using Remote Sensing (Georg-August-Universität Göttingen). https://doi.org/10.13140/RG.2.1.5122.2249

ESA. (2018, April 9). Comparing the atmospheres of Mars and Earth. Retrieved October 4, 2020, from ESA website: https://exploration.esa.int/web/mars/-/60153-comparing-the-atmospheres-of-mars-and-earth

Franz, H. B., Trainer, M. G., Malespin, C. A., Mahaffy, P. R., Atreya, S. K., Becker, R. H., … Wong, M. H. (2017). Initial SAM calibration gas experiments on Mars: Quadrupole mass spectrometer results and implications. Planetary and Space Science, 138(December 2016), 44–54. https://doi.org/10.1016/j.pss.2017.01.014

Gaffey, S. J. (1986). Spectral reflectance of carbonate minerals in the visible and near infrared (0.35-2.55 microns): calcite, aragonite, and dolomite. American Mineralogist, 71(1–2), 151–162.

Gilmore, M. S., Thompson, D. R., Anderson, L. J., Karamzadeh, N., Mandrake, L., & Castaño, R. (2011). Superpixel segmentation for analysis of hyperspectral data sets, with application to Compact Reconnaissance Imaging Spectrometer for Mars data, Moon Mineralogy Mapper data, and Ariadnes Chaos, Mars. Journal of Geophysical Research, 116(E7), E07001. https://doi.org/10.1029/2010JE003763

Goudge, T. A., Milliken, R. E., Head, J. W., Mustard, J. F., & Fassett, C. I. (2017). Sedimentological evidence for a deltaic origin of the western fan deposit in Jezero crater, Mars and implications for future exploration. Earth and Planetary Science Letters, 458, 357–365. https://doi.org/10.1016/j.epsl.2016.10.056

Goudge, T. A., Mustard, J. F., Head, J. W., Fassett, C. I., & Wiseman, S. M. (2015). Assessing the

mineralogy of the watershed and fan deposits of the Jezero crater paleolake system, Mars. Journal of Geophysical Research: Planets, 120(4), 775–808. https://doi.org/10.1002/2014JE004782

Horgan, B. H. N., Anderson, R. B., Dromart, G., Amador, E. S., & Rice, M. S. (2020). The mineral diversity of Jezero crater: Evidence for possible lacustrine carbonates on Mars. Icarus, 339, 113526. https://doi.org/10.1016/j.icarus.2019.113526

Koppal, S. J. (2014). Lambertian Reflectance. In Computer Vision (pp. 441–443). https://doi.org/10.1007/978-0-387-31439-6_534

Michalski, J. R., Cuadros, J., Bishop, J. L., Darby Dyar, M., Dekov, V., & Fiore, S. (2015). Constraints on the crystal-chemistry of Fe/Mg-rich smectitic clays on Mars and links to global alteration trends. Earth and Planetary Science Letters, 427, 215–225. https://doi.org/10.1016/j.epsl.2015.06.020

Morgan, M. F., Seelos, F. P., & Murchie, S. L. (2017). The Crism Analysis Toolkit (CAT): Overview and Recent Updates. Planetary Data Workshop, 3, 1–2. https://doi.org/10.1029/2006JE002682

Mustard, J. F., Ehlmann, B. L., Murchie, S. L., Poulet, F., Mangold, N., Head, J. W., … Roach, L. H. (2009). Composition, Morphology, and Stratigraphy of Noachian Crust around the Isidis basin. Journal of Geophysical Research, 114(12), E00D12. https://doi.org/10.1029/2009JE003349

NASA. (2018). Mars in our Night Sky. Retrieved June 17, 2020, from National Aeronautics and Space Administration website: https://mars.nasa.gov/all-about-mars/night-sky/close-approach/

NASA. (2019a). CRISM. Retrieved September 21, 2020, from National Aeronautics and Space Administration website: https://mars.nasa.gov/mro/mission/instruments/crism/

NASA. (2019b). Mars - Facts. Retrieved June 17, 2020, from National Aeronautics and Space Administration website: https://mars.nasa.gov/all-about-mars/facts/

Naß, A., Di, K., Elgner, S., Van Gasselt, S., Hare, T., Hargitai, H., … Wählisch, M. (2017). Planetary cartography and mapping: Where we are today, and where we are heading for? International Archives of the Photogrammetry, Remote Sensing and Spatial Information Sciences - ISPRS Archives, 42(3W1), 105–112. https://doi.org/10.5194/isprs-archives-XLII-3-W1-105-2017

PDS Geosciences Node. (2017). Mars Orbital Data Explorer. Retrieved October 12, 2020, from https://ode.rsl.wustl.edu/mars/index.aspx

Pelkey, S. M., Mustard, J. F., Murchie, S., Clancy, R. T., Wolff, M., Smith, M., … Gondet, B. (2007a). CRISM multispectral summary products: Parameterizing mineral diversity on Mars from reflectance. Journal of Geophysical Research E: Planets, 112(8), 8–14. https://doi.org/10.1029/2006JE002831

Pelkey, S. M., Mustard, J. F., Murchie, S., Clancy, R. T., Wolff, M., Smith, M., … Gondet, B. (2007b). CRISM multispectral summary products: Parameterizing mineral diversity on Mars from reflectance. Journal of Geophysical Research E: Planets, 112(8), 8–14. https://doi.org/10.1029/2006JE002831

Podwysocki, M. H., Segal, D. B., & Jones, O. D. (1983). Mapping of hydrothermally altered rocks using airborne multispectral scanner data, Marysvale, Utah, mining district. Advances in Space Research, 3(2), 101–112. https://doi.org/10.1016/0273-1177(83)90109-6

Pontual, S., Merry, N., & Gamson, P. (1997). Spectral Interpretation Field Manual (G-MEX). AusSpec International Pty. Ltd.

PSA. (2017). OMEGA FTP Directory. Retrieved October 18, 2020, from ftp://psa.esac.esa.int/pub/mirror/MARS-EXPRESS/OMEGA/

Ritzer, J. A., & Hauck, S. A. (2009). Lithospheric structure and tectonics at Isidis Planitia, Mars. Icarus, 201(2), 528–539. https://doi.org/10.1016/j.icarus.2009.01.025

Ruitenbeek, F. J. A. Van, Goseling, J., Bakker, W. H., & Hein, K. A. A. (2020). Shannon Entropy as an Indicator for Sorting Processes in Hydrothermal Systems. 1–13. https://doi.org/10.3390/e22060656

Shannon, C. E. (1948). A Mathematical Theory of Communication. The Bell System Technical Journal, 27, 379–423. https://doi.org/10.1002/j.1538-7305.1948.tb01338.x

Singh, D. (2019). Venus nightside surface temperature. Scientific Reports, 9(1), 1–5. https://doi.org/10.1038/s41598-018-38117-x

Sun, V. Z., & Stack, K. M. (2020). Geologic Map of Jezero Crater and the Nili Planum Region, Mars. Scientific Investigations Map 3464. https://doi.org/10.3133/sim3464

Tanaka, K. L., Skinner, J. A., Dohm, J. M., Irwin, R. P., Kolb, E. J., Fortezzo, C. M., … Hare, T. M. (2014). Geologic Map of Mars. U.S. Geological Survey Geologic Investigations, 3292. https://doi.org/10.3133/sim3292

Tanaka, M., & Yamanouchi, T. (1977). Absorption properties of the near infrared CO2 bands. Journal of Quantitative Spectroscopy and Radiative Transfer, 17(3), 421–432. https://doi.org/10.1016/0022-4073(77)90121-2

Van Ruitenbeek, F. J. A., Bakker, W. H., Van Der Werff, H. M. A., Zegers, T. E., Oosthoek, J. H. P., Omer, Z. A., … Van Der Meer, F. D. (2014). Mapping the wavelength position of deepest absorption features to explore mineral diversity in hyperspectral images. Planetary and Space Science, 101, 108–117. https://doi.org/10.1016/j.pss.2014.06.009

Viviano-Beck, C. E., Seelos, F. P., Murchie, S. L., Kahn, E. G., Seelos, K. D., Taylor, H. W., … Morgan, M. F. (2014). Revised CRISM spectral parameters and summary products based on the currently detected mineral diversity on Mars. Journal of Geophysical Research E: Planets, 119(6), 1403–1431. https://doi.org/10.1002/2014JE004627

Wiseman, S. M., Arvidson, R. E., Wolff, M. J., Smith, M. D., Seelos, F. P., Morgan, F., … McGuire, P. C. (2016). Characterization of artifacts introduced by the empirical volcano-scan atmospheric correction commonly applied to CRISM and OMEGA near-infrared spectra. Icarus, 269, 111–121. https://doi.org/10.1016/j.icarus.2014.10.012

Appendices

Appendix 1. RLUB of the CRISM Nili Fossae image log-residual output.

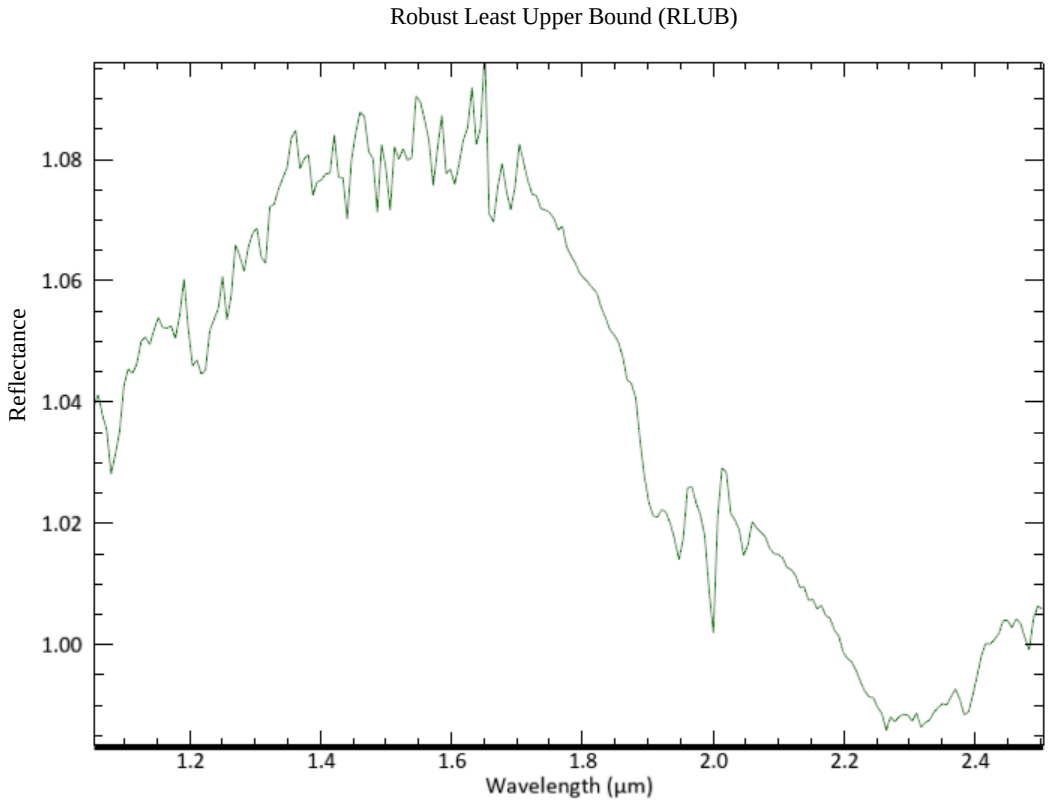

Appendix 2. RLUB of the CRISM Jezero Crater image log-residual output.